

UNIVERSITY OF SOUTHAMPTON

**AN INVESTIGATION OF THE ADHESION AND AGEING OF
POLYSULFIDE SEALANT SYSTEMS**

A thesis submitted to the University of Southampton in support of
candidature for the degree of Doctor of Philosophy

by Fabrice Birembaut

Department of Chemistry, April 2002

UNIVERSITY OF SOUTHAMPTON

ABSTRACT

FACULTY OF SCIENCE

DEPARTMENT OF CHEMISTRY

Doctor of Philosophy

**AN INVESTIGATION OF THE ADHESION AND AGEING OF
POLYSULFIDE SEALANT SYSTEMS**

by Fabrice Birembaut

The recent changes in the European laws about pollutants are forcing the Aerospace industry to find new formulas for the sealants used in the aircraft fuel tanks. The current formulas contain chromium, which is a very dangerous pollutant for the environment. The first aim of this thesis is to design an accelerated ageing test to help in screening the new formulae that will be used in the future. The use of an ultrasonic heating bath reveals itself to be of great advantage compared to other devices in which the sealant is enclosed for the time of the experiment. The several techniques, including hardness testing, mini-peel testing, mass spectrometry coupled with gas chromatography and UV/Visible spectroscopy are assessed and give invaluable clues to validate a new formula. In another chapter, the microscopic point of view is investigated. The Surface Enhanced Raman Scattering (SERS) technique is thus used to investigate the behaviour of the polysulfide molecules used in the Aerospace industry when they adsorb onto the metal surface. First, various smaller molecules, a disulfide and a collection of thiols and dithiols, will be studied to create a model. Using this model it will be possible to interpret the spectrum of the liquid polymer molecule. Moreover, some calculations will be used to decide, between two remaining possibilities, on the most credible behaviour of the molecule.

There will finally be two aims in the last chapter. The first one will be to look at the coupling agents used to promote the adhesion of the polysulfide sealants in the aeroplanes, using the same SERS technique. Because of the commercial sensitivity of the product and because of its complexity, a model will be created to help understanding what happens at the surface neighbourhood. The second aim will be to combine the two model systems to study the interactions between the polysulfide and the adhesion promoter, at the microscopic level, when they are both adsorbed on the same metal surface.

Acknowledgements

I would like to express my gratitude to the following people for their help and support while completing this research:

First, all my thanks are going to my Supervisor Dr. Andrea Russell for making it possible for me to study for this degree, to believing in me all the time (even when I did not) and for her help and support through the years. I also would like to thank Prof. Patrick Hendra for his useful help and our discussions about Raman spectroscopy. Many thanks also go out to my advisor and current boss Dr. Jeremy Frey.

I also would like to thank Dr. Steve Harris and Dr. Mike Taylor from BAe Systems for their help and financial support. My thanks also go out to Dr. Tony Martin for giving me a roof and entertainment when I was in Bristol. Special thank you for Mr. Colin West, even though our collaboration has been short, it was great.

To the past and present members of the Russell group and specially: Anne, Jun, Stéphanie, Abbe (thanks for reading the whole of this manuscript!), Chris, Linda, Becky, Colm, and Gurjit. To all of you a big thank you and good luck for the future. To Claire, Maria-Inmaculada de la Concepcion, Santy and Yu-May, thank you for your support.

A special thank you goes out to Anne-Margot. For her support and for those invaluable hours spent on the phone. De tout coeur merci et bon courage pour ta troisième année de thèse.

Another special thank you to the “Italian Connection”: Fabrizio, Lucia, and Loredana. ‘Grazie mille’ for teaching all those *useful* Italian words and sharing your culture (Ricchi e Poveri).

Least but not last, I think my parents deserve the biggest thank you of all. Thanks for reminding me *everyday* that I had to work hard to get this thesis finished. Merci.

To my Parents
Michel and Francine Birembaut

Table of Contents

<i>General Introduction</i>	1
<i>Chapter 1. Theory and Background</i>	16
1 VIBRATIONAL SPECTROSCOPY	16
1.1 MOLECULAR VIBRATIONS	16
1.2 CLASSICAL EXPLANATION OF THE RAMAN EFFECT	20
1.3 RAMAN INTENSITIES	24
1.4 FLUORESCENCE	27
1.5 SURFACE ENHANCED RAMAN SCATTERING (SERS)	29
1.5.1 Image Field Theories	29
1.5.2 Modulated Reflectance Theories	32
1.5.3 Adsorption Induced Resonance	33
1.5.4 Geometrically Defined Resonance	34
1.5.5 Microscopic (or electron – hole excitation) Theories	35
1.5.6 Summary	36
2 EXPERIMENTAL METHODS	39
2.1 CONVENTIONAL RAMAN INSTRUMENTATION	39
2.2 FOURIER TRANSFORM SPECTROSCOPY	42
2.3 CONFOCAL RAMAN MICROSCOPY	45
2.4 THE RENISHAW 2000 SYSTEM	48
3 MASS SPECTROMETRY	49
3.1 INTRODUCTION	49
3.2 CONSTITUENT PARTS	50
3.3 INTRODUCTION OF THE SAMPLE	50
3.4 IONISATION AND FRAGMENTATION	52
3.5 ELECTRON IMPACT IONISATION	53
3.6 THE MASS ANALYSER	53
3.7 INSTRUMENTATION	54

4	REFERENCES	56
	<i>Chapter 2. Designing an accelerated screening test</i>	<i>59</i>
1.	INTRODUCTION: THE PROBLEM	59
2.	EXPERIMENTAL	61
2.1.	SEALANT PREPARATION	61
2.2.	SOXHLET EXTRACTION	62
2.3.	ULTRASONIC BATH	63
2.4.	EXPERIMENTAL CONDITIONS	64
2.5.	INSTRUMENTATION	66
2.5.1.	Hardness Testing	66
2.5.2.	Mass Spectrometry	66
2.5.3.	Mini-peel testing	66
2.5.4.	UV-Visible Spectroscopy	68
3.	RESULTS AND DISCUSSION	68
3.1.	WEIGHT AND HARDNESS RESULTS	69
3.1.1.	Error in measurements	69
3.1.2.	Results	70
3.2.	MASS SPECTROMETRY	79
3.2.1.	Technique	79
3.2.2.	Results	79
3.3.	MINI-PEEL RESULTS	89
3.3.1.	Measurements	89
3.3.2.	Calibration	89
3.3.3.	Results and Discussion	91
3.4.	UV-VISIBLE SPECTROSCOPY	94
3.4.1.	Instrument	94
3.4.2.	Results and Discussion	94
4.	CONCLUSION	98
5.	REFERENCES	99

<i>Chapter 3. Investigation on the polysulfides bonding</i>	101
1. INTRODUCTION	101
2. EXPERIMENTAL	102
2.1. ROUGHENING PROCESS.....	104
2.2. MOLECULE ADSORPTION.....	104
2.3. STUDIED MOLECULES.....	105
2.4. SPECTRAL CONDITIONS.....	107
3. RESULTS AND DISCUSSION	108
3.1. DIPHENYL DISULFIDE.....	108
3.2. 1-BUTANETHIOL.....	110
3.3. DITHIOLS COLLECTION.....	112
3.4. THE SEALANT MOLECULES.....	118
4. CONCLUSION	125
5. REFERENCES	127
 <i>Chapter 4. Study of Adhesion Promoters</i>	 128
1. INTRODUCTION	128
1.1. ORGANOSILANES.....	132
1.2. ORGANIC TITANATES.....	133
2. EXPERIMENTAL	133
1.3. EXPERIMENTAL DETAILS.....	133
1.4. MOLECULES STUDIED.....	134
1.5. INTERACTIONS.....	135
3. RESULTS AND DISCUSSION	136
1.6. THE MODEL MOLECULES.....	136
1.6.1. Organosilane.....	136
1.6.2. Organotitanate.....	141
1.7. REAL ADHESION PROMOTER.....	143
1.8. INTERACTIONS.....	145
1.8.1. Organosilane and DDS.....	145
1.8.2. Organosilane and LP2C.....	148
1.8.3. Organotitanate and DDS.....	150

1.8.4.	<i>Organotitanate and dithiol</i>	153
1.8.5.	<i>Organotitanate and LP2C</i>	155
1.8.6.	<i>ADP1 and the molecules</i>	157
4.	CONCLUSION	160
5.	REFERENCES	163

	<i>General Conclusion and Future Work</i>	165
--	---	-----

General Introduction

Introduction

The research project presented in this thesis was funded by BAe System / Airbus and involves the study of the polysulfide sealants used in the Aerospace industry. In this introduction, polysulfide sealants will be introduced and the motivation behind the thesis project described.

Polysulfide Sealants

Sealants are widely used in the aerospace industry because of their high resistance to jet fuel. They are mainly composed of a liquid polysulfide polymer that was first discovered by Patrick [1] who obtained the first of a series of patents. He mixed ethylene dichloride and sodium polysulfide to produce a material similar to natural rubber. The most interesting property of these polymers was their unusual inertness to solvents and aliphatic hydrocarbons in contrast to the easy swelling of natural rubber. They had, however, some less desirable properties: they were difficult to process, had a bad odour that remained even when fully cured, and gave off irritating fumes during processing. It was subsequently found that the polymers prepared from *bis* (2-chloroethyl) ether were free of this problem, were more readily processed and gave improved physical properties. Later on, the dichloro monomer of the greatest general utility was found to be *bis* (2-chloroethyl) formal. It polymerised to high yields of polymer, having excellent solvent resistance, very low odour and higher flexibility at low temperatures. At the present time, almost all the polysulfide polymers produced use this monomer as the major organic reactant. In most cases it is used in combination with a small amount of 1,2,3-trichloropropane, the function of which is to produce branching in the polymer chains [2].

In early 1942 work began that led to the invention by J.C. Patrick and H.R. Ferguson of a polymer with thiol ($-SH$) chain terminals, called Liquid Polysulfides. The liquid

polymers were to become the most widely used of the polysulfide polymers and had the trademark designation LP [3]. The ageing properties and excellent weather resistance of the cured LPs have expanded their use well beyond their original applications based on solvent and fuel resistance, for example, sealing the joints of aircraft in the integral wing fuel tanks.

Sealants based on polysulfide liquid polymers originally found wide acceptance for applications requiring flexible, adherent, chemically resistant compositions of matter. Since they were the first liquid polymers available that could be cured at room temperature, they were soon specified for a number of military applications. Their use as aircraft sealants for fuel tanks still remains a major outlet. Other military applications included a quick hose repair compound, a sealant for bottled steel tanks for quick assembly on the battle front, electrical potting compounds, caulks for wooden flight decks which were designed as a stop gap in the early days of aircraft carriers, sealing and adhering methacrylate bubbles on aircraft, sealing cocoons in the mothballed fleets, adhering aluminium strips on wings for reducing air turbulence during the flight, and many others. Most of these were emergency measures adopted for immediate use during the early 1940s and covered by quick-issue military specifications [4]. The use of polysulfide is at present largely restricted to their application as sealants.

As will be seen later, polysulfide sealants may be cured using a chromium oxide salt. However, the changes in environmental legislation introduced in the early 1990's following the Montreal agreement and the growing public awareness of environmental and health issues, has resulted in the need for sweeping changes in the surface treatments used in the aerospace industry [5,6]. Major changes have been forced upon this particular industrial sector, which if not rapidly addressed, will make it increasingly difficult for the European based aerospace companies to remain competitive this century. The main areas affected by the recent environmental legislation and growing public concern include [7]:

- *replacement or reduction in the use of organic solvent based processes, such as those currently based on methyl-ethyl ketone (MEK) or 1,1,1, trichloroethane ,*
- *environmentally friendly pre-treatment and cleaning processes,*

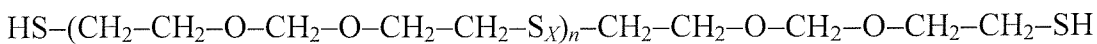
- *better waste management,*
- *the gradual elimination of the toxic hexavalent chromium ion from industrial corrosion protection systems, and*
- *the replacement of cadmium as a protective coating.*

It is also well-known in the aerospace industry that minor formula changes in sealants often result in major property changes such as: chemical compatibility and permeability, mechanical properties, adhesion, dynamic performance, colour, stability, flammability, toxicity, reparability, ease of application, surface preparation, cost, consequences of joint failure, and so on [8]. These changes take all their importance when one realises that 27 meter long wing may flex 5 meters vertically under operating conditions, thus the sealant must have the flexibility to facilitate this movement [9].

The following literature review deals with the structure, the curing, the ageing, the adhesion and the techniques used to study liquid polysulfides. The literature on liquid polysulfide is quite extensive. The present work will be limited to the curing process, the adhesion to a metal and to the various spectroscopic techniques used to study these polymers.

Liquid polysulfide structure curing and aging

Liquid polysulfide polymers are produced by the aqueous polymerisation of short chain of dichloro-hydrocarbons with sodium polysulfide. The most common polymers are based on *bis*-(2-chloro ethyl) formal ($\text{ClCH}_2\text{--CH}_2\text{--O--CH}_2\text{--O--CH}_2\text{--CH}_2\text{Cl}$), which following polymerisation and molecular weight reduction yields linear polymers of type:



Where,

X is the average degree of polysulfidity and is typically between 1.9 and 2.2

n can vary from 6 to 42.

Cross-linking or branching sites are produced by small additions of 1,2,3-trichloropropane (TCP). The TCP is normally added at levels of 0.5 to 2 % by weight of the *bis*-(2-chloro ethyl) formal [10]. The molecular weight of produced LPs can vary from 600 to 4000 (See table 1)

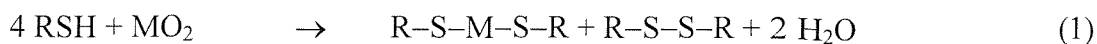
Table 1: Thiol terminated polysulfide polymers [2]

Polymer	Mole % of TCP	Molecular Weight	Viscosity (poise)	Approx. % of SH
LP-8	2	600	3	11
LP-3	2	1000	13	6.6
LP-5	2	2500	100	2.6
LP-2	2	4000	400	1.6
LP-33	0.5	1000	13	6.6
LP-32	0.5	4000	400	1.6
LP-31	0.5	7000	1100	0.9
LP-12	0.1	4000	400	1.6
Rubber	2	80,000	30	N/A

Todorova and Oreshkov developed, in 1999, a method to calculate the average molecular weight of polysulfide polymers using IR spectroscopy [11]. They were also able to ratio the S – S stretching band situated at 492 cm^{-1} to determine the degree of polysulfidity X of the polymer.

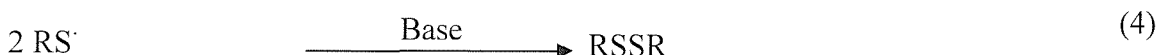
Over the years, it has been found that a wide variety of materials are capable of affecting cure in polysulfide polymers. The main products used for curing agents are metal peroxides and other metal oxy- salts which make use of the reducing properties of the thiol group to cause cross linking. Such materials include the dioxides of lead, manganese, calcium, barium, sodium and zinc (the letter M used in the equations below represents these metals) together with chlorates, dichromates and permanganates. Other oxidising agents, including organic peroxides and hydroperoxides, have been used commercially and many others have been tried experimentally. An extensive but not exhaustive list is given by Lucke [12].

A simplified curing mechanism has been suggested to be as follows [13]:

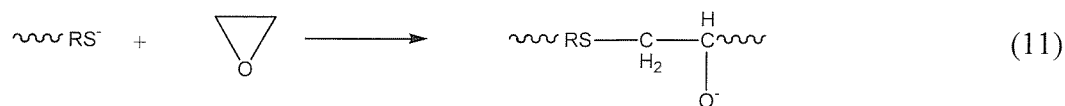
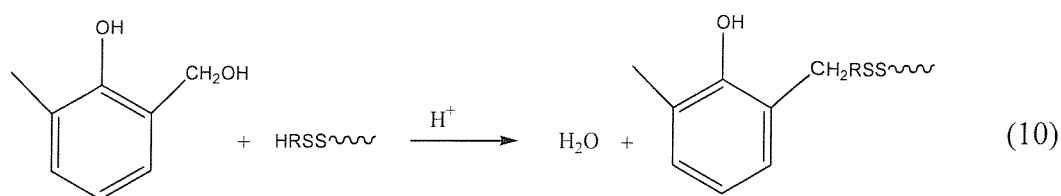


The cure of the sealant begins on the surface with the formation of a cured skin. Full cure of the bulk of the sealant will then follow as the catalysing agents (moisture/oxygen) diffuse through the body of the material. This model is, however, quite a naive view of what is happening during the curing. The following model probably represents a more realistic approach to the problem.

Lowe [10] showed that the curing process is preceded, as described below (equation 3 through 9), by a more complex mechanism. Many different parameters are taking part in this process, such as the presence of water and addition of base, both used as catalysts for the reaction or presence of acid or mono mercaptans which can have severe retardation effects on the cure.

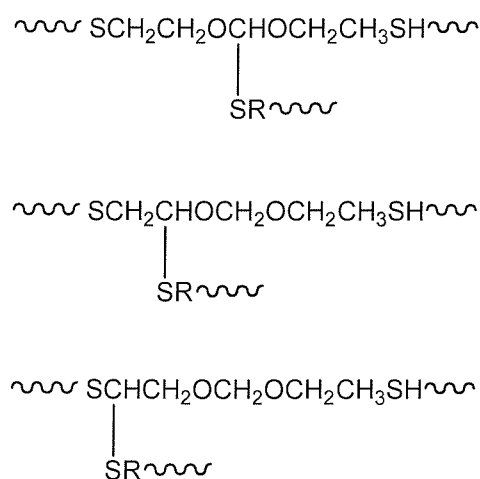


Parallel to metal oxides, other organic agents can be used to cure LPs and modify sealant performance. For example, hydroxymethyl groups of phenolic resins, or the epoxide rings in epoxy resins, both introduced to improve adhesion, can interact with thiols [14]:



However, these resins, present in sealant formulation, only work as a long-time curing system and cannot be used on their own as a full curing system.

In 1999, Matsui and Miwa [15] used the Intensive Nuclei Enhanced by Polarisation Transfer (INEPT) method to determine new sites of cross-linking in polysulfide polymers. According to the toughening theory, OH terminals in LP are removed and their concentration decreases during the toughening period [2]. The authors found that during their study OH terminals did not change or even increased slightly. This inconsistency suggested to them that additional cross-linking sites concerning tertiary carbon atoms were produced during polymerisation in addition to those related to the TCP. Those new cross-linking sites are as follows:



Research is still carried out on curing rates and how to improve sealants and their resistance to solvents. In 1989, Hanhela *et al.* [16] found that nitrile oxides reacted quite rapidly with thiols. They then tried to use these organic compounds as curing agents.

They assessed that both terephthalonitrile oxide and 4,4'-sulfonylbisbenzonitrile dioxide cured liquid polymer LP-2 at 90% in under 4h. These materials exhibited hardness and elasticity properties close to the existing sealants. Unfortunately, a year later the same authors [17] published an article reporting that these new sealants degraded under heat. This then leads to another widely studied aspect of LPs and LP sealants: degradation.

Degradation

There are different kinds of possible degradation mechanisms for these polymers, affecting various part of the cured sealant (see Table 2 for the composition of the sealants used in the aerospace industry) and the first one is called ageing. Ageing materialises mainly as hardening and lost of elasticity. In 1971, Stargel [18] proposed that the hardening could be caused by ozone attack, chemical spills, solvent evaporation, ultraviolet attack, migration of plasticisers and “many other factors”. He also suggested that hardening could occur due to the cyclic loads of tension and compression.

Table 2 Formulation of Cr1 and Mn1 sealants, respectively chromium and manganese cured (data obtained from BAe Systems)

	Base		Activator	
Cr1	Sulphide	59.2 %	Water	21.3 %
	Water	0.6 %	DMA	30.0 %
	Toluene + MEK	1.5 %	Dichromate	25.1 %
	Phenolic resin	7.5 %	Clay	22.6 %
	CaCO ₃	31.2 %	Carbon black	1.0 %
	Ti species	Nil		
Mn1	Sulphide	60.1 %	Acid soluble MnO ₂	55.0 %
	Water	0.3 %	Carbon black	12.4 %
	Toluene + MEK	Nil	Hydrogenated terphenyls	29.7 %
	Phenolic resin	4.0 %	NN'-diphenyl guanidine	1.7 %
	CaCO ₃	35.6 %	Sodium stearate	2.1 %
	Ti species	v. small	Water	0.4 %

Now we know that the main causes of degradation are heat, water and fuel [19]. Different methods have been developed, through the years, to assess the effect of these agents on the curing rate and the properties of the polymer. Hardness, viscosity, glass transition, thermogravimetric methods, NMR and IR are the most commonly used. Wilkie and Mittleman [20] in 1994 described a new technique to study the thermal degradation of polymers; Infrared Spectroscopy coupled with thermogravimetric analysis. This new technique was shown to be very useful in providing information about degradation process and details of degradation pathways. Nevertheless, TGA/IR is not a solution to all problems in the study of polymer degradation and the authors advise the reader not to neglect other techniques, which are required to completely identify the reaction scheme.

In 1987, Paul *et al.* [14] compared the effect of the environment on manganese and chromium cured sealants. The critical changes that occurred at high temperatures on uncured sealants were in viscosity (eventually accompanied by skinning and a drop in thiol concentration) and in the rate of cure. Mn(IV) curing agents did not lose activity although Cr(VI) ones showed a loss of solvent. They also showed that the higher the relative humidity, the faster the curing time. They carried out work on cured sealants as well, finding that the use of dichromate and manganese dioxide curing systems had produced sealants with stability up to 120 °C (continuous exposure) and in some cases up to 180 °C (short-term exposure) and that thermal failure was often indicated by embrittlement, cracks and weight loss. Three years later, the same authors [21] repeated their experiment over a wider range of sealants. They found that the uncured sealant lifetime could be extended to 2 to 3 years (although the manufacturers advise 9 months) by lowering the storage temperature to 2 °C.

As seen above, another important property of the sealants is their high resistance to jet fuel. Stout [22] described how some polysulfide sealants used by U.S. Air Force in 1981 were chalking when in contact with fuel. He examined this “chalk” using X-ray analysis and found it was mainly composed of calcium carbonate. He arrived at the conclusion that this material was left as the sealant polymers were gradually extracted by the chemical action of fuel and that this phenomenon was accelerated by the presence of mercaptans and metal ions in the fuel. He also found that when sealants were in contact

with fuel (or water) and high temperatures ($\sim 150^\circ\text{C}$), the sealants were “sponging”, i.e. they were absorbing the liquid and swelling.

Continuing with the difference between chromate cured and manganese dioxide cured sealants, Hanhela [23] described how adhesion problems were ascribed to water swelling rather than thermal effects. He also showed that chromate cured sealants are much more effective in hot water than those cured with manganese dioxide. The manganese cured sealants expanded to a high level of swell (80-120 %). Water was then transported through the matrix with little resistance and chemical attacks on the sealant-primer interface caused adhesion failure. The authors decided then to compare these results with the cross-linking ratio in these sealants [24]. However, no relationship between stability and cross-linking was observed. They were able to show that the significant swell differences between dichromate- and manganese dioxide-cured sealants derive from the respective abilities of these sealants to counter autoxidation. Sealants prepared from LP-2 for which the manganese dioxide-cure is used afford an acidic solution, whereas the materials cured by dichromate do not.

In 1993, Ennis [25] studied the influence of moisture ageing on the cross-linking density of an epoxy resin used in the aerospace industry. He found that small amounts of hydrolysis could lead to an effective reduction in cross-linking density. He also assessed that a modified network structure and reduced cross-link density gave a cured material of an inherently lower strength, and lower T_g . According to him, the measurement of flow or softening point of the uncured adhesive, and the T_g of the cured adhesive would appear to offer the best assessment of the quality of this particular material, when the more demanding formation and testing of joints is not required.

Recently, Choi [26] showed that the degradation process resulting in the ageing of vulcanised rubbers was due to an increase of the cross-link density. Apparently, the origins of the change of the cross-link density are the dissociation of the existing sulphur cross-links and the formation of new cross-links. The new cross-links are formed by the reaction of curing agents remaining in the vulcanizates and the combination reaction of the pendent sulfide groups.

Adhesion

Adhesion at polymer interfaces is a complex problem. Various types of bonding interactions – chemical, electrostatic and mechanical, with the possible formation of weak boundary layers – contribute to the ultimate adhesion strength between two materials and must be considered in explanations of cohesive and adhesive failure modes. In terms of the chemical component, the macroscopic adhesive bond is comprised of an aggregate of microscopic interactions in an interface region that can be morphologically and structurally complex. Part of the complexity of the metal-polymer interface arises from the fact that polymer surfaces are not usually as well characterised as the metal surface. Furthermore, chemical reactions might dissociate the polymer, breaking bonds and making available free radicals as additional source of reaction sites with the possible formation of residual reaction products. The connection to be made between microscopic surface chemistry and macroscopic adhesion lies in the fact that chemically reactive metal-polymer systems generally result in strongly bonded interfaces. Modification of the surface of the polymers by roughening, sputtering or reactive etching can enhance adhesion [27].

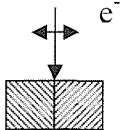
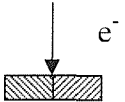
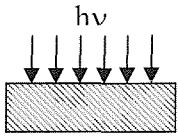
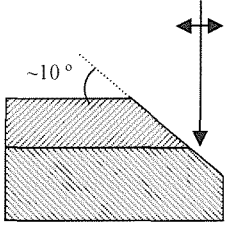
A thermodynamic study of the effect of a liquid environment on polymer-metal adhesion has been carried out by Carre and Schultz [28]. They found that in the case of an adhesive failure, the decrease of the adhesive strength due to the presence of a liquid environment could be quantitatively predicted by taking into account the surface characteristics of the solids and liquid; whereas in the case of cohesive failure in the elastomer, the contributions of both physical and chemical interactions to the cohesion energy of the cross-linked elastomer should be considered. The values they obtained experimentally were in good agreement with those calculated using network models.

Vibrational spectroscopy of polymer interfaces is far more complex than studying organic molecules adsorbed on single crystal metal surfaces due to the difficulty in assigning the variety of modes observed, particularly if they are not well-resolved due to instrumental limitations.

Watts, in 1988, [29] showed that the best techniques to study the degradation of polymer-to-metal adhesion are as presented in Table 3.

DiNardo described a large number of techniques appropriate to different cases [27]. It would be too long to develop each case in here. The most important techniques he recommends for the study of interfaces are Electron Energy Loss Spectroscopy (EELS), Infrared reflection spectroscopy (IRAS) and Surface Raman Enhanced Spectroscopy (SERS).

Table 3 Techniques presented by Watts to study the interface polymer – metal

Technique	Schematic of the technique	Sample preparation	Resolution (spatial and chemical)
1. SEM ¹ / EDXA ²		Easy (cross section)	Poor
2. TEM ³ / EELS ⁴		Very difficult (microtome or ion thin)	Good
3. XPS ⁵		Varies (mechanical electrochemical or chemical separation)	Very good
4. AES ⁶		Fair (ball cratering or angle lapping)	good

¹ SEM: Scanning Electron Microscopy

² EDXA: Energy Dispersive X-ray Analysis

³ TEM: Transmitting Electron Microscopy

⁴ EELS: Electron Energy Loss Spectroscopy

⁵ XPS: X-ray Photoemission Spectroscopy

⁶ AES: Auger Electron Spectroscopy

In surface chemistry, EELS has been used principally to measure vibrations of atomic and molecular adsorbate species on single crystal surfaces [30]. Not only can Vibrational modes be determined, but bonding sites, symmetries, and molecular orientations can be obtained. The disadvantage of this technique is that it must be carried out in ultra high vacuum. Infrared and Raman spectroscopy, if giving less information about the orientation or symmetries work very well in air or even in solution.

Boeirio *et al* [31] used Reflection – Absorption InfraRed Spectroscopy (RAIRS) to determine the mechanisms responsible for adhesion at the Natural Rubber (NR)/ primer interface. They also tried to determine the structural changes in the model rubber compounds during cross-linking using Fourier Transform Infrared (FTIR) spectroscopy. They simulated NR using a mixture of mainly either squalene ($C_{30}H_{50}$) or squalane ($C_{30}H_{62}$) and N,N-dicyclohexyl-benzothiazole-sulfenamide (DCBS), carbon black, sulphur and stearic acid. They found that although poor reactions occurred between squalane and DCBS, the squalene reactions were interesting. They concluded that an intermediate formed in the reaction that was responsible for cross-linking between squalene and the primer in the model system and for adhesion at the NR/primer interface in a chemical bond.

To summarise, many techniques are available to study the liquid polymer either in the bulk or at a microscopic level. They have also been extensively studied. However, no work has been done to study how the long chains of liquid polysulfide adsorb onto the surface of metal and what orientation they adopt. This is thus the aim of this thesis, as well as the interaction of the liquid polymer with the adhesion promoter molecules. The principal technique will be Surface Enhanced Raman Scattering because of the information it gives on what is happening close to the surface of the metal used.

Thesis Plan

Chapter 1 is dedicated to the development of Raman spectroscopy as an analytical tool and discusses the various advantages of FT Raman spectroscopy and Conventional Raman spectroscopy. It also introduces the Surface Enhanced Raman Scattering (SERS)

technique with a literature review on the subject. The second part of this chapter deals with the Mass Spectrometry technique that has also been used in this work.

Part of this project was to design an accelerated ageing test to enable the testing of new formulations of sealants. The ageing test will be based upon immersion of the sealants into different solvents and some evaluation techniques, such as mass spectrometry, UV/Visible spectroscopy, mass uptake, hardness testing and mini-peel testing. These techniques will be introduced / discussed in **Chapter 2**.

After looking at the macroscopic point of view, it will then be interesting to look closer and to study what happens at the interface between the polymer and the metal. To do so, the Surface Enhanced Raman Scattering technique will be used, as it provides spectroscopic information on the molecules adsorbed onto the surface of the metal. These results are presented in **Chapter 3**.

Also used in aerospace industry, adhesion promoters are quite an important part of the joint / adhesion system. The way they work is, however, unclear. For this reason the adsorption of adhesion promoters onto the surface of a metal and how their interaction with the liquid polymer molecules was also investigated, see **Chapter 4**.

Finally, a general conclusion will be proposed at the end of this manuscript. It will also set out some suggestions for future work.

References

- [1] Patrick, J. C. In *Ferguson* H.R. U.S. Patent, **1925**; Vol. 466; pp 963.
- [2] Bertozzi, E. R. *Rubber Chemistry and Technology* **1968**, 41, 114.
- [3] Duell, A. A. *Surface Coating* **1965**, 1, 1.
- [4] *Handbook of Adhesives*, 3rd ed.; Van Nostrand Reinhold: New York, **1989**.
- [5] McLauchlan, W. M. *Corrosion Management* **August/September 1996**, 8.
- [6] Storey, D. S. *Corrosion Management* **August/September 1996**, 10.
- [7] Hitchen, C. J.; Gostelow, C. R.; Gostelow, J. C. AGARD, report no 816, **1996**, pp. 4.1.
- [8] Amstock, J. S. High Performance Sealants. In *The Construction Specifier*, **July 1995**; pp 61.
- [9] Meyer, R. E. *Sampe Journal* **1982**, 18, 6.
- [10] Lowe, G. B. *International Journal of Adhesion and Adhesives* **1997**, 17, 345.
- [11] Todorova, D.; Oreshkov, T. *Spectroscopy Letters* **1999**, 32, 773.
- [12] Lucke-Huthig, H.; Verlag, W. *Aliphatic polysulfides*; Springer-Verlag: Heidelberg, **1994**.
- [13] Allen, K. W.; Hutchinson, A. R.; Pagliuca, A. *International Journal of Adhesion and Adhesives* **1994**, 14, 117.
- [14] Paul, D. B. *Abstracts of Papers of the American Chemical Society* **1987**, 193, 109.
- [15] Matsui, T.; Miwa, Y. *Journal of Applied Polymer Science* **1999**, 71, 59.
- [16] Hanhela, P. J.; Paul, D. B. *Australian Journal of Chemistry* **1989**, 42, 1257.
- [17] Ennis, B. C.; Hanhela, P. J.; Paul, D. B. *Australian Journal of Chemistry* **1990**, 43, 109.
- [18] Stargel, S. *Journal of Elastoplastics* **1971**, 3, 222.
- [19] Comyn, J.; Day, J.; Shaw, S. J. *International Journal of Adhesion and Adhesives* **1997**, 17, 213.
- [20] Wilkie, C. A.; Mittleman, M. L. *ACS Symposium Series* **1994**, 581, 116.

- [21] Barber, J. W.; Hanhela, P. J.; Huang, R. H. E.; Paul, D. B. *Polymer Testing* **1990**, 9, 291.
- [22] Stout, R. J. Service sensitivity of polysulfide sealants. In *13th National SAMPE Technical conference*, **1981**; Vol. 13; pp 64.
- [23] Hanhela, P. J.; Huang, R. H. E.; Paul, D. B. *Industrial & Engineering Chemistry Product Research and Development* **1986**, 25, 321.
- [24] Hanhela, P. J.; Huang, R. H. E.; Paul, D. B.; Symes, T. E. F. *Journal of Applied Polymer Science* **1986**, 32, 5415.
- [25] Ennis, B. C.; Pearce, P. J.; Morris, C. E. M. *Journal of Applied Polymer Science* **1989**, 37, 15.
- [26] Choi, S. S. *Bulletin of the Korean Chemical Society* **2000**, 21, 628.
- [27] DiNardo, N. J. *Proceedings of the International Conference on Vacuum Web Coatings* **1991**, 5, 35.
- [28] Carre, A.; Schultz, J. *Journal of Adhesion* **1984**, 18, 171.
- [29] Watts, J. F. *Surface and Interface Analysis* **1988**, 12, 497.
- [30] DiNardo, N. J.; Avouris, P.; Demuth, J. E. *Journal of Chemical Physics* **1984**, 81, 2169.
- [31] Boerio, F. J.; Tsai, Y. M.; Kim, D. K. *Rubber Chemistry and Technology* **1999**, 72, 199.

Chapter 1. Theory and Background

1 Vibrational spectroscopy

In any molecule, the atoms are in continual motion, vibrating or oscillating around their equilibrium position. When exposed to electromagnetic radiation the molecule may experience a force. The study of this interaction between the incident radiation and the molecular vibrations, as a function of the energy of the radiation, is known as vibrational spectroscopy. To interpret vibrational spectroscopic data, an understanding of how molecules vibrate, and the type of properties of the vibrations that can be measured, is required.

1.1 Molecular vibrations

The energy of a molecule is divided between translational, rotational, vibrational and electronic forms. All four of these are said to be quantized. The translational energy levels are extremely close together and translational energy can be regarded as continuous for all practical purposes. However, rotational, vibrational and electronic energy levels are well spaced and transitions between these levels can be observed using various forms of spectroscopy in different regions of the electromagnetic spectrum.

Molecules can be thought of as collections of point masses (atoms) connected by weightless springs (chemical bonds) which follow simple harmonic motion when they oscillate. Each spring obeys Hooke's law and has a force constant according to the following equation (the units are given in parenthesis):

$$F = k \cdot x \quad (\text{N}) \quad (1-1)$$

where,

k = force constant ($\text{N} \cdot \text{m}^{-1}$)

x = extension (m)

A diatomic molecule can thus be viewed as two point masses M_1 and M_2 connected by a spring of force constant k . The resonant vibrational frequency of such arrangement is given by:

$$\nu_{vib} = \frac{1}{2\pi} \sqrt{\frac{k}{\mu}} \quad (\text{s}^{-1}) \quad (1-2)$$

where

$$\mu = \frac{M_1 M_2}{M_1 + M_2} \quad (\text{kg}) \quad (1-3)$$

μ is known as the reduced mass. The potential energy function for a harmonic oscillator is a parabola, and when this is used to solve the Schrödinger equation, a series of allowed energy values are obtained according to the following equation:

$$E_{vib} = h \left(v + \frac{1}{2} \right) \nu_{vib} \quad (\text{J}) \quad (1-4)$$

where

h = Planck's constant (J.s)

v = vibrational quantum number

ν_{vib} = vibrational frequency (Hz)

In this model the vibrational energy levels form a regular ladder spaced ν_{vib} apart. The vibrational quantum number is a positive integer (including zero), and transitions are allowed between levels such as $\Delta v = \pm 1$. The vibrational ground state still has an energy of $\frac{1}{2}h\nu_{vib}$ and thus molecules undergo constant vibration, even at 0 K. The simple harmonic model however fails on two main counts. Firstly, the parabolic potential function does not allow bonds to break. Secondly, in reality transitions can be observed for which $\Delta v \geq \pm 1$ and these reveal that the energy levels are not equally spaced but instead converge, i.e. an anharmonic oscillator model is needed. A more realistic potential energy function was suggested by P.M. Morse [1]:

$$E = D_{eq} [1 - \exp(-a(r_{eq} - r))]^2 \quad (\text{J}) \quad (1-5)$$

where

D_{eq} = Dissociation Energy (J)

r_{eq} = Equilibrium bond length (m)

r = internuclear distance (m)

a = constant for a particular molecule (m^{-1})

When this is used to solve the Schrödinger equation the vibrational energy levels are given by:

$$E_{vib} = h \left[\left(v + \frac{1}{2} \right) \nu_{vib} - \left(v + \frac{1}{2} \right)^2 x_e \nu_{vib} \right] \quad (\text{J}) \quad (1-6)$$

Where

x_e = anharmonicity constant

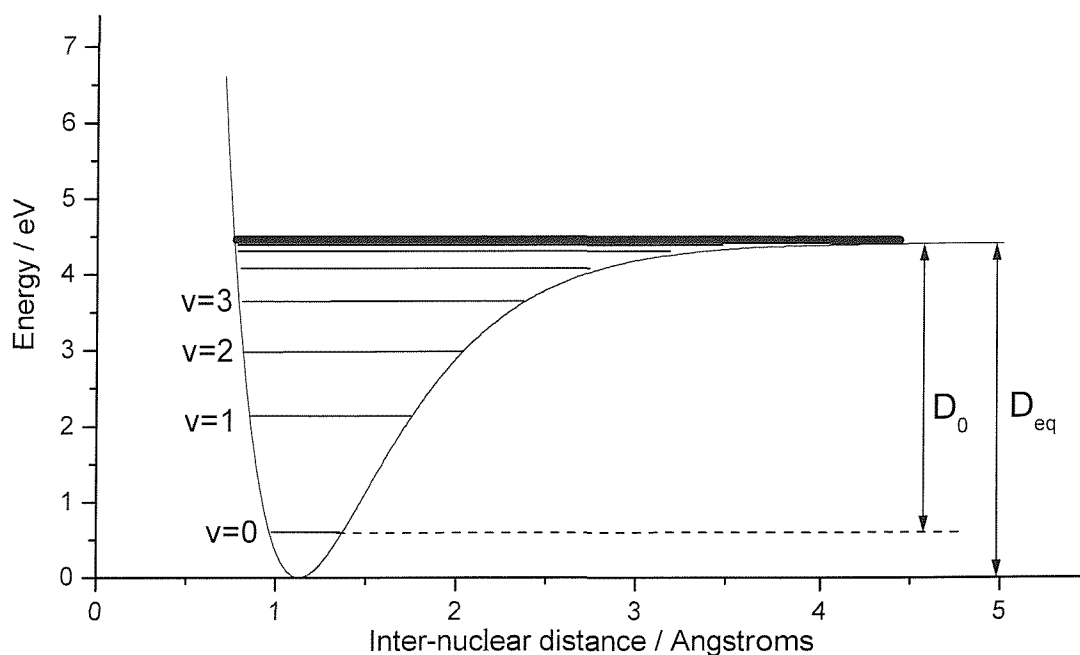


Figure 1-1 The Morse potential energy curve for $^1\text{H}^{35}\text{Cl}$ with the total vibrational energy levels superimposed.

The Morse curve is not thought to be an exact description of the inter-atomic potential function and others have been suggested, but it is much more realistic than the parabolic function of the harmonic oscillator model. Equations 1-4 and 1-6 determine the total vibrational energy which is the sum of potential and kinetic energy of the vibrating molecule. The intersection of the horizontal energy levels (total energy) with the potential curve represents the turning point of a classical oscillator where all the vibrational energy is potential and none is kinetic. For a given value of the vibrational quantum number there is a range of possible values of the internuclear distance. If

molecules behaved exactly as classical oscillators, this range would be defined by the locus of points which lie on the horizontal lines of total vibrational energy between the two points of intersection with the potential energy curve (figure 1-1)

It is at this point that another aspect of the quantum mechanical nature of molecular vibrations become apparent. In addition to the vibrational energy levels, solutions of the Schrödinger equation also yield to the vibrational wavefunctions, ψ_v , which provide further information about the oscillator. In particular, the square of the vibrational wave function, ψ_v^2 , determines the probability of a molecule having a particular value of internuclear distance at any instant and is known as the probability density distribution. Figure 1-2 shows the vibrational wavefunction for a harmonic oscillator for several values of the vibrational quantum number.

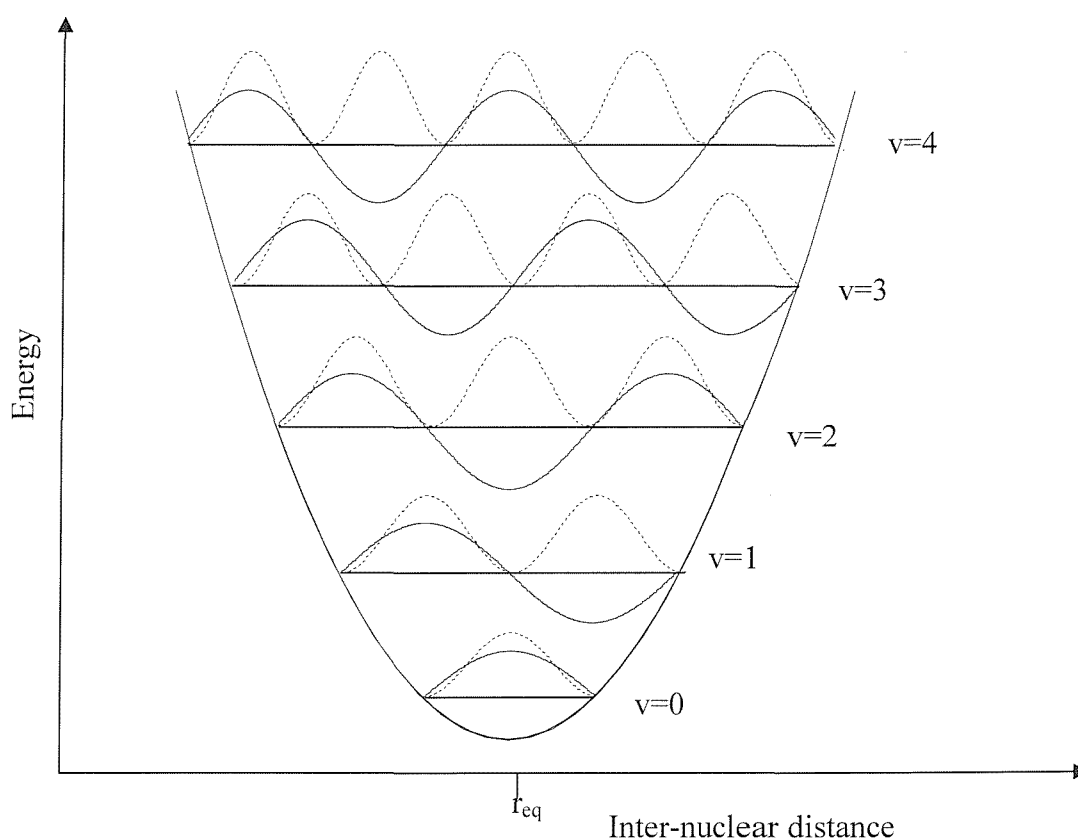


Figure 1-2 The vibrational wavefunctions ψ_v (solid lines) and probability density distributions ψ_v^2 (dashed lines) for a harmonic diatomic oscillator superimposed on a parabolic potential function. r_{eq} indicates the equilibrium position for the inter-nuclear distance.

By examining ψ_v^2 for the $v = 0$ level it is clear that the oscillator spends most of its time around the equilibrium bond length. This is completely opposite to a classical harmonic oscillator which is most likely to be found at its turning points. However, as the vibrational quantum number increases the quantum mechanical oscillator approaches the behaviour of a classical harmonic oscillator. Also evident is the fact that there is a finite probability of having a bond length outside the region defined by the potential energy curve. The probability density distributions for anharmonic oscillators are asymmetric with the position of greatest probability lying close to the maximum bond length as defined by the potential curve.

1.2 Classical Explanation of the Raman Effect

When a molecule is placed in an electric field of strength E , the molecular electron cloud becomes distorted and an instantaneous dipole μ is induced. Thus,

$$P = \alpha \cdot E \quad (\text{V} \cdot \text{m}^{-1}) \quad (1-7)$$

Where

E = Electric field ($\text{V} \cdot \text{m}^{-1}$)

α = polarisability

Polarisability can be visualised as the ‘ease’ with which a molecular electron cloud is distorted by an applied electric field. Polarisability is a tensor. The polarisability of a molecule tends to be anisotropic. It is easier to distort the electron cloud along the bond axis than perpendicular to it. The variation in the polarisability of a molecule, as a function of direction is usually represented in the form of a polarisability ellipsoid. This is a three dimensional surface whose distance from the electrical centre of the molecule is $1/\sqrt{\alpha_x}$, where α_x is the polarisability in that direction.

If a molecule is exposed to a beam of radiation, the oscillating electric field, which it experiences, is given by

$$E = E_0 \cos(2\pi\nu_0 t) \quad (1-8)$$

Where

E_0 = maximum electric field strength (V.m^{-1})

ν_0 = frequency of light (Hz)

t = time (s)

Thus, it can be seen that the induced dipole will also oscillate with the frequency ν . This is shown in Equation 1-9.

$$P = \alpha.E = \alpha.E_0 \cos(2\pi\nu_0 t) \quad (1-9)$$

Such an oscillating dipole will emit radiation at a frequency ν ; this is Rayleigh scattering. As we have seen the molecule will be undergoing constant vibration wherein the progress through the vibration can be described in terms of q , its distortion from the equilibrium position.

$$q = q_0 \cos(2\pi\nu_{vib} t) \quad (1-10)$$

Where

q_0 = maximum displacement

ν_{vib} = vibrational frequency (Hz)

The molecular polarisability may change as the vibration proceeds. This can be written in terms of a Taylor series:

$$\alpha = \alpha_0 + \left(\frac{\delta\alpha}{\delta q} \right)_0 q + \frac{1}{2!} \left(\frac{\delta^2\alpha}{\delta q^2} \right)_0 q^2 + \dots \quad (1-11)$$

Where

α_0 = polarisability at the equilibrium position

$\left(\frac{\delta\alpha}{\delta q} \right)_0$ and $\left(\frac{\delta^2\alpha}{\delta q^2} \right)_0$ are the first and second differentials of the polarisability with respect

to distortion around the equilibrium structure. However, for most purposes only the first two terms of equation 1-11 are significant. Hence the variation in polarisability as the molecule vibrates will be of the form,

$$\alpha = \alpha_0 + \left(\frac{\delta\alpha}{\delta q} \right)_0 q_0 \cos(2\pi\nu_{vib} t) \quad (1-12)$$

The variation in polarisability is very slight and the second term of the equation 1-12 is very much smaller than the first. Substituting for α from equation 1-12 into equation 1-9 we obtain:

$$P = \alpha_0 E_0 \cos(2\pi\nu_0 t) + \left(\frac{\delta\alpha}{\delta q} \right)_0 q_0 \cos(2\pi\nu_{vib} t) \cos(2\pi\nu_0 t) \quad (1-13)$$

However, since

$$\cos A \cos B = \frac{1}{2} (\cos(A+B) + \cos(A-B)) \quad (1-14)$$

We can rearrange equation 1-13 to give,

$$P = \alpha_0 E_0 \cos(2\pi\nu_0 t) + \frac{1}{2} \left(\frac{\delta\alpha}{\delta q} \right)_0 q_0 (\cos(2\pi[\nu_0 + \nu_{vib}] t) + \cos(2\pi[\nu_0 - \nu_{vib}] t)) \quad (1-15)$$

The induced electric dipole will have components oscillating at frequencies ν_0 , $\nu_0 + \nu_{vib}$ and $\nu_0 - \nu_{vib}$. An oscillating electric dipole will emit electromagnetic radiation of its own frequency, and thus light at these three frequencies will be scattered. The vast majority of light will be elastically scattered at a frequency of ν_0 and this is known as Rayleigh scattering. However, a small fraction of the incident radiation will be inelastically scattered at frequencies $\nu_0 - \nu_{vib}$ and $\nu_0 + \nu_{vib}$. This radiation is known respectively as Stokes and anti-Stokes Raman scatter and is very weak, of the order of 10^{-8} of the intensity of the excitation radiation. As can be seen from equation 1-15, for Raman light to be emitted $\left(\frac{\delta\alpha}{\delta q} \right)_0$ must be non zero, i.e. there must be an asymmetric change in molecular polarisability as the vibration occurs. This criteria is investigated for the vibrational modes of CO_2 in figures 1-3 and 1-4.

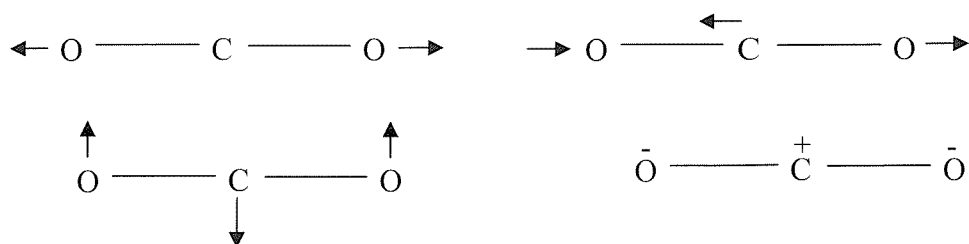


Figure 1-3 The fundamental vibrational modes of carbon dioxide

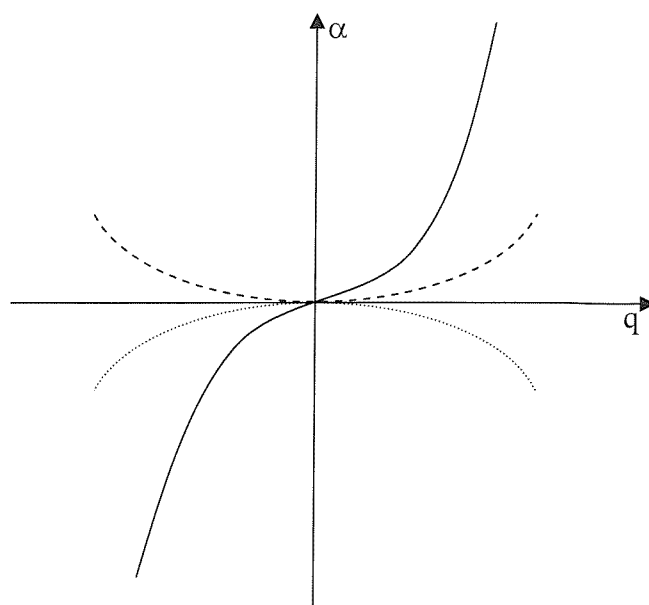


Figure 1-4 Graphs of polarisability α for the vibrational modes of carbon dioxide as a function of normal coordinates. The plain line corresponds to the symmetric vibration, the dashed line is the antisymmetric stretching vibration and the dotted line is the antisymmetric bending vibration.

Raman scattering can also be explained in relation to the quantised nature of vibrational energy levels. When a photon of light interacts with a molecule with a given set of vibrational quantum numbers, one of each mode (most probably $v=0$), it places it in a polarized ‘virtual state’ with a lifetime of the order of femtoseconds. From here it can relax back to its original state by emitting a photon with the same energy as the incident one, thus giving rise to the elastic Rayleigh scattering. Alternatively, the relaxation can be accompanied by a positive change in one or more vibrational quantum number, emitting a Stokes Raman photon. This is most likely to be a change of $\Delta v=+1$ from $v=0$ to $v=1$, although for an anharmonic oscillator other changes are possible but far less probable. If there is a significant population of the $v=1$ level or higher, relaxation can occur with a negative change of vibrational quantum number giving rise to an anti-Stokes Raman photon. An energy diagram summarising these possibilities is shown in figure 1-5. A schematic Stokes and anti-Stokes spectrum is also given in figure 1-6. The polarisability, α , is not a vector quantity but a tensor linking the three Cartesian components of the incident electric field to those of the induced dipole. Consequently, the spatial distribution of Raman scattering is complex.

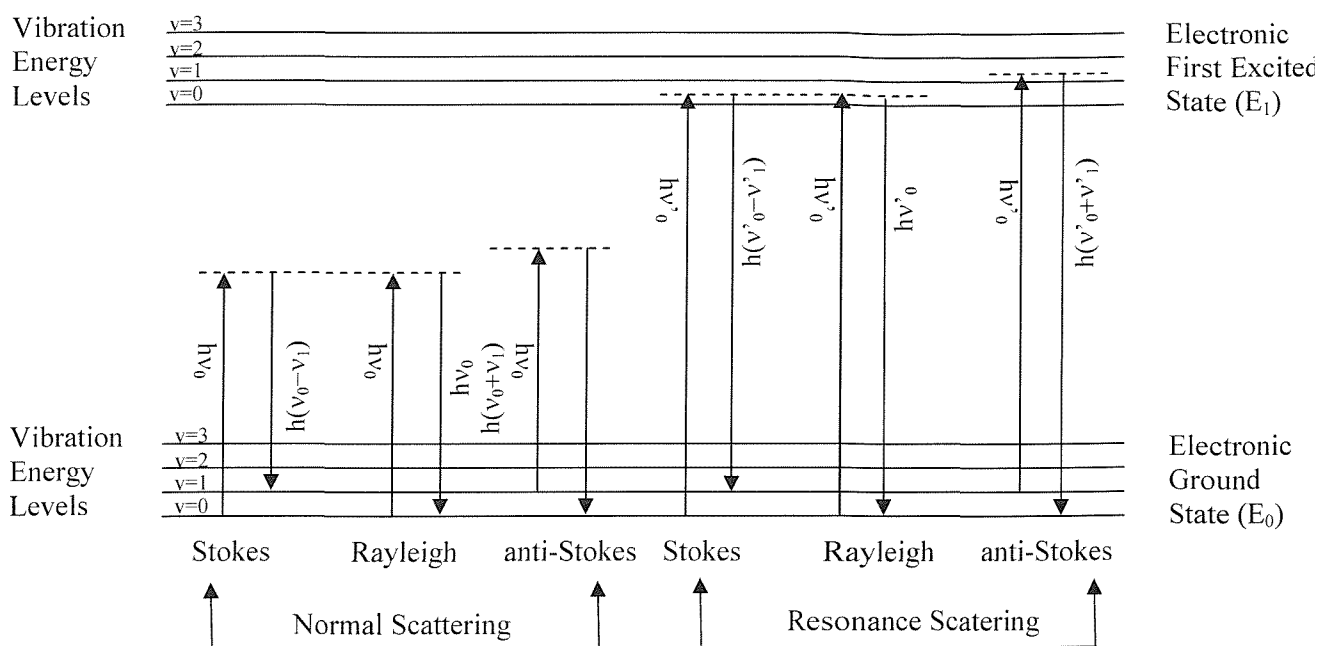


Figure 1-5 An energy level diagram for Rayleigh and Raman scattering

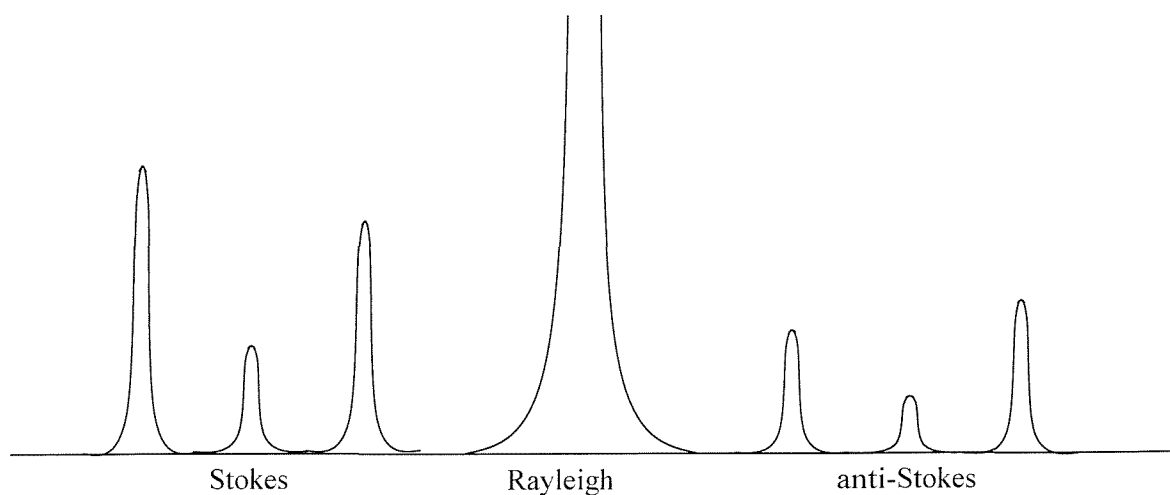


Figure 1-6 A schematic Stokes and anti-Stokes spectrum

1.3 Raman Intensities

The classical interpretation of the Raman effect informs us about the energies of the scattered light but does not account for the intensity of the Raman signal. To evaluate its intensity, the following relation has been used:

$$I = K(\nu_0 - \nu_{vib})^4 I_0 \left(\frac{d\alpha_{zz}}{dr} \right)^2 \quad (1-16)$$

Here, the Stokes process is considered, involving the tensor component α_{zz} and where K is a constant, I_0 is the incident light intensity and r the distance separating the m_1 and m_2 nuclei. Equation 1-16 demonstrates that the intensity of the Raman scattering is proportional to the fourth power of the frequency of the scattered light. This gives rise to the so-called ν^4 law and shows that there is a natural barrier to extending Raman studies towards the infrared region of the optical spectrum since the ν^4 factor becomes small with diminishing values of ν . Additionally, it is apparent that the intensity depends on the change in polarisability with the change in r , caused by the molecule vibrating along the bond linking m_1 and m_2 .

In the quantum mechanical treatment of the Raman intensity, the factor $d\alpha_{zz}/dr$, (or in more general terms $d\alpha_{\sigma\rho}/dq$, where $\alpha_{\sigma\rho}$ is one of the nine elements of the tensor and q is a normal coordinate) is replaced by the transition polarisability tensor $|\alpha_{\sigma\rho}|_{kn}$. Thus, the total intensity of the scattered light is resulting from a molecular transition between states k and n given by:

$$I_{n \leftarrow k} = K(\nu_0 \pm \nu_{kn})^4 I_0 \sum_{\sigma\rho} |\alpha_{\sigma\rho}|_{kn}^2 \quad (1-17)$$

where,

$$(\alpha_{\sigma\rho})_{kn} = \frac{1}{h} \sum_r \left\{ \frac{[\langle n | \mu_\rho | r \rangle \langle r | \mu_\sigma | k \rangle]}{[\nu_{rk} - \nu_0 + i\Gamma_r]} + \frac{[\langle n | \mu_\sigma | r \rangle \langle r | \mu_\rho | k \rangle]}{[\nu_{rk} + \nu_0 + i\Gamma_r]} \right\} \quad (1-18)$$

In these expressions the molecule is considered to be in the molecular state k . It is perturbed by an electromagnetic wave of frequency ν_0 and intensity I_0 , causing the transition to a state n and scattering light of frequency $\nu_0 \pm \nu_{rk}$. The sum over index r covers all the quantum mechanical eigenstates of the molecule, h is Planck's constant and Γ_r is a damping constant which takes into account the finite lifetime of each state of the molecule. The $\langle n | \mu_\rho | r \rangle$, etc. are the amplitudes of the electric dipole transition moments, where μ_ρ is the electric dipole moment operator operating along direction ρ . Immediately, it can be seen from Equation 1-18 that as ν_0 approaches the energy of an

allowed molecular transition, ν_{rk} , the term $\nu_{rk} - \nu_0 + i\Gamma_r$ becomes small; consequently one term in the sum becomes very large. This is the resonance condition.

In practical experiments, the Stokes scattering is more intense than the anti-Stokes. The classical approach cannot indicate this nor the intensities of the Raman lines. On the other hands, simple quantum mechanical theory can give a clearer interpretation of this phenomenon as shown in Figure 1-5.

According to the Boltzmann distribution, at room temperature, the population of molecules is much larger at $v=0$ than at $v=1$. Hence, the ratio of intensities of Stokes lines to the anti-Stokes lines is given by:

$$\frac{I_{Stokes}}{I_{anti-Stokes}} = \frac{(\nu_0 - \nu_{vib})^4 g_1}{(\nu_0 + \nu_{vib})^4 g_0} \exp\left(-\frac{\Delta E}{k_B T}\right) \quad (1-19)$$

Where,

- g_0 and g_1 = Degeneracy factors of levels $V=0$ and $V=1$ respectively
- h = Planck's constant (6.63×10^{-34} J.s)
- k_B = Boltzmann's constant (1.38×10^{-23} J.K⁻¹)
- T = Temperature (K)
- ΔE = Energy difference between levels $v=0$ and $v=1$

In general, Rayleigh and Raman scattering are relatively inefficient processes; only about 10^{-3} to 10^{-5} of the intensity of the incident radiation will appear as Rayleigh scattering, and about 10^{-7} to 10^{-12} as Raman scattering. However, the Raman scattering efficiency can be improved by factors as high as 10^4 or even 10^6 times when a resonance condition exists [2].

Resonance Raman scattering occurs when the frequency of the incident radiation falls within an electronic absorption band of the sample (see Figure 1-5). This process then lead to a great increase of the population density of the relevant excited state. In resonance Raman scattering, the term $(\alpha_{op})_{kn}$ in Equation 1-18 dominates all the other terms and results in a great enhancement of the Raman signals. The intensities still follow the ν_0^4 term but this is not dominant in this case. Three of the major problems in using the resonance Raman effect routinely are the restriction to molecules exhibiting a

strong resonance effect, the great amount of fluorescence (see next paragraph) associated with this effect and also the interpretation of resonance Raman spectra. The polarisability tensor becomes asymmetric and the analysis of the symmetry properties of resonance Raman lines is much more complicated. In fact, quite frequently, the resonance gain is shown only by one or two molecular vibrations; therefore molecular orientations deduced from relative band intensities can be completely misleading.

1.4 Fluorescence

In addition to higher vibrational levels, molecules also possess excited electronic states whose existence can present difficulties when recording Raman spectra. Aromatic molecules and conjugated hydrocarbons have π to π^* electronic transitions which can lie between the near infrared and the ultraviolet. Transition metal complexes also have strong electronic absorptions over the same range as a result of d to d transitions. The intense laser illumination sources used in Raman spectroscopy frequently promote sample molecules from the electronic ground state, E, to some electronically excited state E^* . The force constants and equilibrium bond lengths of this state will be different, and hence the shape of the Morse curve and the spacing of vibrational energy levels will also be altered. In transition between electronic states there can be any change in vibrational and rotational quantum numbers, and the electronically excited molecule may also be in an excited vibrational state as well. The excited state E^* is unstable and the molecule will rapidly return to the electronic ground state. Transitions to the vibrational ground state of E^* usually occur without the emission of radiation, but instead by exchange with other vibrational modes and with nearby molecules through collisions. These are known as radiationless transitions. If several electronic excited states lie close together, the molecule will usually fall to the lowest lying state by similar means. From here transitions occur to any vibrational level of the electronic ground state with the emission of a photon. This process is known as fluorescence and is summarised in Figure 1-7.

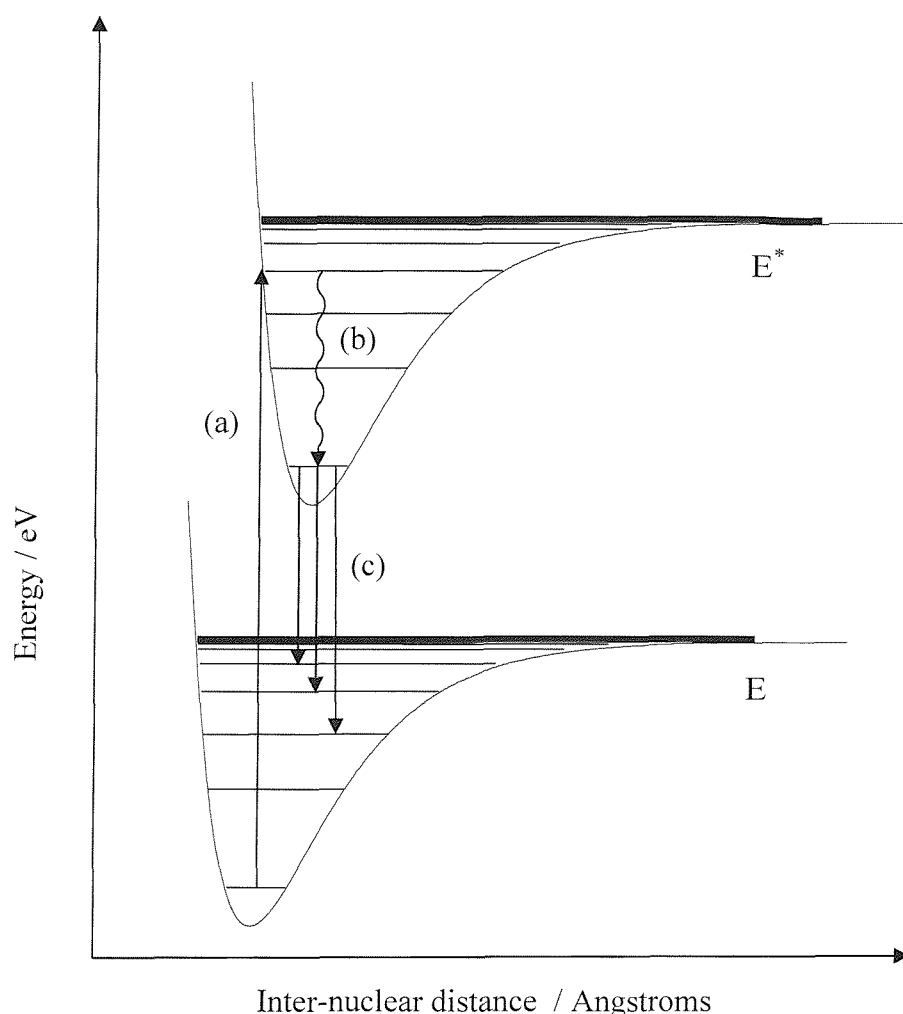


Figure 1-7 The origin of fluorescence as a result of electronic excitation and subsequent relaxation. (a) is the absorption process, (b) the radiationless decay and (c) the fluorescence.

As mentioned in section 1.2, Raman scattering is very weak indeed. Unfortunately, the intensity of fluorescence emission can be several orders of magnitude more intense, and this is one of the principal failings of conventional Raman spectroscopy. In condensed phases electronic absorptions are broad and this, coupled with the existence of many electronic excited states and vibrational modes, results in a large number of possible transitions all with a significant bandwidth. As a consequence, the fluorescent emission is broad and featureless, and small Raman bands superimposed on this background can be very difficult to observe.

1.5 Surface Enhanced Raman Scattering (SERS)

Surface Enhanced Raman scattering is a process in which the Raman Scattering intensity arising from molecules adsorbed on microscopically rough metal surfaces, is enhanced by factors of 10^4 to 10^6 compared with the intensity expected from non-adsorbed species at the same concentration. Such enormous enhancements totally overcome the traditional low sensitivity problem, thus enabling the in-situ characterization of the chemical identity, structure and orientation of surface species. In 1974, Fleischmann, Hendra and McQuillan [3] first demonstrated surface Raman results of Pyridine on a silver electrode that had been electrochemically processed. The SERS active surface is obtained by chemical or electrochemical roughening or by depositing colloids onto it.

The interpretation of the origin of the SERS effect is still a controversial matter despite the enormous amount of work already done in this field. There are many theoretical models which have been proposed to explain the origin of the enhancement. It is now becoming clear that several effects are in operation at the same time, but a consensus view on their relative significance has not yet been reached by the various investigators. The calculations involved in the explanations of these enhancement mechanisms can be very complicated. So, in this section, we will only try to expose a qualitative and concise review of the current theories. A fuller account of each model can be obtained from the original papers, from a review by Furtak and Reyes [4], from a paper by Otto [5], from a book by Chang and Furtak [6] and from a review Moskovits [7].

1.5.1 *Image Field Theories*

King, Van duyné and Schatz [8]; Efrima and Metiu [9]; and Eesley and Smith [10]; all proposed three main image field type theories.

Van Duyne *et al* proposed a macroscopic explanation in terms of an increase in molecular polarisability and hence increased Raman scattering. They approximate the molecule to a point dipole and suggest that the dipole, P , induced in the adsorbed

molecule by the high electric field at the surface, images itself in the metal and is given by:

$$P = \alpha_0 (E_0 + E_d) \quad (\text{V.m}^{-1}) \quad (1-20)$$

Where

α_0 = polarisability of the free molecule

E_0 = the incident field due to the excitation (V.m^{-1})

E_d = field at the molecule caused by its own image within the metal (V.m^{-1})

The effective polarisability (α_{eff}) will be considered larger than α_0 , because of the high polarisability of the electron cloud in the metal. It is thus defined as:

$$\alpha_{\text{eff}} = \frac{P}{E_0} = \frac{\alpha_0}{\left(1 - \frac{\alpha_0 E_d}{P}\right)} \quad (1-21)$$

and then using the electrostatics, the image field can be calculated as

$$E_d = P \frac{(\epsilon_m - \epsilon_{\text{sol}})}{(\epsilon_m + \epsilon_{\text{sol}})} \frac{1}{4R^3} \quad (1-22)$$

Where,

ϵ_m = dielectric function of the metal

ϵ_{sol} = dielectric function of the solution

R = effective molecule - surface separation

This theory predicts a strong dependence upon proximity of the adsorbate to the metal, but does not include details of the bonding. Perturbations of the molecule are ignored. Van Duyne's model does not apply to molecules in the diffusion layer, because there must be coulombic interaction between the surface and the molecule, which means that it must be either chemisorbed or physisorbed. The model also indicates a surface coverage dependence, because the field of one molecule will shield its neighbours from the full effect of the voltage drop across the double layer and also because the image

field will be greatest when the molecular dipole is perpendicular to the surface. Although this coverage dependence is in agreement with some experimental results, the potential drop across the double layer will reach a minimum at the point of zero charge (pzc) and adsorption of a neutral molecule such as pyridine will be at maximum. Experimentally it is found that the spectrum of pyridine on silver is most intense at the pzc and this result cannot be predicted from Van Duyne's theory. This is accurate for visible and near infrared excitation. This theory does not explain either why surface roughness is important in obtaining strong enhancement and why the enhancement is restricted to a few metals. The image field theory requires the assumption that the surface is perfectly flat, with no inhomogeneity in the field across the interface. On the other hand, it should be noted that the theory predicts that the scattering enhancement will increase (due to the nature of the dielectric function of metals) as the frequency of the incident radiation approaches the infrared region of the electromagnetic spectrum. The other main characteristic of a SERS spectrum, the intense background, which is also present in the near infrared SERS spectra, cannot be explained by the image field theory. So, it seems that while this theory brings forward an interesting mechanism for increasing the effective polarisability of a molecule, it does not explain all the experimental results.

Efrima and Metiu as well as Eesley and Smith have based their work on Van Duyne's model. Efrima and Metiu assesses the polarisability enhancement resulting from the incident light radiation field as well as the field produced by the scattered radiation. These are relatively small effects which increase the scattering cross-section by a factor of as much as 32 and hence are not dominant.

Eesley and Smith used a quantum mechanical approach so that the approximation of point dipoles was not needed. Their modification includes the deshielding effect of neighbouring molecules' image field. This lowers the effective polarisability.

To summarise, the image field models offer a qualitative assessment of the scattering enhancement, but only account for a few characteristics of SERS. In addition, they all favour perpendicular dipoles, and take no account of surface roughness. This is in line with the experimental results obtained by Van Duyne's group [11] showing that weak SERS spectra of pyridine and tetracyanoplatinate can be obtained from mechanically

polishing silver electrodes without anodisation. They concluded that the enhancement due to features greater than 250-500 Å is only a factor of 100, compared to typical enhancements of 10^6 for pyridine on silver.

1.5.2 *Modulated Reflectance Theories*

Modulated reflectance theories have been put forward by Otto [12] and by McCall and Platzmann [13]. They both derived their enhancement mechanism from the interaction between incident photons and electrons within the metal, rather than by molecular imaging, as proposed by the image field theories. In his work, Otto suggests that the molecule vibrations modulate the surface charge density of the metal and he uses electroreflectance theory to calculate the interaction between the incident photons and the modulated metal electrons. This results in a quadratic dependence of the scattering intensity upon the frequency of the radiation used to excite the molecule.

McCall and Platzmann followed a similar argument to Otto. However, they suggested that the modulation of the electron density between a chemisorbed molecule and the metal surface produces the Raman enhancement and therefore incident photons interact with a metal - molecule complex. Their model predicts no dependence of the mechanism upon the excitation frequency and further contends that surface roughness is not important to enhancement. They also pointed out that gold and copper should give rise to more efficient photon – electron coupling than silver at argon ion laser frequencies. This is in complete contradiction –with experimental observations.

Although Otto's theory predicts the same behaviour for gold, copper and silver and is limited to physisorbed molecules, it does on the other hand offer an explanation of the background continuum accompanying the SERS spectra. He explained this in terms of metal phonon collisions that he included in his mechanism for modulated reflectance coupling. These phonon collisions offer a way of coupling incident electromagnetic waves parallel to the surface to phonons of much lower frequency that would normally be allowed and would increase the scattering enhancement from 10 times (predicted solely on the basis of modulated reflectance) to 10^6 times.

To summarise, these theories offer a possible explanation of the enhancement, but do not take into account the role of surface roughness. There are also some contradictions with experimental evidence.

1.5.3 Adsorption Induced Resonance

Since electronic absorption spectra of molecules and metal complexes often show blue or red shifts on changing their environment, a shift of the electronic energy levels of an adsorbed molecule is expected with respect to molecule in vacuum or in a bulk solution. This was predicted by Philpott [14] before SERS was discovered. Other proposals have come from Wenning and Kolb [15], King and Schatz [16] and Efrima and Metiu [17]. Although Philpott and Efrima and Metiu used different methods, they both contended that upon adsorption, the electronic levels of the molecule would shift and broaden to produce a number of bands characteristic of the surface electronic states. Photoexcitation between these new bands is possible and therefore, a genuine resonance Raman effect will take place. This coupling between molecular electronic states and the metal surface may be due to either surface plasmons or surface phonons. Roughness is not necessary for such coupling, but may be beneficial to the electronic state – surface plasmon coupling.

Hexter and Albrecht [18] have tried to quantify the work of Philpott by deriving a mathematical model for the plasmon – molecular orbital interaction-. Since in their model they have used the approximation of a point dipole, their conclusion that such an interaction is feasible seems rather unrealistic. This is because, for perturbation of the molecular energy levels to take place, the molecules must actually be in contact with the surface. Nevertheless, a possible mechanism is as follows:

- Resonant Raman scattering causes an incident photon to be directly converted to an emitted photon
- A surface plasmon oscillation is excited by an incident photon, and it then decays and emits a photon by resonance Raman scattering or decays into a phonon.

As can be seen from the above, these mechanisms are particularly attractive if the molecule itself is resonant Raman active. Efrima and Metiu proposed that plasmon coupling would produce a very complex excitation energy profile. Complex excitation profiles have been reported for SERS and an increase in efficiency towards the infrared is observed. The main drawback to these mechanisms is that they do not include weakly adsorbed or physisorbed species, where little electronic perturbation can be expected.

Pettinger, Wenning and Kolb discuss a similar mechanism, but consider all the bonding at the metal surface to be due to solvent molecules, solvated adsorbates and the adsorbate itself. In this way, surface complexes of molecules are considered and hence the surface chemistry of the interface becomes more important. This is interesting because SERS spectra reported so far showed a very marked dependence on the surface composition and detailed analysis of low frequency Raman bands has indicated the presence of surface complexes on silver electrodes in cyanide and chloride solutions [19].

The work of King and Schatz is based on a calculation of scattering from an adsorbed molecule that is resonance enhanced in the free state.

To conclude, adsorption induced resonance theories are largely in agreement with experimental data and show particular relevance to silver surfaces, where the surface plasmon energy is notably lower than that of other metals.

1.5.4 Geometrically Defined Resonance

This group of theories covers the electron resonance models of Creighton, Blatchford and Albrecht [20] and Moskovits [21]. Both groups proposed the particle size is critically important in determining whether enhancement of the scattering occurs and that the mechanism is that of a resonance phenomenon in which the surface plasmons of small metal particles are excited and energy is exchanged with specifically adsorbed molecules. Excitation can be individual, within one metal particle or collective if many particles are closely packed. Creighton, Blatchford and Albrecht dealt with a metal sol, whilst Moskovits is concerned with modelling a rough metal surface. Plasmon excitation frequencies have been calculated for individual spheroids [22] and close packed spheroids [23] and a large particle size dependence is predicted. Both groups proposed that the scattering intensity will deviate from the usual $(\nu_0 - \nu_{\text{vib}})^4$ rule. They do

not quantify resonance conditions, but expect an optimal excitation frequency dependent upon the size of the scattering particles and packing density.

In conclusion, geometrically defined resonance theories are supported by the experimental evidence as far as surface roughness and critical particle size are concerned. The observation of SERS from silver and gold sols by Creighton's group is particularly interesting as the size of the particles is controlled by chemical reduction. However, the predicted resonance excitation frequency dependence is not in agreement with the experiment.

1.5.5 Microscopic (or electron – hole excitation) Theories

So far, all the theories described in this chapter have taken a macroscopic approach, i.e. they have attempted to explain increases in the polarisability of the scattering molecule as a result of adsorption and the effects of adsorption are quantified by the dielectric function of the metal substrate. As a result, all the theories have difficulties in accurately describing a molecule as a point dipole or in describing its scattering behaviour as linear in an highly non-linear environment. In order to avoid these problems, Gerstern, Birke and Lombardi [24], Burstein, Chen, Chen, Lundquist and Tosatti [25] and Fuchs [26] have proposed the electron – hole models for SERS.

Upon adsorption at a metal surface, the molecular orbital energy levels of the molecule are broadened and shifted. Further, there is a photo-chemically induced electron transfer between the metal and the adsorbate. Photoexcitation of the molecule has two results:

- (i) either there is a radiative decay of the electron (fluorescence, Rayleigh scattering or Raman scattering) or non-radiative decay (vibrational relaxation)
- (ii) or the electron is injected into the conduction band of the metal

By considering the vibrational energies of the ground and excited states, radiative decay of the excited state will lead to a broad luminescence background from the metal and sidebands of vibrational frequencies on either sides of the excitation frequency ν_0 . Furthermore, sidebands will be greatly enhanced in intensity compared to the normal

Raman spectrum of the molecule, if the excited state is stable. On the other hand, the electron – hole theories did not predict any frequency dependence for the enhancement or that the surface roughness is important. In addition, since electron transfer is involved, it is expected that chemisorbed species would be more greatly enhanced than physisorbed ones. This is in contradiction with the experimental observation made in the case of pyridine [26,27]. Otto *et al* [5,28] proposed similar mechanisms involving electron – hole pair interactions, but with more emphasis on atomic scale roughness and adatoms.

1.5.6 Summary

The above review demonstrates the difficulties in explaining the SERS phenomenon. Most of the models do not fit all the experimental evidence and some do not provide enhancement factors great enough to account for all of the effect. It is most likely that two or more of these effects are in operation at the same time.

Since 1981, it has been generally accepted that the SERS mechanisms consist of two major models. The first one is the electromagnetic model (EM) in which it is thought that the incoming photons used to produce Raman scattering also excite surface plasmons. These are oscillations in the density of the electron cloud in small metal particles or in irregularities at the surface. The plasmon resonance frequency is related to the size and shape of the particles and the electrical and optical properties of the metal from which they are made. Once the plasmon is excited, it cannot re-radiate easily and the result is a greatly enhanced electric field surrounding the metal particles. Thus, the Raman scattering from molecules close to this particle is greatly enhanced. The EM model is able to produce quantitative estimates of the enhancement factor, definitive dependence on the incident wavelength and qualitative predictions of the decrease of SERS intensity as the separation between the molecule and the surface is increased. This model has been comprehensively reviewed by Moskovits [7]. The EM enhancement is, in general, not sensitive to the chemical nature of the molecule and produces spectra that should be similar to the Raman or Resonance Raman spectra of the molecules in solution.

The other well accepted theory on SERS is called the Chemically Enhanced mechanism. It is widely recognised that the factors which influence the contribution of the

chemically enhanced mechanism to the SERS intensity include: the bonding interaction between the adsorbed molecule and surface metal atoms, and the orientation and coverage of the adsorbed molecules and metal surface structures. How these factors could influence the SERS intensity depends on the charge transfer mechanism involved. In Raman scattering, the charge transfer process is a process of virtual excitation in which the charge-transfer state can be partially resonated with the exciting radiation. This will lead to a large contribution to the Raman scattering cross section of the molecule-metal complex. It is assumed, and it is possibly the case in most experimental systems, that normally a weak interaction is involved in the substrate-molecule system. In this situation the molecular energy level partially overlaps with the metal conducting band. Generally, the detailed process of charge transfer can be described by the following four steps:

- (i) a photon is annihilated, then an electron is excited from a donor (the substrate or the adsorbed molecule) into a hot electronic state
- (ii) the hot electron is transferred to an acceptor, such as the adsorbed molecule or the metal substrate
- (iii) the hot electron comes back to the donor from the acceptor and at the same time a Raman photon is radiated
- (iv) the complex metal – adsorbed molecule is present at the special vibrationally excited level of the initial electronic state

However it is found that charge transfer SERS can have a rather complicated dependence on factors, such as the excitation frequency, the vibrational mode, the adsorbing site and the coverage. All these factors will affect the resonance of the charge transfer band with the excited radiation, and hence yield a significant influence on the SERS intensity.

More recently, Mrozek and Otto [29] have proposed a quantitative separation of the contribution of the classical electromagnetic enhancement and chemical effect, to SERS. By using silver island films, prepared on sapphire under clean vacuum condition, as substrates for various adsorbates and condensates, they have been able to demonstrate a strong “first layer effect”. According to the authors, the “first layer

effect” is assigned to the “chemical” effect at sites of atomic scale roughness as it is chemically specific, vibrationally selective [30], quenched by oxygen and has analogies with resonance Raman scattering by matrix isolated silver complexes [31] and does not exist at atomically smooth surfaces. The chemical effect is thus assigned to sites of atomic scale roughness. They also indicate that a contribution of a short range quasi first layer effect of about two orders of magnitude, at roughness features of very small local radii of curvature less than 10 Å cannot be excluded.

It is thus generally accepted that the electromagnetic mechanism contributes to about 10^4 of the overall enhancement, and that the chemical effect contributes to about 10^2 . It should be noted that, although the increased intensity of the spectra is still a mystery, information about adsorbates can be derived from the spectra.

Nowadays, it is considered that the Electromagnetic Mechanism does not only benefit to Raman spectroscopy but also to other methods including Surface Enhanced Second Harmonic Generation (SESHG) and Surface Enhanced Hyper-Raman Spectroscopy (SEHRS) [32]. The EM model is also much more understood and a number of calculations of the enhancement based on this idea have appeared in the literature, including work Yang *et al.* [33] and Kottmann *et al.* [34] on isolated particles.

In 1995, Yang and co-workers [33] used the discrete dipole approximation (DDA) method to determine extinction and Raman intensities for small particles of arbitrary shape. The Raman intensity calculations involved evaluation of surface electromagnetic fields relevant in SERS intensities. They showed that DDA extinction spectra and Raman enhancements converge with increasing dipole number for representative spheroidal and tetrahedral particles and for two coupled spheroids. They also described how the DDA can be used for metal particles near to a flat surface.

Kottmann *et al* [34], even more recently, studied the plasmon resonances of 10 - 100 nm two-dimensional metal particles with a non-regular shape. Contrary to particles with a simple shape (cylinder, ellipse) non-regular particles exhibit many distinct resonances over a large spectral range. At resonance frequencies, extremely large enhancements of the electromagnetic fields occur near the surface of the particle, with amplitudes several

hundredfold that of the incident field. Implications of these strong and localized fields for nano-optics and surface enhanced Raman scattering (SERS) were discussed.

Although these new calculations are very precise and accurate when compared to the experimental results, there are still black spots left. For example, it is still very difficult to explain why two rough surfaces prepared with slightly different roughening procedures may show orders of magnitude enhancement differences. It is also rather difficult to estimate the fraction of molecules that experience substantial SERS enhancement [32].

The above review is definitely not exhaustive and better work has definitely been done by others. The reviews by Wu and co-workers published in the I.J.V.S. [35] along with the one by Moskovits [21] and the work by Campion and Kambhampati [36] are probably the best place to start understanding SERS. The latest developments in Electromagnetic Mechanism have also been reviewed by Schatz and Van Duyne [32].

2 Experimental methods

2.1 Conventional Raman Instrumentation

From its discovery up until late 1950s the instrumentation for Raman spectroscopy remained very crude to today's standards. The Raman light was excited using powerful arc lamps (usually mercury vapour) and the spectrum recorded using a spectroscope and a photographic plate [2]. Production of the Cary 81, the first instrument based on a double monochromator brought a significant step forward. However, it was not until the introduction of the laser as an excitation source that a revolution in the subject occurred, a result of the initial work done with a ruby laser by Kogelnik and Porto [37]. The development of the continuous wave He-Ne laser and improvements in photomultiplier technology allowed the volume manufacture of automatic scanning recording Raman spectrometers such as the Spex 1401. These formed the basis for modern day conventional Raman instrumentation.

Up until recently, Raman experiments have been performed using multiple monochromators operated either as scanning spectrometers or spectrographs. The most

popular excitation sources have been argon and krypton ion gas lasers, or tunable dye lasers using solutions of dyes such as Rhodamine 6G. Double and triple monochromators have been used to improve spectral resolution and minimise the effect of stray light, thus allowing the observation of very low frequency Raman bands.

Until the mid 1970s photomultiplier tubes were the only practical electronic detectors available for the detection of the very low light levels characteristic of Raman spectroscopy. These devices consist of an electrically charged photocathode which will emit an electron when it is struck by a photon. The emitted electron is accelerated along a chain of electrodes, or dynodes, where further electrons are emitted at each stage. Thus, a single photon striking the front photocathode will generate a large pulse at the detector output. These pulses can be counted using a ratemeter or integrated using analogue circuitry. The great attraction of photomultiplier tubes was their noise equivalent power (NEP). This is the light power that must fall on the detector to generate a signal the same strength as the dark noise (i.e. $S/n=1$) for a bandwidth of 1 Hz. The lower the NEP, the more sensitive the detector and weaker Raman spectra can be recorded. The dark noise in a detector is related to square root of its area and also its bandwidth (Δf), and consequently to allow comparison of different sizes detectors a more useful concept is the specific detectivity D^* :

$$D^* = \frac{\sqrt{Area \cdot \Delta f}}{NEP} \quad (\text{cm} \cdot \text{Hz}^{1/2} \cdot \text{W}^{-1}) \quad (1-23)$$

The dark noise characteristics of a detector are also expressed in terms of the dark current or counts per seconds. The NEP of a small area photomultiplier tube (1 or 2 mm^2) suitable for visibly excited Raman spectroscopy is of the order of $10^{-15} \text{ W} \cdot \text{Hz}^{-1}$ with a peak quantum efficiency of about 25 %. These devices were, however, not sensitive enough for wavelength longer than 900 nm.

A monochromator is essentially a narrow pass filter which only allows a small range of frequencies (or bandpass) to fall on the detector. The transmission over this range of frequencies is about 25 %. In a scanning instrument a spectrum is obtained by tilting the different gratings to allow different regions of the spectral range to pass through the exit slit and reach the photomultiplier. To record spectra of progressively higher resolution the exit slit must be made narrower and narrower. All the light which does not pass

through the exit slit is simply absorbed by the black internal surfaces of the monochromator, a very wasteful process. To counter this problem, multichannel detectors were developed in the mid 1970s. [38]. These consist of a semiconductor chip containing many (more than 500) tiny detectors each of which can be read individually. A spectrograph is used so that a large width of the spectrum falls on the detector, the exact range depending on the dispersion of the instrument. The signal on the detector is accumulated and then each element is read individually by a computer. The integration time is dependent on the dynamic range of the detector and is thus typically small (about 30 ms). Consequently, many “scans” are coadded to obtain the final spectrum. Various types of multichannel detectors have been developed over the years; a typical example is the ISIT tube which consists of an image intensifier mounted before an array of silicon detectors. Overall a multichannel detector is an electronic equivalent of a photographic plate, but with a finite number of spectral elements.

Multichannel detectors based spectrometers offered enormous advantages over their photomultiplier counterparts. This comes from the fact that they can analyse many optical frequencies simultaneously and thus exhibit the “multiplex” advantage [39]. Consequently, the time taken to record a Raman spectrum was drastically reduced, and / or the sensitivity of the spectrometer was greatly improved [40]. Multichannel detectors have enabled the reduced recording of time resolved Raman spectra [41] and the detection of very weak signals [42]. This is despite the fact that the NEP of each channel may be worse than that of a photomultiplier tube.

More recently, the charge coupled device (CCD) has emerged as a superlative multichannel detector. These devices were originally developed for use in astronomy, but, in 1987, were shown to be excellent for recording Raman spectra [43]. CCDs are two dimensional detectors consisting of an array of detector pixels (e.g. 512x512 or 1024x1024) which develop a charge by the photoelectric effect when hit by a photon. These charges can be shuffled along the chip by changing the potential applied to the array of electrodes until they reach the edge of the chip (the serial register). From there, they can be shuffled horizontally and the charge developed by each pixel measured by an output amplifier. The attractions of the CCD are many [44]. They have an incredibly low dark current, typically 1 electron per pixel every 1000 seconds at 140 K. The output amplifier is a source of noise, but over all this is less than the shot noise associated with

the statistical arrival of the Raman photons. The quantum efficiency of a CCD is high, peaking at 45 % and their NEP can be 10^{-18} W.Hz⁻¹ or lower [45]. Because of this they are extremely sensitive, and have been used to record Raman spectra of unenhanced Langmuir-Blodgett films on water surfaces [46]. Their two dimensional nature allows time or spatially resolved experiments to be performed. Alternatively, multiple pixels in the same column can be added (“binned”) to enhance the signal to noise ratio. They are also very resilient and are not damaged by accidental exposure to the Rayleigh line, unlike photomultiplier tubes.

2.2 Fourier Transform Spectroscopy

The first paper on FT Raman spectroscopy was published by Gebbie, Chantry and Hilsum in 1964 [47]. However, due to the instrumental restrictions of the day the results were unimpressive and the paper did not stimulate any interest. The next papers on the subject were published by Chase in 1986 [48], who excited Raman spectra with a Nd:YAG laser at

1.067 μm and analyzed the light produced with a modified Nicolet 7199 FTIR spectrometer. Chase demonstrated that acceptable quality Raman spectra could be obtained by the FT method and a significant reduction in fluorescence was attained by using near infrared excitation.

FTIR and FT Raman spectrometers are built around a Michelson interferometer (Figure 1-8). Light entering the interferometer strikes a beamsplitter which divides it into two beams of ideally equal intensity. These two beams then hit separate mirrors, which reflect them back to the beamsplitter where interferences take place. One of the mirrors is fixed, the other can be scanned in a controlled fashion. By scanning the movable mirror the relative distance traversed by one of the beams is altered, and the light reflected back to the beamsplitter along one path may be in or out of phase with that reflected from the other. The beam reflected off the movable mirror is said to have experienced an optical delay. When the two beams are recombined at the beam splitter half of the light is reflected towards the detector and the remaining half passes out of the interferometer.

The function of the interferometer can be illustrated by considering what happens when it is illuminated with a source of monochromatic light of wavelength λ

and intensity I_λ . When the optical path difference is equal to an integer number of wavelength ($n\lambda$), constructive interference will occur and the detector will register a maximum signal. Conversely, when the path difference equals $n\lambda/2$ destructive interference will occur and no light will reach the detector. The interference pattern at any value of optical delay, x , is governed by the following cosine relationship:

$$I(x) \propto I_\lambda \cos\left(\frac{2\pi x}{\lambda}\right) \quad (1-24)$$

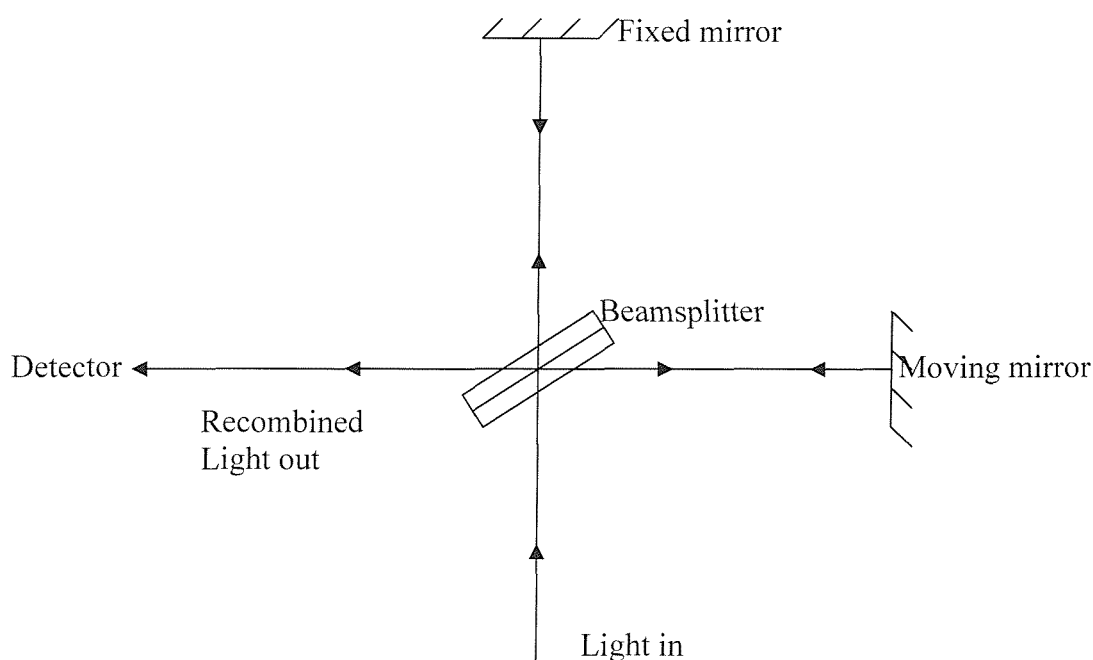


Figure 1-8 Interferometer of Michelson

Thus the interference pattern will be a cosine wave with a maximum at an optical path difference of zero. In an FTIR or FT Raman spectrometer the interferometer is illuminated with a polychromatic source. The total interference pattern produced is then the linear sum of the individual interference waveforms of each of the wavelengths of light present:

$$I(x) \propto \sum_{\lambda=0}^{\lambda=\infty} I_\lambda \cos\left(\frac{2\pi x}{\lambda}\right) \quad (1-25)$$

All of the radiation will be in phase when the optical delay is zero, and hence the detector signal will be a maximum. At other values of optical delay the different wavelengths will be gradually going in and out of phase and a complex trace called an

interferogram is produced. The maximum of the interferogram is called the centreburst.
A series of spectra and their interferograms are shown in Figure 1-9

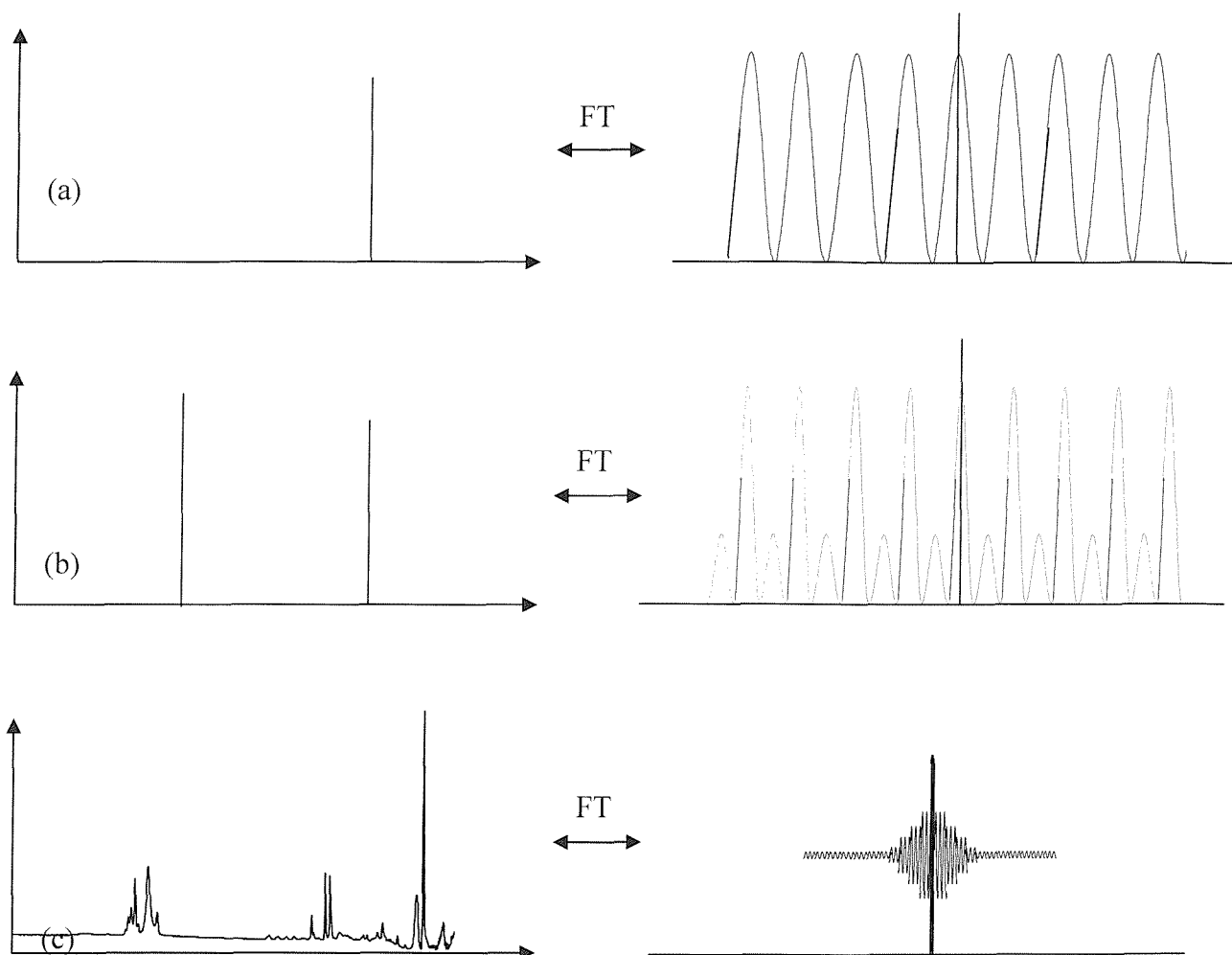


Figure 1-9 Interferogram produced by (a) a monochromatic source, (b) two monochromatic sources and (c) a polychromatic source. The axes are not to scale

The most overwhelming advantage of FT Raman spectrometers is their ease of use. A well designed FT Raman spectrometer is simple to operate. This simplicity stems from the design of the front end collection optics. The Perkin Elmer 2000 series spectrometer uses a 180° back scattering geometry. The preset position of the prism ensures that the laser is automatically coincident with the viewed patch and no laser alignment is necessary.

There are several techniques with which it is possible to study polymers, such as NMR, Infrared absorption measurements or ATR spectroscopy. However, Raman samples require little or no preparation because Raman is a scattering technique and the sample needs only to be held in the laser beam.

A further advantage of the Raman method is that glass is a perfect window material; polymer solutions, lattices and emulsions may be studied easily in glass vials.

Fourier Transform methods also allow excellent quality spectra to be accumulated rapidly. However, the most important factor influencing the analysis of polymeric materials is the use of a longer wavelength, near infrared rather than visible excitation source. This decreases the incidence of sample fluorescence and extends the range of materials which can be studied.

2.3 Confocal Raman Microscopy

The first experimental Raman microprobes, conceived and developed in the early seventies [49], effectively employed two conjugated spatial-filtering diaphragms, one for the laser and the other for the measurement of Raman scattered light. However, the inherent weakness of Raman signals and the lack of sensitivity of the existing photodetection systems available at the time did not allow the reduction of the pinhole diameters to achieve the diffraction limit.

The concept of confocal scanning microscopy was introduced by Minsky [50] to overcome some of the limitations of the conventional optical microscope. With this technique a significant improvement in both contrast and spatial resolution may be obtained when a point source is focused at the diffraction limit onto the specimen, while the enlarged image of the illuminated spot is analyzed through a pinhole diaphragm. Unlike a conventional microscope, where the entire field is illuminated, the confocal system measures at any one time the intensity of the light reflected or transmitted by a very small area of the sample.

Without entering into complicated calculations, the essential features of confocal microscopy may be summarized as follow:

- (i) An exact optical conjugation onto the sample of the pinhole apertures which are employed for both illumination and detection of the specimen results in combined spatial filtering effects. They produce a narrower 'point spread function' than can be obtained with a conventional microscope
- (ii) The stray light background due to the out-of-focus regions of the specimen is strongly attenuated by spatial filtering, so that the main contribution to the signal comes selectively from a thin layer of sample close to the exact focal plane. This capability of optical sectioning undoubtedly constitutes the most important advantage of the confocal configuration, which benefits from both contrast enhancement and improved depth of field.

The main features of a Raman confocal system can be described by the basic layout shown in Figure 1-10 and Figure 1-11.

The laser excitation beam is first filtered by an illumination pinhole D_1 . This initial spatial filtering removes the appearance of diffraction rings and speckle noise around the focused spot and results in a clean point source waist which is imaged onto the sample. The scattered Raman radiation is collected by a wide aperture objective and focused on an adjustable pinhole D_2 placed in the image plane of the microscope. A beam splitter insures a coaxial illumination and light collection by the same objective in the backscattering configuration. The pinholes D_1 and D_2 are called confocal diaphragms. Their exact optical conjugation with the point source in the object plane ensures that only the light originating from the sample region, which coincides exactly with the illumination spot, is transmitted to the spectral analyser and detector. The two effects of spatial filtering, both for illumination and collection, multiply and increase the spatial resolution by eliminating stray light coming from the out of focus regions of the sample. This configuration accounts for the ability of the system to provide optical sectioning [51].

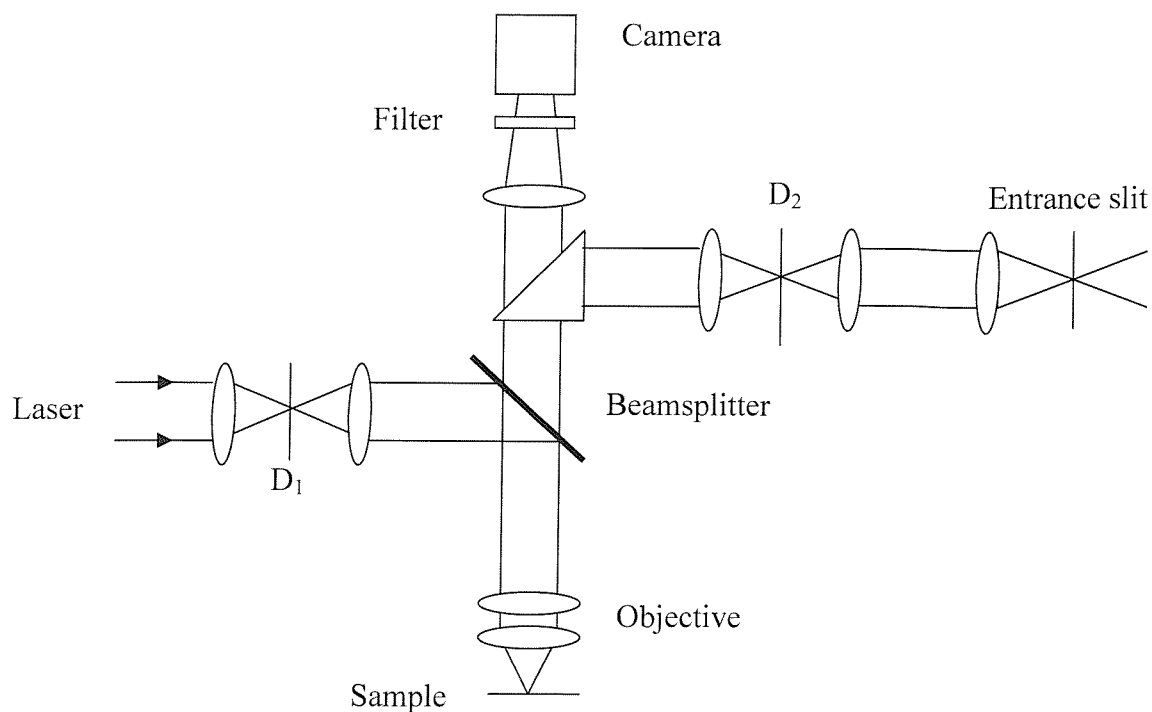


Figure 1-10 Raman microscope set up for use of confocal mode

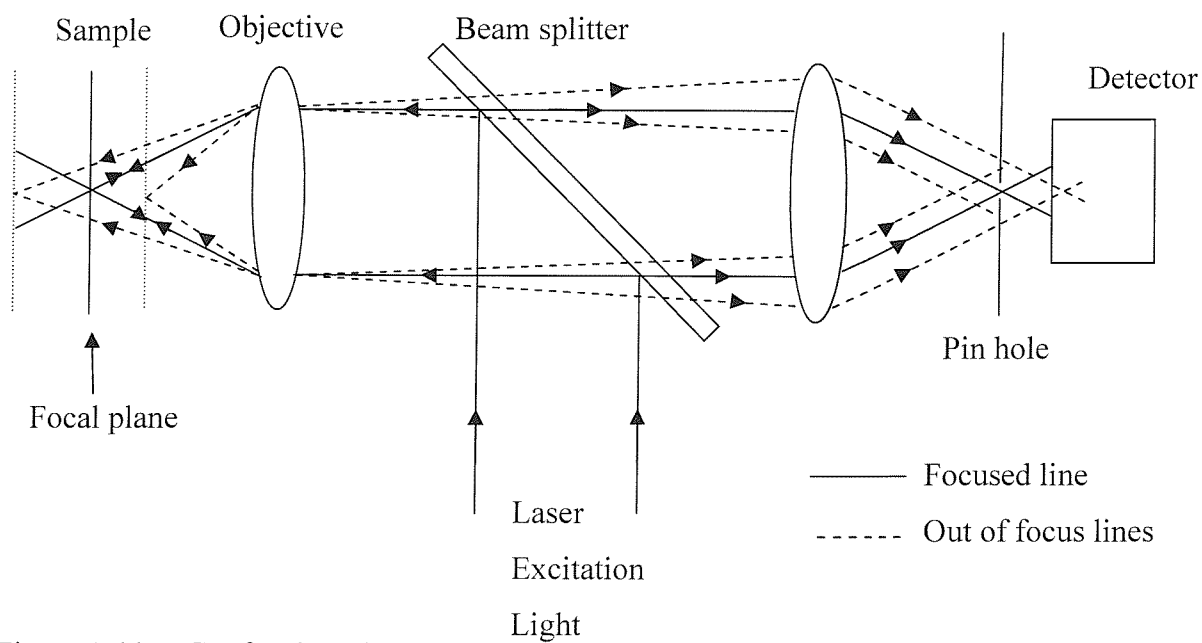


Figure 1-11 Confocal mode

2.4 The Renishaw 2000 System

The layout of the Renishaw imaging microscope is shown in the diagram below.

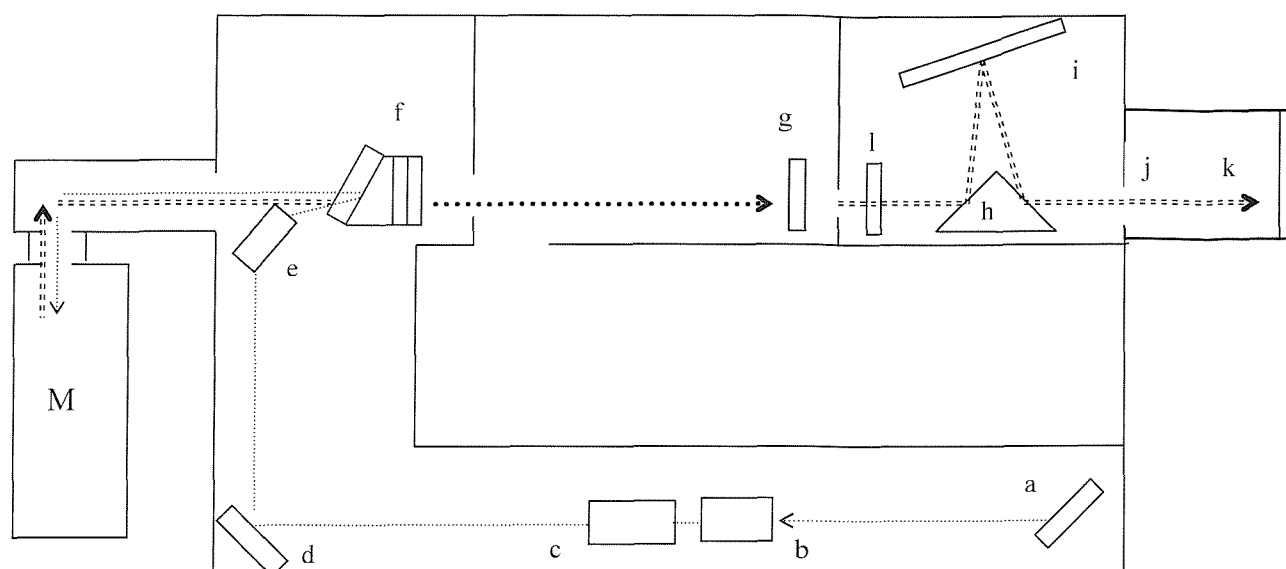


Figure 1-12 Raman optical main assemblies.

Key:

- a Laser alignment mirror.
- b x40 objective lens and 10 μm pinhole.
- c x4 objective.
- d Adjustable mirror.
- e Fixed mirror.
- f Holographic notch filter and polariser/ waveplate.
- g Spectrographic entrance slit assembly
- h Prism mirror
- i Diffraction grating assembly
- j CCD focusing lens
- k CCD detector
- l Collimating lens
- M microscope

..... Laser light

===== Raman light

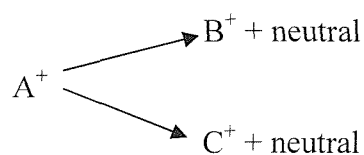
The laser light is directed along a, b, c, d, e and f, the laser and Raman scattering is directed back through the microscope to f, Raman light only is then directed along g, h, i, j, k, when in the grating mode. When a static scan is performed the grating (i) is held motionless during the experiment; hence the experiment is called a static scan. An extended scan is used when the spectra need to have a larger range of wavenumbers. In the case of the extended scan the grating moves during the experiment. [52]

3 Mass spectrometry

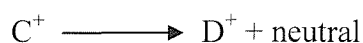
3.1 Introduction

In its simplest form, the mass spectrometer is designed to perform three basic functions: to vaporise compounds of widely varying volatility, to produce ions from the resulting gas-phase molecules (except where the volatilisation process directly produces ion rather than neutrals), and to separate ions according to their mass-to-charge ratios (m/ze), and subsequently detect and record them. Since multiply charged ions are produced only rarely relative to singly charged, z can normally be taken as one; and since e is a constant (the charge of one electron), m/z then gives the mass of the ion. Thus, the mass spectrometer is a device for the production and weighing of ions.

The devices that are used to produce gas-phase ions almost always put sufficient vibrational energy into the ion that it will, to some extent, fragment to produce new ions with loss of neutrals, e.g.



Given sufficient vibrational energy, B^+ and/or C^+ may decompose further, e.g.



When the array of ions (A^+ , B^+ , C^+ , etc) has been separated and recorded, the output is known as a mass spectrum. It is a record of the abundance of each ion (plotted vertically) against its m/z value (plotted horizontally). The most abundant ion is

arbitrarily assigned a value of 100 per cent. Obviously, if A^+ is produced by simple ionisation of the sample, then the mass of A^+ gives the molecular weight of the sample.

It can be seen that the mass spectrum is a result of a series of competing and consecutive unimolecular reactions. Therefore, it is determined by chemical reactivity and is not a true spectroscopic method. However, since it complements information provided to the chemist by UV, IR, Raman and NR, it is conveniently considered alongside them. [53]

3.2 Constituent parts

A mass spectrometer consists of the following basic units:

- (i) an ion source where ions are formed from the sample
- (ii) an analyser which separates the ions according to their m/z values
- (iii) a detector which gives the intensity of the ion current for each species;
the detector output can be displayed or stored, to yield the mass spectrum
- (iv) electronics of power supply and control of the three units above
- (v) various pumping systems [54]

3.3 Introduction of the sample

The system used for introduction of the sample into the ion source depends on the physical state of the sample: liquid, gas or solid. The following section will only deal with gas chromatography coupling, as this technique was used in this project.

The main use of a Gas Chromatography column before the mass spectrometer is to separate the different constituents of a mixture. The separation and detection of components is readily achievable by gas chromatography. Furthermore, limited characterisation of unknown components is often possible from retention times appropriate to the particular column used. Mass spectrometry, because of its high sensitivity and fast scan speeds, is the technique most suited to provide definite structural information from the small quantities eluted from a gas chromatograph. The association of the two techniques has, therefore, provided a powerful means of structure identification for the components of natural and synthetic organic mixtures.[53]

The main problem in coupling a chromatograph to a mass spectrometer is the increase in pressure caused in the ion source by the carrier gas from the chromatograph. Two different types of coupling can be used, depending on the type of chromatographic column: with capillary columns direct introduction of the capillary into the ion source is possible, whereas packed columns require ‘separators’, a more complex type of interface.

The molecular jet separator, one of the possible interfaces between a packed column and a mass spectrometer, is based on the fact that the velocity of a gas molecule is a function of its molecular weight (Graham’s law of diffusion). Thus low molecular weight species such as carrier gases are preferentially removed by pumping down during their passage towards the ion source. The gas flow reaching the source is thereby enriched in the higher molecular weight species present. In practice, the separators may have one or more stages, each of which can be pumped separately (Figure 1-13).

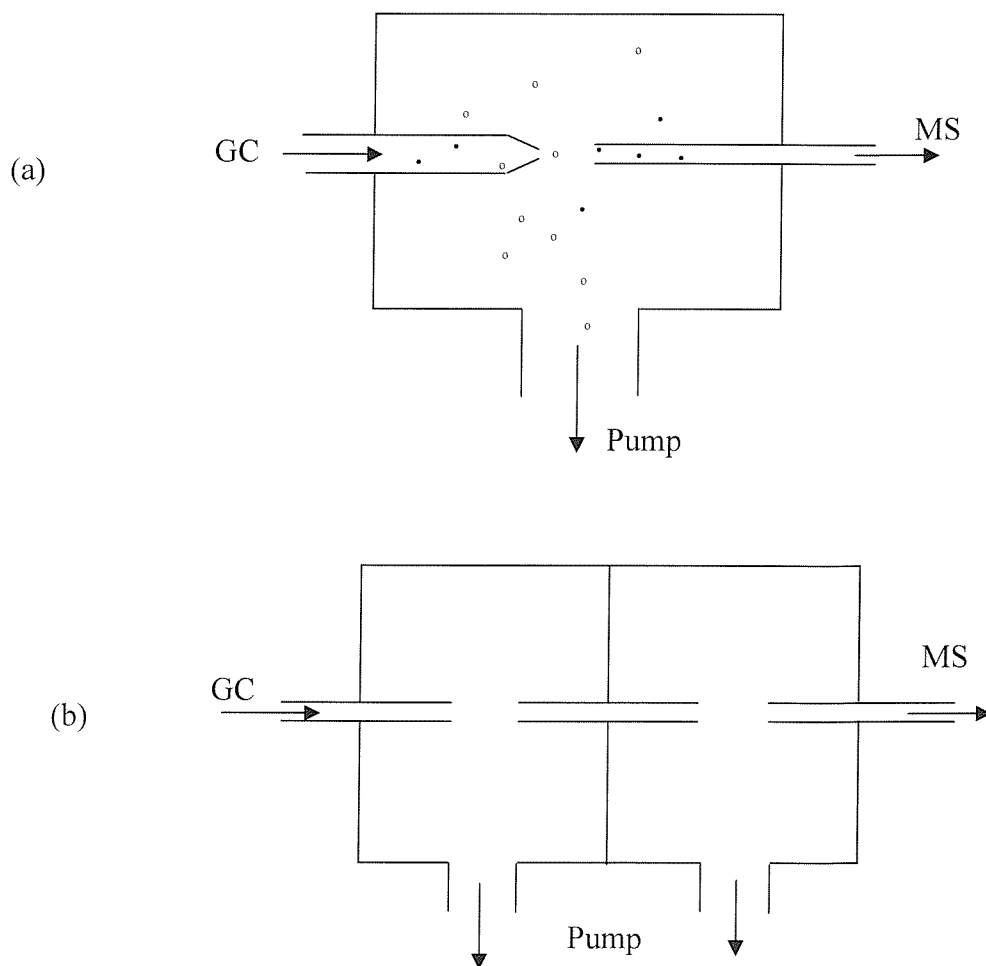


Figure 1-13 Molecular jet interface for coupling a gas chromatograph with a mass spectrometer. (a) Single-stage separator and (b) Two-stage separator.

A second type of interface, the membrane separator, is based on the relative permeability of a membrane for different molecules (Figure 1-14) [54]

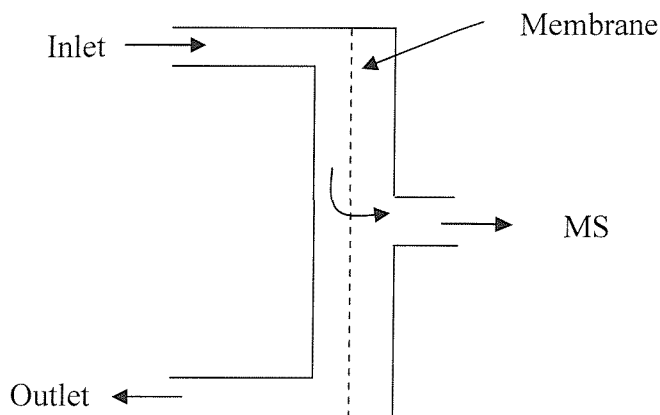


Figure 1-14 Membrane interface for coupling a gas chromatograph with a mass spectrometer.

3.4 Ionisation and fragmentation

Various methods of ionisation can be used, the choice depending on the physical state of the sample and the volatility and thermal stability of the material. Electron-impact ionisation gives satisfactory results for gas-phases molecules. For inorganic solids such as salts, thermal ionisation, field desorption and laser desorption are used. Atom or ion bombardment is suitable for ionisation of organic compounds of high molecular weight. Table 1-1 gives a résumé of some ionisation methods commonly used:

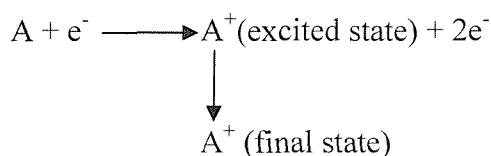
Table 1-1 Ionisation methods [54]

Gases	Liquids	Solids
electron impact	volatilisation, and	thermal ionisation
photon impact	ionisation as for gases	laser desorption/ionisation
		ion bombardment
		atom bombardment

3.5 Electron impact ionisation

In a mass spectrometer the ions are formed in the ionisation chamber of a unit called the ion source. Several techniques can be used to convert the initially neutral sample into an ionised species in the gas phase. Nevertheless, the one that has been used in this thesis is called electron impact ionisation.

This is the oldest and most widely used method. The substance is volatilised into the ionisation chamber, where its molecules are bombarded with electrons and transformed into positively charged ions:



The ion current, I , for the ions produced is given by Equation 1-26 [54]:

$$I = ai_e \rho \sigma l \quad (1-26)$$

where,

- i_e = electron current
- ρ = sample pressure in the ionisation chamber
- σ = ionisation cross section of the molecules
- l = effective path length of the electrons in the chamber
- a = efficiency of extraction of the ions

3.6 The mass analyser

Various devices may be used to analyse the ions coming out of the ionisation chamber, such as a magnetic analyser, a time of flight analyser, a cyclotron resonance analyser or as used in this project, a quadrupole analyser:

The quadrupole analyser: they are commercial rivals of magnetic instruments, especially in the range up to m/z 1000, where high resolution is not required and where simplicity of operation may be an advantage. They are used particularly where GC and/or HPLC instruments are directly coupled to the mass spectrometer, although magnetic sector instruments also perform this function very well. The arrangement of electrodes in a quadrupole mass filter is given in Figure 1-15.

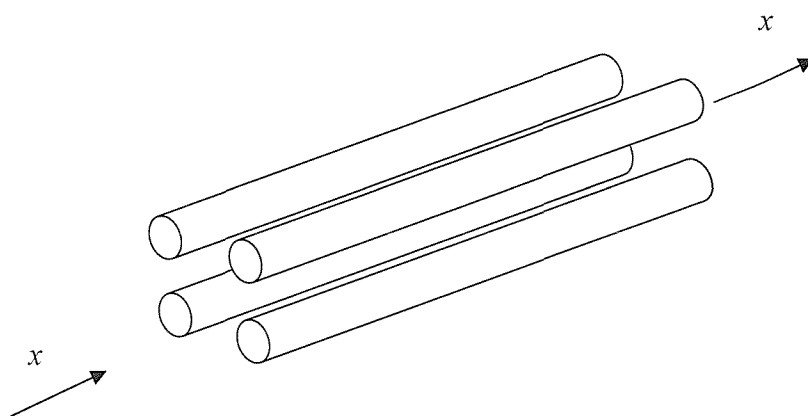


Figure 1-15 Electrodes of a quadrupole

A constant voltage U and a radiofrequency potential V are applied between opposite pairs of four parallel rods. The rods are between 0.1 and 0.3 m long in most commercial instruments. Ions are injected along the x direction and the mass spectrum scanned either by varying the amplitude of U and V , while keeping the ratio u/v constant, or by varying the frequency of the radiofrequency potential. Mixture analysis can be achieved by three quadrupole mass spectrometers connected in sequence. The first quadrupole is used to separate the molecular ions, the second as a collision chamber and the third to separate the products of collision-induced decomposition.[53]

3.7 Instrumentation

The Mass spectrometer that has been used in this thesis is a ThermoQuest TraceMS gas chromatography mass spectrometer and can be seen in

Figure 1-16.

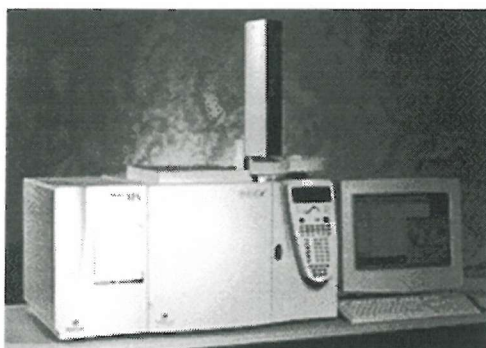


Figure 1-16 ThermoQuest TraceMS gas chromatography mass spectrometer

The ionisation technique is electron ionisation and the mass analyser is a quadrupole.

4 References

- [1] Morse, P. M. *Physics Reviews* **1929**, 34, 57.
- [2] Hendra, P. J.; C., J.; Wanes, G. M. In *Fourier Transform Raman Spectroscopy*; Ellis Horwood Ltd.: Chichester, 1991.
- [3] Fleischmann, M.; Hendra, P. J.; McQuillan, A. J. *Chemical Physics Letters* **1977**, 26, 163.
- [4] Furtak, T. E.; Reyes, J. *Surface Science* **1980**, 93, 351.
- [5] Otto, A.; Timper, J.; Billman, J.; Pockrand, I. *Physical Review Letters* **1980**, 45, 46.
- [6] Chang, R. K.; Furtak, T. E. *Surface Enhanced Raman Scattering*; Plenum: New York, 1982.
- [7] Moskovits, M. *Reviews of Modern Physics* **1985**, 57, 783.
- [8] King, F. W.; Van Duyne, R. P.; Schatz, G. C. *Journal of Chemical Physics* **1978**, 69, 4472.
- [9] Efrima, S.; Metiu, H. *Journal of Chemical Physics* **1979**, 70, 2297.
- [10] Eesley, G. L.; J.R., S. *Solid State Communications* **1979**, 31, 815.
- [11] Schultz, S. G.; Janik-Czachor, M.; Van Duyne, R. P. *Surface Science* **1981**, 104, 419.
- [12] Otto, A. Proceedings of the International Conference on Vibrations in Adsorbed Layers, 1978, Munich.
- [13] McCall, S. L.; Platzmann, P. M. *Bulletin of American Physical Society* **1979**, 24, 340.
- [14] Philpott, M. L. *Journal of Chemical Physics* **1975**, 62, 1812.
- [15] Pettinger, B.; Wenning, U.; Kolb, D. M. *Ber. Bunsenges. Phys. Chem.* **1978**, 82, 1326.
- [16] King, F. W.; Schatz, G. C. *Chemical Physics* **1979**, 38, 245.
- [17] Efrima, S.; Metiu, H. *Surface Science* **1980**, 92, 432.
- [18] Hexter, R. M.; Albrecht, M. G. *Spectrochimica Acta* **1979**, 35A, 233.
- [19] Fleischmann, M.; Hill, I. R.; Pemble, M. E. *J. Electroanal. Chem. Interfacial Electrochem.* **1982**, 136, 361.

- [20] Creighton, J. A.; Blatchford, C. G.; Albrecht, M. G. *Journal of Chemistry Society: Faraday Transactions* **1979**, 75, 790.
- [21] Moskovits, M. *Journal of Chemical Physics* **1978**, 69, 4159.
- [22] Kerker, M.; Wang, D. S.; Chew, H. *Applied optics* **1980**, 19, 3373.
- [23] Wang, D. S.; Kerker, M. *Phys. Rev. B: Condens. Matter* **1982**, 25, 2433.
- [24] Gersten, J. I.; Birke, R. I.; Lombardi, J. R. *Physical Review Letters* **1979**, 43, 147.
- [25] Berstein, E.; Chen, Y. L.; Chen, C. Y.; Lundquist, S.; Tosatti, E. *Solid State Communications* **1979**, 29, 567.
- [26] Fuchs, R. *Bulletin of American Physical Society* **1979**, 24, 339.
- [27] Van Duyne, R. P. *Chemical and Biological Applications of Lasers*; 4 ed.; Moore, C. B., Ed.; Academic Press: New York, 1980; pp 101.
- [28] Billman, J.; Kovacs, G.; Otto, A. *Surface Science* **1980**, 92, 153.
- [29] Mrozek, I.; Otto, A. *Journal of Electron Spectroscopy and Related Phenomena* **1990**, 54/55, 895.
- [30] Otto, A. *Indian Journal of Pure and Applied Physics* **1988**, 26, 141.
- [31] Brings, R.; Mrozek, I.; Otto, A. *Journal of Raman Spectroscopy* **1991**, 22, 119.
- [32] Schatz, G. C.; Van Duyne, R. P. *Electromagnetic Mechanism of Surface-enhanced Spectroscopy*. In *Handbook of Vibrational Spectroscopy*; J.M.Chalmers, P.R.Griffiths, Eds.; John Wiley and Sons Ltd.: Chichester, 2002.
- [33] Yang, W.-H.; Schatz, G. C.; Van Duyne, R. P. *Journal of Chemical Physics* **1995**, 103, 869.
- [34] Kottmann, J. P.; Martin, O. J. F.; Smith, D. R.; Schultz, S. *Optics Express* **2000**, 6, 213.
- [35] Wu, D. Y.; Ren, B.; Tian, Z. Q. *Internet Journal of Vibrational Spectroscopy* **2000**, 4, edition 2 section 9.
- [36] Campion, A.; Kambhampati, P. *Chemical Society Reviews* **1998**, 27, 241.
- [37] Kogelnik, H.; Porto, S. P. S. *Journal of Optical Society of America* **1963**, 53, 1446.
- [38] Bridoux, M.; Delhay, M. In *Advances in Infrared and Raman Spectroscopy*; Hester, H. E., Ed.; Heyden: London, 1976.
- [39] Felgett, P. *Journal de Physique et le Radium* **1958**, 19, 187.

- [40] Hamaguchi, H. *Applied Spectroscopy Reviews* **1988**, 24, 137.
- [41] Hamaguchi, H. In *Vibrational Spectra and Structure*; Durig, J. R., Ed.; Elsevier: Amsterdam, 1987.
- [42] Okazaki, T.; Sanda, F.; Endo, T. *Journal of Polymer Science Part A-Polymer Chemistry* **1997**, 35, 2487.
- [43] Dierker, S. B.; Murray, C. A.; Legrange, J. D.; Schlotter, N. E. *Chemical Physics Letters* **1987**, 137, 453.
- [44] Batchelder, D.N. *European Spectroscopy News* **1988**, 80, 28.
- [45] Pemberton, J. E.; Sobocinski, R. L.; Bryant, M. A.; Carter, D. A. *Spectroscopy International* **1990**, 2, 26.
- [46] Takenaka, T. 12th International Conference on Raman Spectroscopy, 1990, Columbia, South Carolina, J.R. Durig and J.F. Sullivan Eds; Wiley and Sons: New York.
- [47] Chantry, G. W.; Gebbie, H. A.; Hilsum, C. *Nature* **1964**, 203, 1052.
- [48] Chase, D. B.; Hirschfield, T. *Applied Spectroscopy* **1986**, 40, 133.
- [49] Delhaye, M.; Dhamelincourt, P. *Journal of Raman Spectroscopy* **1975**, 3, 33.
- [50] Minsky, M. *Scanning* **1988**, 10, 128.
- [51] Turrell, G.; Corset, J. In *Raman Microscopy: Development and Applications*; Academic Press Ltd.: London, 1996.
- [52] Rose, A. *Spectroscopic Studies of Substrates used for Solid-Phase Synthesis and Combinatorial Chemistry: Fundamentals and Applications*. MPhil, Southampton, 2000.
- [53] Williams, D. H.; Fleming, I. In *Spectroscopic Methods in Organic Chemistry*; 5th ed.; McGraw-Hill Publishing Company: Maidenhead, 1995.
- [54] Constantin, E.; Schnell, A. In *Mass Spectrometry*; Ellis Horwood Ltd.: Chichester, 1990.

Chapter 2. Designing an accelerated screening test

1. Introduction: the problem

Sealants, which are currently used in aircraft fuel tanks to seal every rivet, joint or screw (see Figure 2-1), contain chromium. There is increased legislative pressure to control environmental pollutants such as chromium. BAE SYSTEMS have a number of strategies for addressing environmental issues but are particularly interested in the removal of chromates from fuel tank sealants. As a supplier of wing sets for the Airbus programme, they currently deliver assemblies for more than 300 aircraft per year and this number is now increasing rapidly. Each wing set requires up to 200 kg of fuel tank sealant.

At one of the larger production facilities for major airframes, up to 50 000 l of sealants are used per annum and this requires an additional 250 l of solvent containing adhesion promoter. Up to 25% of the sealant becomes waste and is disposed at cost. Even after disposal, a 'duty of care' situation applies which means that this waste remains the responsibility of BAE SYSTEMS which in turn generates future potential responsibilities and costs.

Chromate containing sealants have been used historically because they have always been relatively weight efficient with a density of 1.5 g.cm^{-3} . In contrast, the alternative manganese cured systems have generally had a higher density of 1.65 g.cm^{-3} . For this reason, the introduction of manganese sealants has been relatively slow because of the weight penalty, which is often prohibitive for airframe applications.

In 1981, the first reports were made that polysulfide sealants were chalking after prolonged contact with fuel [1]. They thought that this chalking was a condition wherein the surface of the sealant in contact with fuel undergoes chemical and physical changes that results in sealant deterioration. They found that this chalking was caused by fuel extraction of the elastomeric component of the sealant, leaving a layer of inorganic fillers. They also claimed

that fuel, water and high temperatures were initiating factors that create sponging in the sealants.

Cured sealants have been widely studied through their history, using various methods. The most common ones are probably the peeling test [2-5]: used from a normal angle to the surface up to 180 °, and the shear technique [6-8]. They give a good idea of the adhesion properties of the sealant. Other techniques, such as swelling [9] and modulus testing [10,11], give information about the ageing process that takes place when the sealant is in contact with different solvents. More destructive methods have also been used in the past, such as Differential Scanning Calorimetry [12] or even techniques that require an ultra high vacuum environment: Electron Energy Loss Spectroscopy or even Auger Spectroscopy [13]. These last three methods give deeper information on the structure of the sealant as well as on the interface with the metal.

The aim of this project was to establish a fast ageing system to test new formulations of sealants. It was originally started with a soxhlet extractor but the efficiency of this technique and its replacement will be discussed. The proposal of several techniques, such as hardness testing, mass uptake, mass spectrometry, mini-peel testing and UV-Visible spectroscopy, to screen the behaviour of the sealants during the extraction process will also be presented in this report. Finally the conclusion will focus on the relevance of this process as well as the help that the various techniques can provide to understand the behaviour of the sealants during the ageing process.

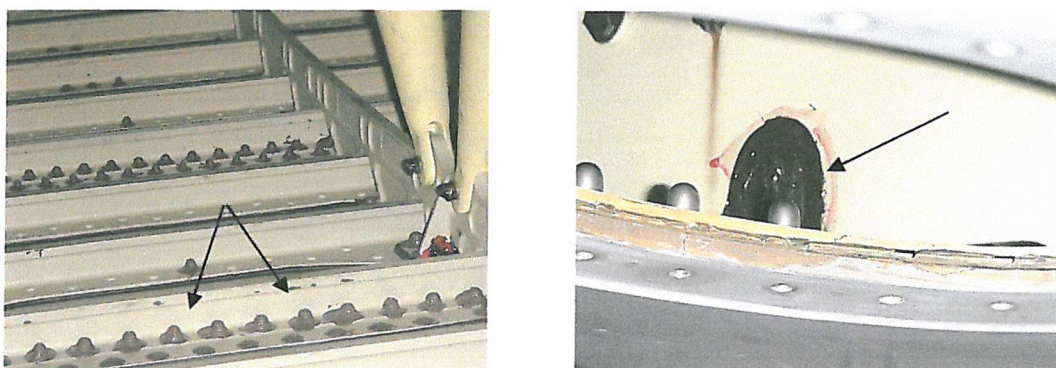


Figure 2-1 Pictures of the inside of an aircraft fuel tank. The arrows indicate sealant

2. Experimental

2.1. Sealant preparation:

Sealants were prepared following the protocol and using materials supplied by British Aerospace [14]. They were prepared in a mould as shown in Figure 2-2.

Samples were prepared with and without the backing plate, representing the wing components . The sealant samples with the plate are composed of four parts: a painted aluminium plate (the paint used was a chromate leaching paint currently used in aircraft manufacture), a first layer of polymer, a stainless steel gauze and a second layer of polymer. The samples without plate are only composed of polymer.

Three polymers were studied: one chromium cured (Cr1), and two manganese cured (Mn1 and Mn2).

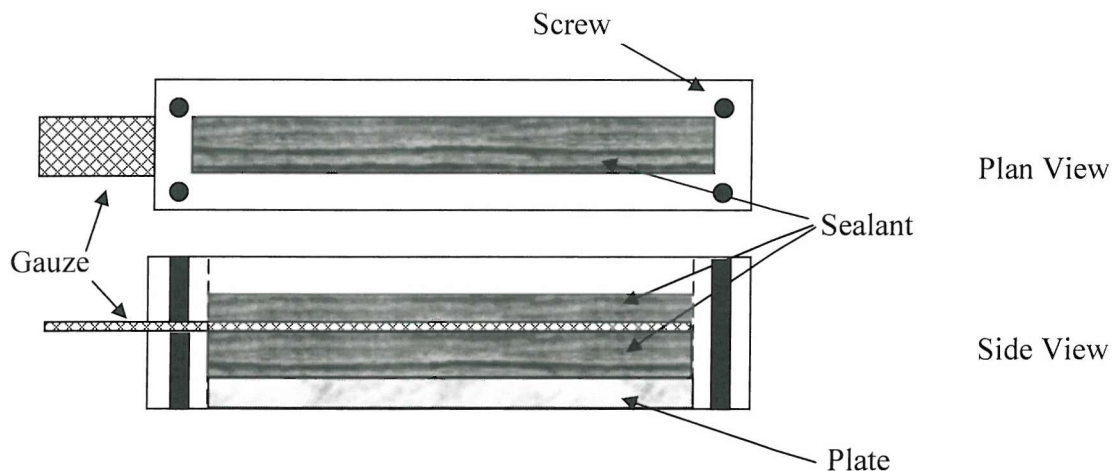


Figure 2-2 Plan and side views of sealant mould. Prepared sample dimensions: 155x35x8 mm

Three cures have been used:

- Long cure: 28 days at $24\text{ }^{\circ}\text{C} \pm 1\text{ }^{\circ}\text{C}$ and $50\% \pm 5\%$ of relative humidity
- Normal Cure: 14 days at $24\text{ }^{\circ}\text{C} \pm 1\text{ }^{\circ}\text{C}$ and $50\% \pm 5\%$ of relative humidity

- Short cure: 24 hours at $24\text{ }^{\circ}\text{C} \pm 1\text{ }^{\circ}\text{C}$ and $50\% \pm 5\%$ of relative humidity followed by 48 hours at $50\text{ }^{\circ}\text{C} \pm 1\text{ }^{\circ}\text{C}$ and $50\% \pm 5\%$ of relative humidity

2.2. Soxhlet Extraction

The project started using Soxhlet extraction to accelerate the ageing process. The principle of the Soxhlet extraction is shown in Figure 2-3. The fuel or the mixture composed of fuel and water is heated until evaporation, the vapor is condensed in the cooler and fills the extractor. When the level reaches the top of the tube outside, all the fuel goes down into the flask and a new cycle is begun.

To lower the boiling points of the fuel mixture, the system was run under reduced pressure. Thus the temperature at which each mixture was boiling was $80\text{ }^{\circ}\text{C}$ for the fuel alone and $50\text{--}55\text{ }^{\circ}\text{C}$ for the mixture of fuel and water.

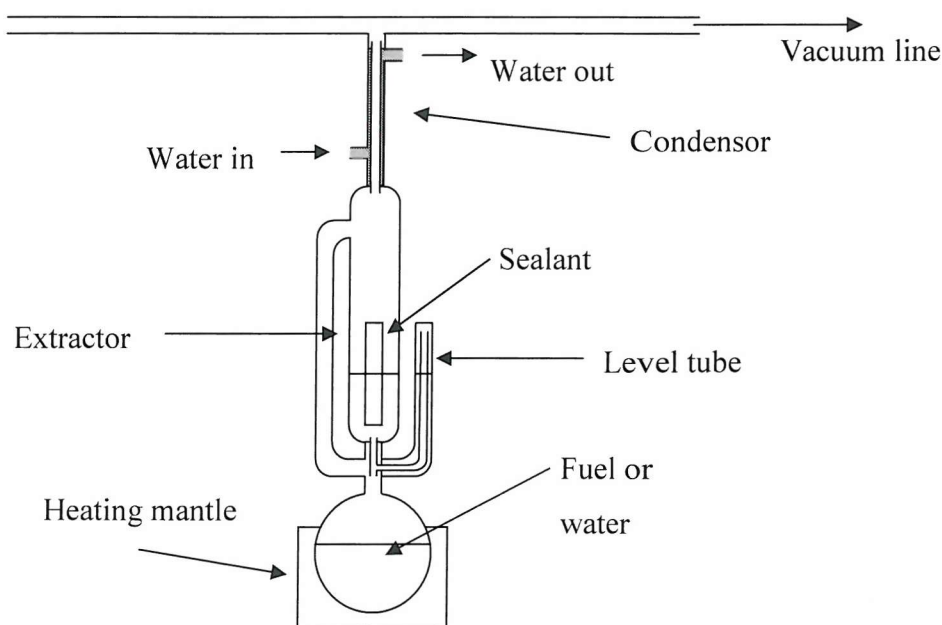


Figure 2-3 The Soxhlet extractor.

Because of the lower pressure, and because of the difficulty of balancing this pressure, it has been impossible to carry out this experiment correctly. The major problem was a leak situated in the system; several months were spent looking for this leak and retesting the system; however, it was not possible to locate it. This leak forced the continual use of the vacuum pump, which revealed itself to be too efficient resulting in either bumping or a foaming process in the extractors containing a fuel and water mixture. Thus, a solution to address the leak problem was to set up an 'air-bleed'. This involved reducing the vacuum by 'bleeding' a small amount of air into the system through a capillary tube. The pump operated continuously at this stage to establish a low pressure. We also decided to use a synthetic fuel (Toluene 30% v/v: 2,2,4 trimethyl pentane 70% v/v) to reduce the boiling temperature, as we were working at a reduce pressure of ~200 mbar. The pump, however, worked too powerfully and caused the vaporised fuel mixture to be pumped out of the system. Two months were spent considering different solutions to this problem, such as using a double condenser or filling the condenser with very cold water (2°C). Both of which failed to solve the problem and after consulting a chemical engineer we finally found that the efficient condensation of the pentane and related solvents is *very* difficult and would require an enormous condensation system. The soxhlet extraction was thus abandoned.

2.3. Ultrasonic Bath

An ultrasonic heating bath has been used instead of the former procedure for vaporising the fuel and re-condensing it: the sealants and the fuel mixture were placed in bottles, and placed in the bath. The ultrasonic action was used to agitate the fuel, which is held between 50-55°C. There are several advantages to this method. Firstly, boiling is no longer required; this will then reduce considerably the risks of having boiling solvents. Secondly, the new apparatus is cheaper to run: the bottles are placed in the ultrasonic bath and it is possible to run up to 9 extractions at the same time in a 50x30x40 cm sized bath compared to a maximum of 5 Soxhlet extractors in a fume cupboard. It also recreates more accurately the conditions of an aeroplane as you can switch on the ultrasonic action to provide a good agitation of the solvent mixture around the sealant. Finally, the sealant sample itself could

be taken out to measure its mass and hardness during the extraction whereas this was not possible in the Soxhlet extractor as it was sealed and no tests could be run on the sealant during the extraction.

2.4. Experimental Conditions

The following table summarises the various samples that have been studied. However, only the significant results will be displayed in this chapter.

Sealant samples have been cut into small pieces (~25 mm long) to fit into the bottles. About 80 ml of solvent was then added into the bottles which were placed into the ultrasonic heating bath. The bath temperature was raised to a temperature of 50 °C. Three times a day the ultrasonic action was switched on. As this action was increasing the temperature of the bath, we decided to limit it to 3 times for 20 minutes each day. After 20 minutes of exposure to ultrasound the bath temperature had increased by about 10 °C but returned to 50 °C within another 20 minutes following the exposure.

Every 1 day, 2 days, 6 days, 10 days and 14 days, the sealant samples were taken out of the solutions weighed and tested for hardness. A 10mL aliquot of solvent was also taken and analysed using mass spectrometry and UV/Visible spectroscopy. The aliquot of solvent taken was replaced by a fresh one. After 14 days of extraction, the sealant samples were kept for 14 days at $24\text{ }^{\circ}\text{C} \pm 1\text{ }^{\circ}\text{C}$ and $50\% \pm 5\%$ of relative humidity to allow them to dry. Then, they were once again weighed and hardness tested. Some samples were also studied using a “mini-peel” technique using a stage specially fitted in a Scanning Electron Microscope. This study was conducted at BAe Systems in Filton.

Table 2-1 Studied samples

Sealant Code	Cure	Plate (Y or N)	Fuel
Cr1	Short	✓	SF, W, EG
		✗	SF, W, EG
	Normal	✓	SF, W, EG
		✗	SF, W, EG
	Long	✓	SF, W, EG
		✗	SF, W, EG
Mn2	Short	✓	SF, W, EG
		✗	SF, W, EG
	Normal	✓	SF, W, EG
		✗	SF, W, EG
Mn2	Short	✓	SF, W, EG
		✗	SF, W, EG
	Normal	✓	SF, W, EG
		✗	SF, W, EG
	Long	✓	SF, W, EG
		✗	SF, W, EG

Coding: ✓ = With Plate
✗ = Without Plate

Short cure = 24 hours at 24 °C ± 1 °C and 50 % ± 5 % of Relative Humidity followed by 48 hours at 50 °C ± 1 °C and 50 % ± 5 % of Relative Humidity

Normal Cure = 14 days at 24 °C ± 1 °C and 50 % ± 5 % of Relative Humidity

Long cure = 28 days at 24 °C ± 1 °C and 50 % ± 5 % of Relative Humidity

SF = Synthetic Fuel (70 % v/v 2,2,4 Trimethyl Pentane 30 % v/v Toluene)

W = Water

EG = Antifreeze mixture (50 % v/v Water 50 % v/v Ethylene Glycol)

2.5. Instrumentation

2.5.1. Hardness Testing

All the hardness values have been collected with a BD-2 Duroprobe Durometer equipped with a Shore A probe. Shore hardness measures the indentation into a sample material of a known indenter profile against a known spring force. The indenter extends 0.100 inches (2.5 mm), equal to 100 Shore hardness degrees. The display reads between 00.0 and 100.0, however readings up to 10 ° and above 90 ° should not be recorded because of the non-linearity of the scale outside these values [15]. For each hardness value, a range of 5 points have been collected, well spaced from each others and at least 0.5 mm away from the edge of the sample. The time interval has been set at 3 seconds as recommended by the American Society for Testing Materials (ASTM) [16].

2.5.2. Mass Spectrometry

The Mass spectrometer that has been used to obtain the results presented in this report was a ThermoQuest TraceMS gas chromatography mass spectrometer. The ionisation technique is electron ionisation and the mass analyser is a quadrupole. The details have been discussed in Chapter 1.

2.5.3. Mini-peel testing

The microscope used at BAe systems was a Cambridge 360 SEM fitted with a specially designed Oxford Instruments 100 kg Tensile Stage. It has a ± 100 kg load cell and could operate over a range of -150 to 300 °C.

- *Sample preparation*

Samples have been cut 3.5mm wide and approximately 25mm long to fit into the stage. A Struers Accutom 5 fitted with a 354A cutting blade turning at 3000 r/min has been used. One cut is made in each sample using a sharp, clean scalpel to initiate a crack at the interface sealant / plate (Figure 2-4).

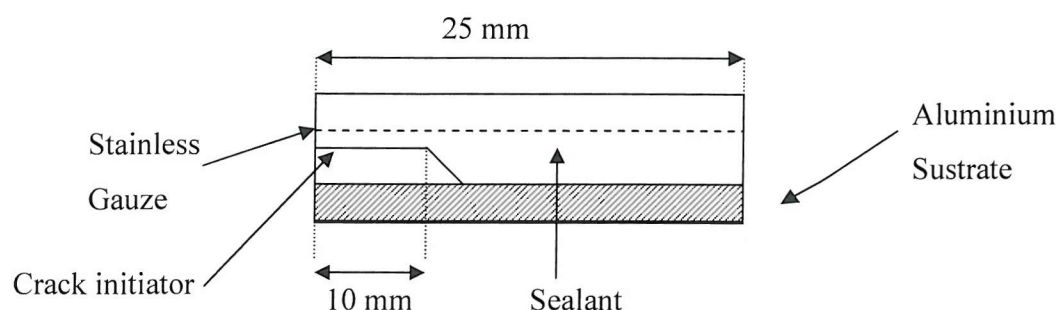


Figure 2-4 Sample preparation for use in the tensile stage

The crack initiator is cut parallel for approximately 10 mm (± 2.5 mm) and then down towards the interface (until it reaches it) at an angle of $\sim 45^\circ$ ($\pm 5^\circ$). It was important to keep this cut as smooth as possible because any slight nicks may act as crack initiators at points other than the interface. The different samples were then gold coated with a sputter coater to increase their conduction, ensuring that good and even coating of gold was obtained.

- *Sample mounting*

The tensile grips of the SEM tensile testing stage were moved to a suitable distance apart for mounting the sample. After this the chart recorder was set to zero. The sample was then mounted as shown in Figure 2-5, ensuring that sealant / substrate interface was visible from above. The grips were then done up hand tight using an Allen screwdriver. The SEM door was shut. The chart recorder was set running, then the tensile stage was started at the test speed of 0.40 mm.min^{-1} .

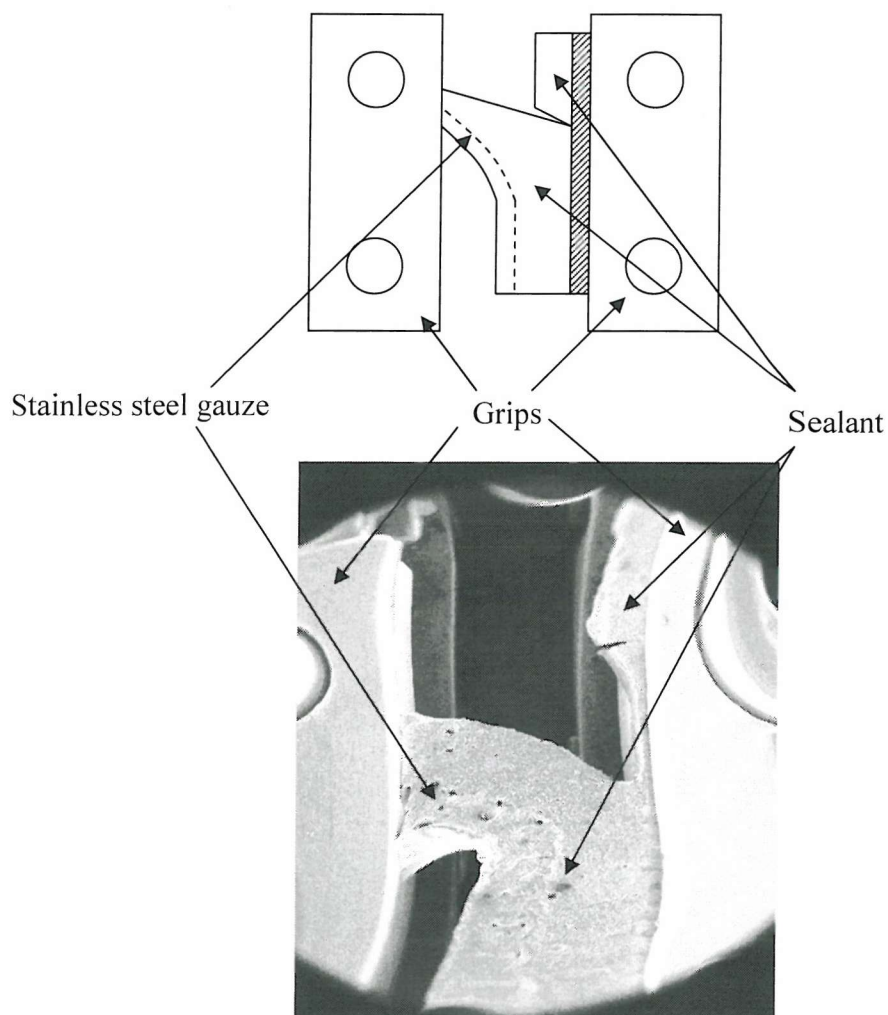


Figure 2-5 Mounting of the sample in the SEM chamber

2.5.4. UV-Visible Spectroscopy

The spectrometer used was a Hewlett Packard 8452A UV-Visible Instrument with a diode array lamp. The resolution of the instrument is 2 nm.

3. Results and Discussion

In this section, several graphs will be displayed, corresponding to the behaviour of the sealants in contact with the different solvents used. However, the highlight of the discussion will not be on this behaviour but on the different factors influencing this behaviour, such as: the solvent, the plate and the cure. Another important point of the

discussion will be the reliability of the accelerated procedure to test the new formulations of sealants.

3.1. Weight and Hardness Results

3.1.1. Error in measurements

The results presented are expressed as a percentage of mass uptake and a percentage of change of hardness (see Equation 2-1)

$$\%X = \frac{X_1 - X_2}{X_2} \cdot 100 \quad (2-1)$$

The error bars were calculated using a simple statistical equation [17]:

$$\sigma_f^2 = \sum_{i=1}^N \left(\frac{\partial f}{\partial x_i} \right)^2 \sigma_i^2 \quad (2-2)$$

Where,

σ_f^2 = the error

f = the function associated to the measurement

x_i = the variable of the function f

σ_i = the error in the measurement

And thus:

$$\Delta X = \frac{100}{X_2} \sqrt{\frac{error_2^2 X_1^2}{X_2^2} + error_1^2} \quad (2-3)$$

Where,

$error_2$ = the error in measurement X_2

$error_1$ = the error in measurement X_1

measurements X_1 and X_2 come from Equation 3-1

The error in the mass measurements comes from the scale limit: ± 0.0001 g. The error on hardness is the standard deviation of the 5 measurements.

3.1.2. Results

All the following results are displayed as a function of the square root of time because of the diffusion law. Diffusion refers to the process by which molecules intermingle as a result of their kinetic energy of random motion. Consider two containers of gas A and B separated by a partition (see Figure 2-6). The molecules of both gases are in constant motion and make numerous collisions with the partition. If the partition is removed as in the lower illustration, the gases will mix because of the random velocities of their molecules. In time, a uniform mixture of A and B molecules will be produced in the container [18].

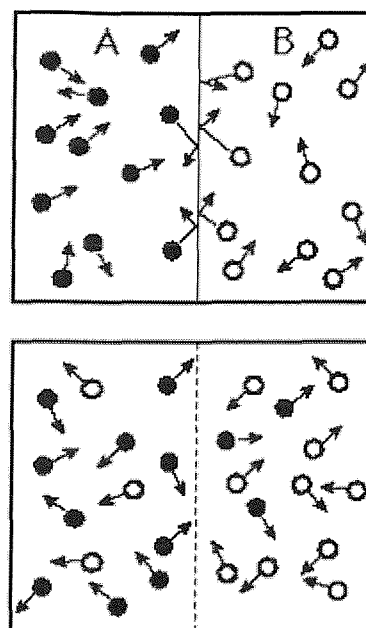


Figure 2-6 Example of a diffusion process. Top – start of process (separated gases). Bottom – end of process (mixed gases).

Since the average kinetic energy of different types of molecules (different masses) which are at thermal equilibrium is the same, then their average velocities are different. Their average diffusion rate is expected to depend upon that average velocity, which gives a relative diffusion rate:

$$\text{Diffusion Rate} = K \sqrt{\frac{t}{m}} \quad (\text{m.s}^{-1}) \quad (2-4)$$

Where the constant K depends upon geometric factors including the area across which the diffusion is occurring, t is the time and m the mass of the particle. This general relationship also applies to motion in the condensed phase.

In the following pictures, the mass uptake and the change of hardness of the specified sealants through the extraction and drying processes are shown. They are displayed on the same graph for each sealant. The left ordinate scale represents the mass uptake in percentage, while the right one is for the change of the change of hardness.

The negative lines represent the change of hardness while the positive ones correspond to the mass uptake.

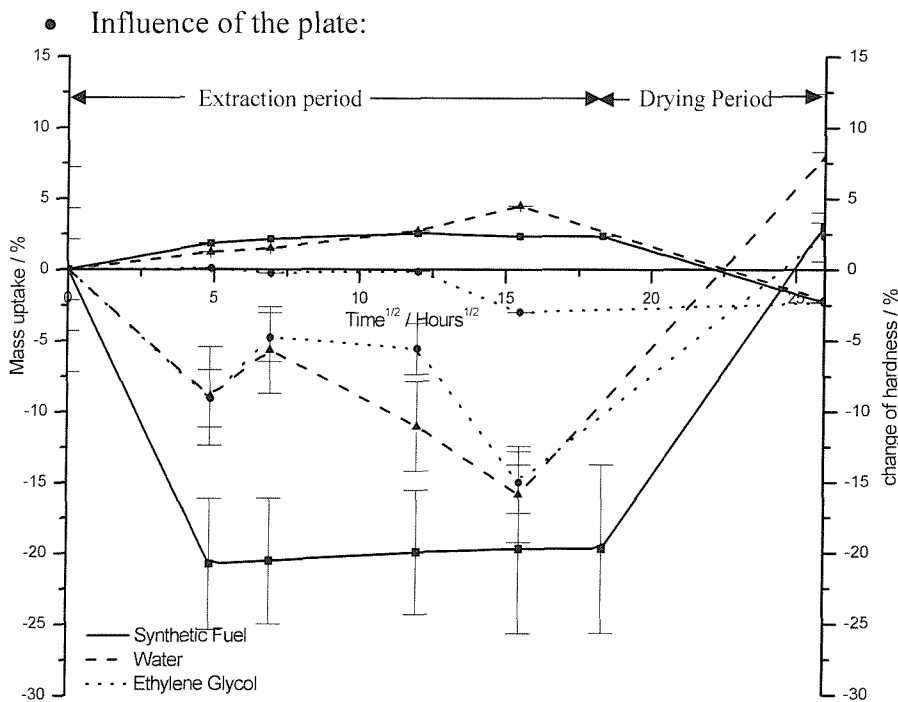


Figure 2-7 Extraction results for Cr1 on plate after short cure

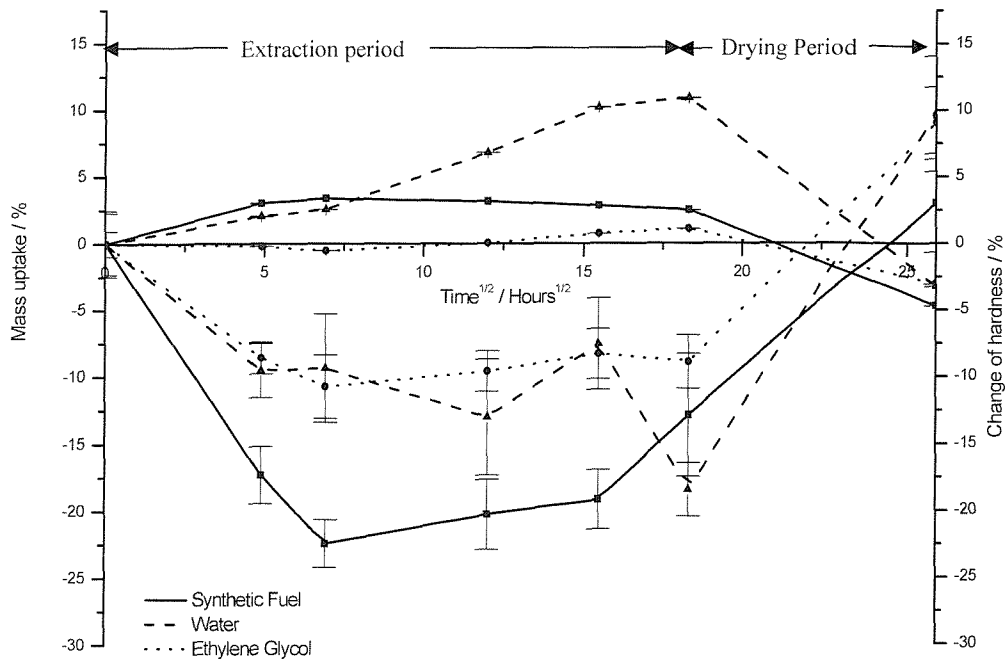


Figure 2-8 Extraction results for CrI after short cure

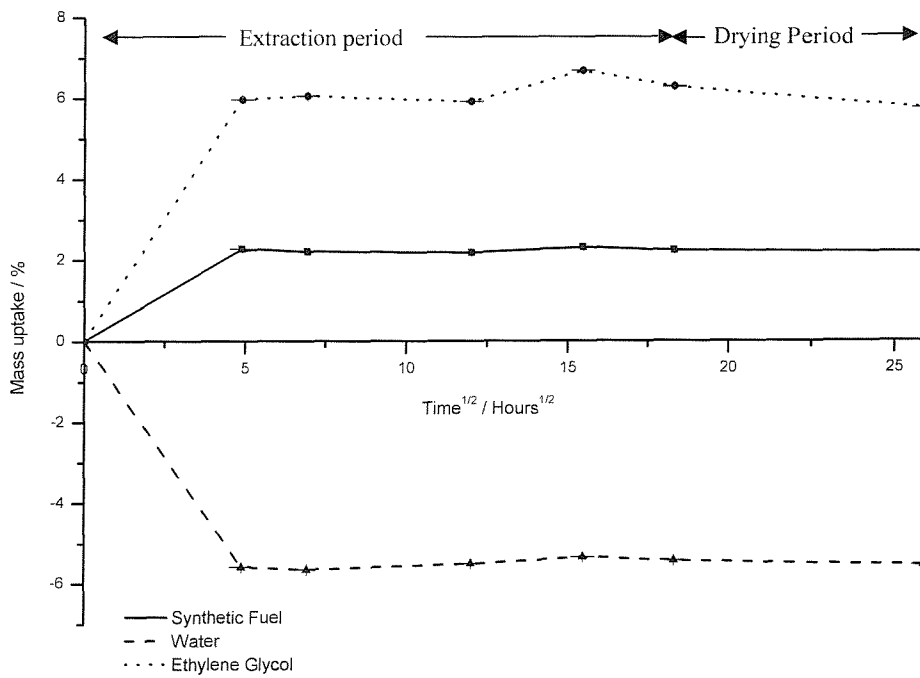


Figure 2-9 Extraction results for the plate and gauze only

The difference of mass uptake between the samples with and without plate is about a factor of 2 for all the studied sealants. As the plate is sticking to one face of the sample, the diffusion of solvent into the sample is thus limited. The Figure 2-9 shows the extraction process on the plate and gauze only. It appears that in the three different solvents, the change of mass passes through an initiation stage before stabilising. The uptake in Synthetic Fuel is not important enough to be taken into consideration in our interpretation of the results. However, the results in water and in ethylene glycol are different but one should keep in mind that the plate and gauze have been exposed to the solvent without any covering at all. Thus, the transfer of matter that occurred (change in mass) should not happen during a normal extraction as the chromium paint and the gauze are not in direct contact with the solvents.

- Influence of the solvents

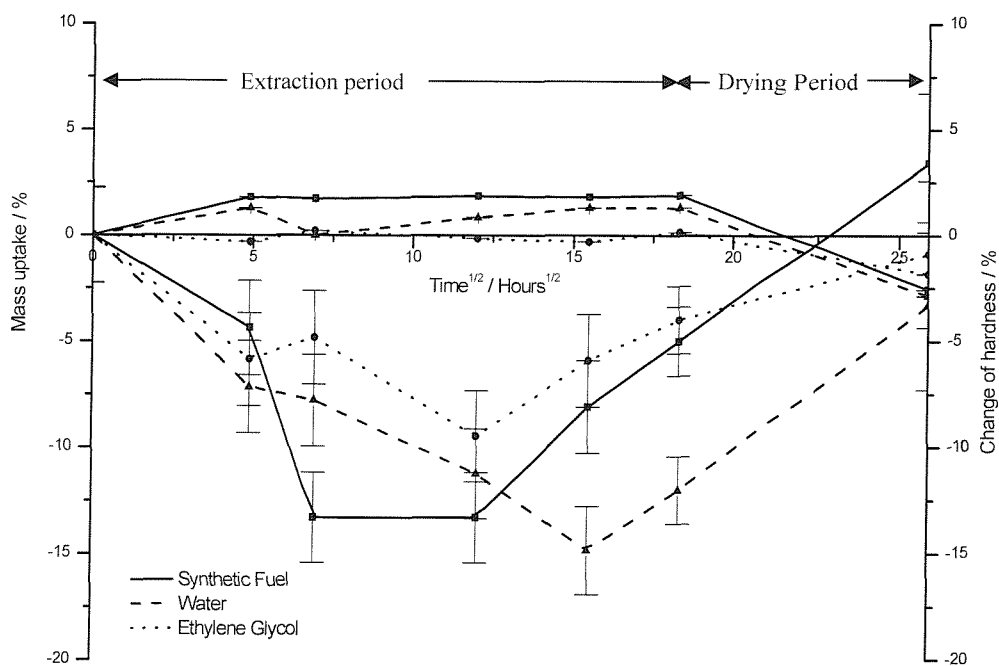


Figure 2-10

Extraction results for CrI on plate after normal cure

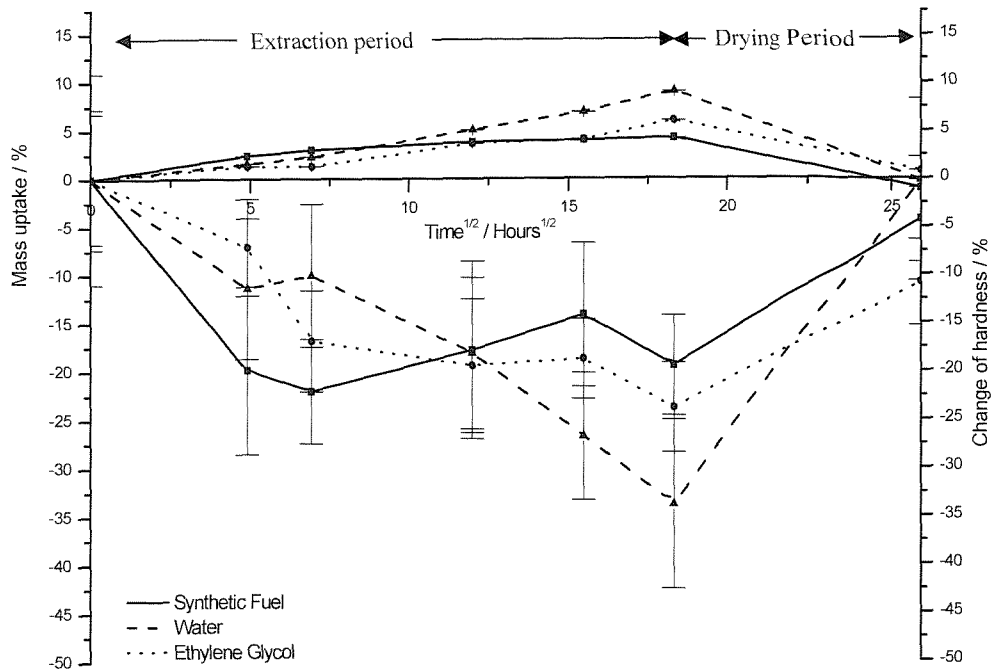


Figure 2-11 Extraction results for Mn1 on plate after normal cure

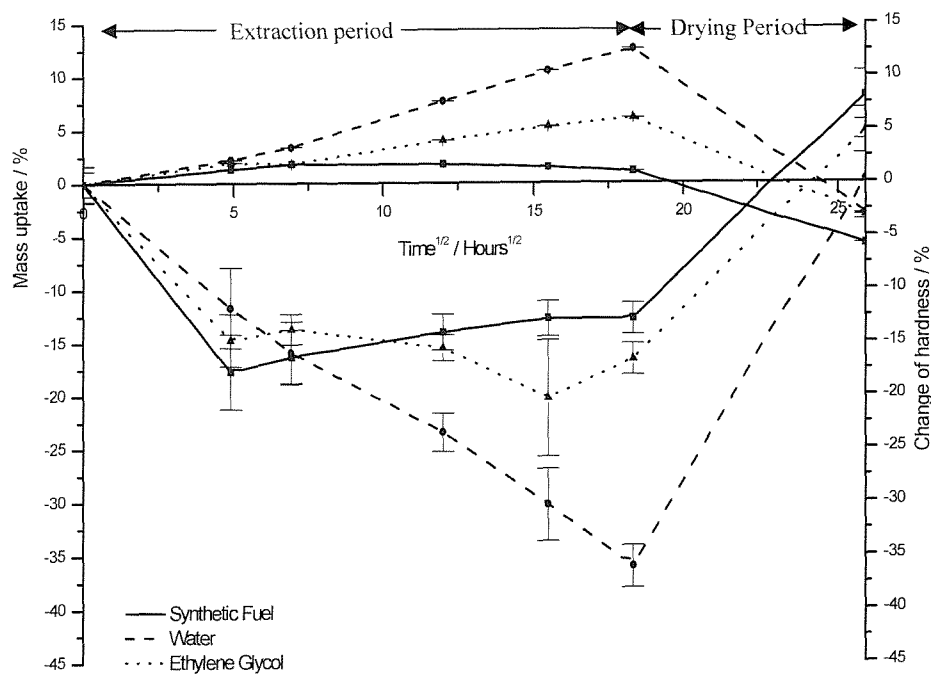
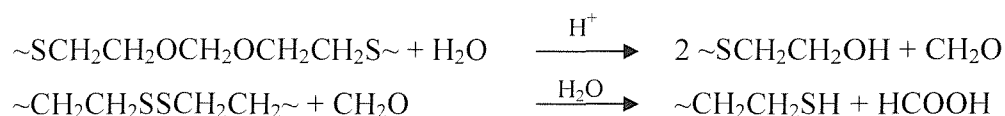


Figure 2-12 Extraction results for Mn2 on plate after normal cure

In this sub-section, only standard cure results will be discussed. Concerning the solvent, the first remark is that the antifreeze mixture (ethylene glycol / water) seems to have the same effect as water itself but in lower proportion (Figure 2-10 to Figure 2-12). Both curves follow the same trajectory, but the ethylene glycol curve is always below the water one. The antifreeze mixture does then not have an impact on the mass uptake of the sealant, only the Water plays a role on the mass uptake. The various sealants that have been studied respond differently to the solvents used. Cr1, which is reported to be the sealant with a “good” response shows that its mass uptake increases slowly during the first hours of the extraction and then stabilises during the rest of the extraction. Its change of hardness also shows a similar response, i.e. a drop of hardness at the beginning of the extraction and then a stabilisation. This sealant has been chosen to be our reference as its response to synthetic fuel and water is very good. The two other samples that have been studied (Mn1 and Mn2) have been qualified as “bad” sealants because of their poor response to contact with synthetic fuel and/or water. The results obtained with both manganese cured sealants show that the intake of water increases throughout the extraction without reaching a stabilisation phase. This is also correlated by the hardness results. Following the same scheme, the hardness continuously drops. Although they both respond badly to water, Mn2 seems to have a better tolerance to the Synthetic Fuel than Mn1, this was confirmed by the literature [19]; sealants cured by manganese dioxide or chromium salts are very little affected after interaction for up to 40 days at 60 °C with fuel.

In their work, Hanhela *et al* give some explanations of what is happening to chromium and manganese cured sealants when in contact with water. For the manganese cured ones, the immersion in hot water induces an autoxidation which results in the formation of an acidic solution. This acidic solution attacks the uncured part of the polysulfide chains as follows[9,20]:



However, this process is inhibited with chromate cured sealants since the chromium ion acts as a radical scavenger.

This process does not explain the abnormal swelling of manganese cured sealants, and hence the loss of hardness. Hanhela *et al* concluded that such behaviour was due to a further reaction of the acid with the calcium carbonate filler. They also drew some conclusion on the influence of hot water immersion of the sealants and the adhesion of those sealants: because of the swell of manganese cured sealants, water encountered low resistance to travel through the matrix and chemical attack on the sealant – primer interface causes adhesion failure.

- Influence of the cure

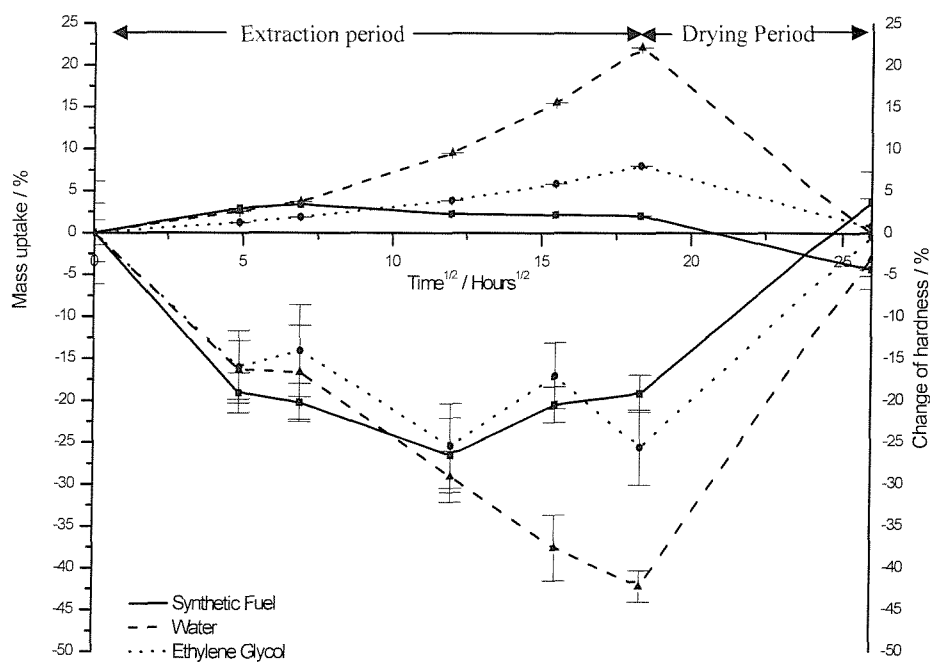


Figure 2-13

Extraction results for Mn₂ after normal cure

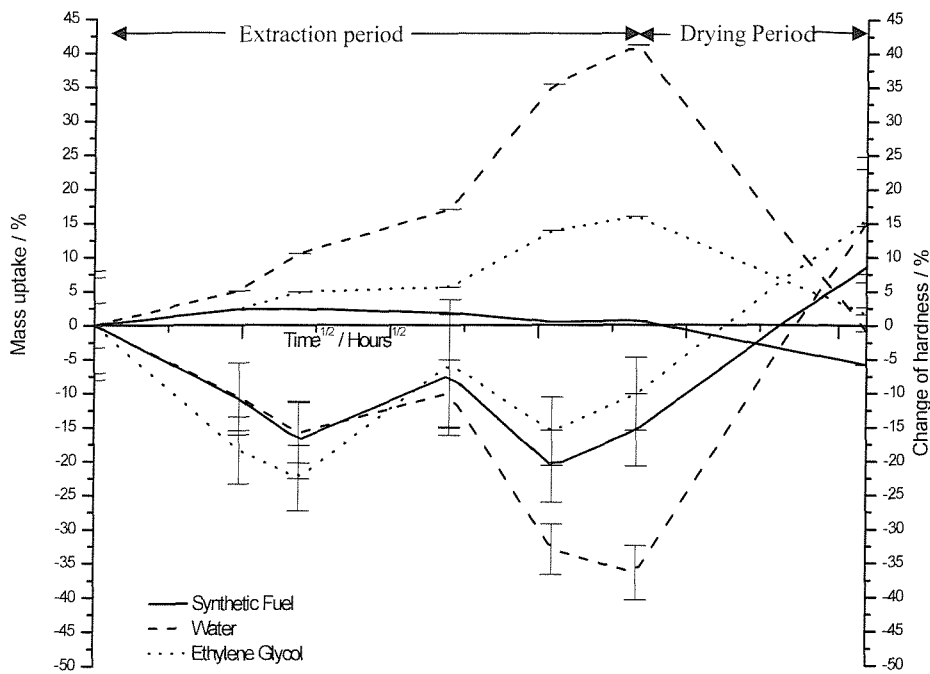


Figure 2-14 Extraction results for Mn₂ after short cure

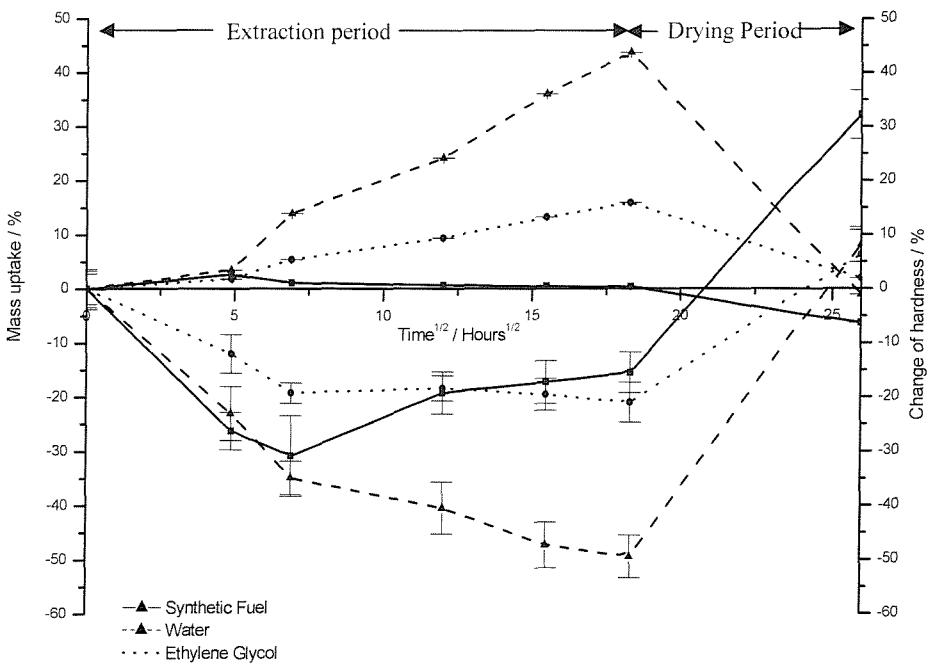


Figure 2-15 Extraction results for Mn₂ after long cure

When comparing the results for the three types of cure, one can see that the short cure dramatically increases the abnormal behaviour of all of the sealants. However, the temptation to use only the short cure to test a new formula of sealant should be disregarded because even good sealants might show a bad response. This cure should be used as a complementary study to the normal cure to accentuate the eventual defaults of the formulation. Surprisingly, the long cure seems to show the same kind of results as the short cure. However, these results must be interpreted with caution as the samples that were prepared for the long cure were prepared with older sealant and thus the control measures were not identical.

The type of cure is obviously a very important factor in the degradation of sealants when exposed to solvents and temperature. Three factors influence the curing rate: the temperature, the humidity and the time. Those three factors were under control all the time and humidity remained constant throughout the experiments (relative humidity was kept constant at $50 \pm 5\%$). It is during the curing process that the cross-linking phenomenon happens. By reducing the time of the cure (Figure 2-14), the amount of crosslinked material decreases subsequently inside the material and thus the amount of the uncured part of the polysulfide increases as well. As seen in the influence of the solvent part, water attacks the manganese dioxide cured sealants thus releasing these uncured chain endings in the solution. The more open structure allows the solvent to penetrate the sealant layer and swelling occurs. If the sealant is not completely cured, the chances to increase dramatically this behaviour are high, and can be observed when comparing Figure 2-13 and Figure 2-14.

These techniques, mass uptake and hardness testing, give a good idea of the behaviour of the sealant when exposed to solvents and heat. They should then be carried out when testing new formulations of sealants. However, they do not give enough information about how the sealant degrades and what part of the sealant passes into solution. This is the reason why Mass Spectrometry and UV-Visible spectroscopy have also been used, to give extra information on the degradation process.

3.2. Mass Spectrometry

3.2.1. Technique

The Synthetic Fuel samples, taken as aliquots during the ultrasonic extraction, have been analysed without any pre-treatment. However, the Water and Ethylene Glycol samples needed to be re-extracted. Water is not a good solvent to use in GC/MS. Thus these samples were placed in a separating funnel alongside with a small amount of Synthetic Fuel to allow the species dissolved in the water to pass into the fuel. This fuel was then analysed by GC/MS.

The technique used was a Generic GC/Electron Impact MS. The substance is volatilised into the ionisation chamber, where its molecules are bombarded with electrons and transformed into positively charged ions and then analysed by the mass analyser.

3.2.2. Results

The Gas Chromatography and mass spectrometry spectra are the same for PR Cr1 and Mn1, and looking at the formulation for each one (see Table 3-1), the extracted material comes from the similar parts of those sealants. This discussion is based on a mass spectrometry online database [21].

Table 2-2 Formulation of CrI and MnI sealants (data obtained from BAe Systems)

	Base		Activator	
CrI	Sulphide	59.2 %	Water	21.3 %
	Water	0.6 %	DMA	30.0 %
	Toluene + MEK	1.5 %	Dichromate	25.1 %
	Phenolic resin	7.5 %	Clay	22.6 %
	CaCO ₃	31.2 %	Carbon black	1.0 %
	Ti species	Nil		
MnI	Sulphide	60.1 %	Acid soluble MnO ₂	55.0 %
	Water	0.3 %	Carbon black	12.4 %
	Toluene + MEK	Nil	Hydrogenated terphenyls	29.7 %
	Phenolic resin	4.0 %	NN'-diphenyl guanidine	1.7 %
	CaCO ₃	35.6 %	Sodium stearate	2.1 %
	Ti species	v. small	Water	0.4 %

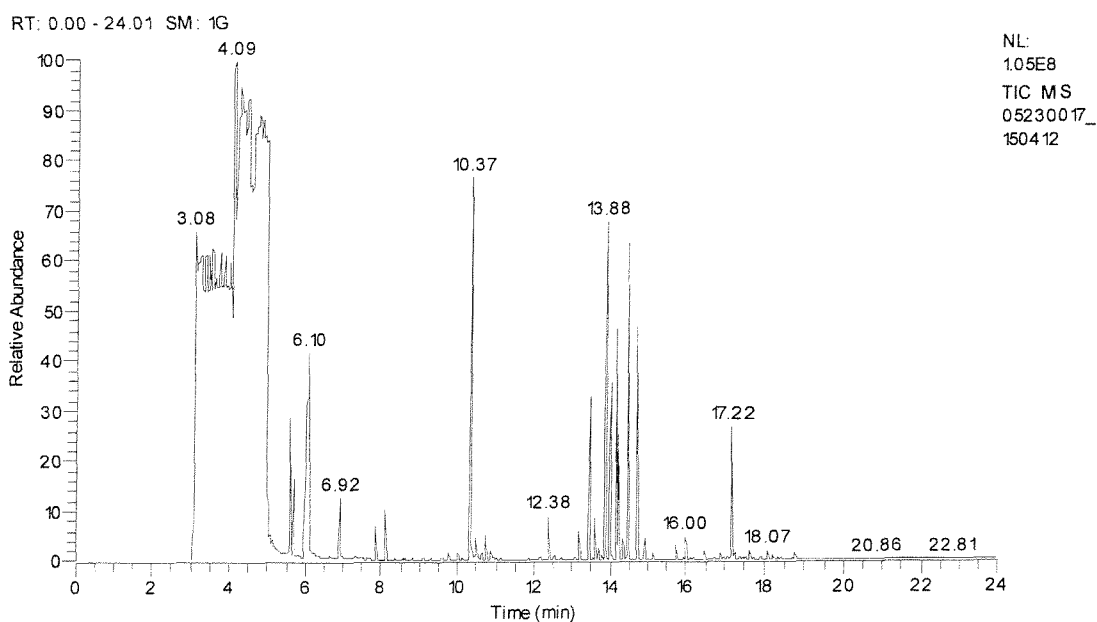


Figure 2-16 Gas Chromatography of Synthetic Fuel extracted from CrI and MnI

08140016_110845#125 RT: 4.05 P: + AV: 5 SB: 12 118-123 127-132 NL: 2.75E6
F: {0,0}+c EI det=350.00 Full ms [20.00-560.00]

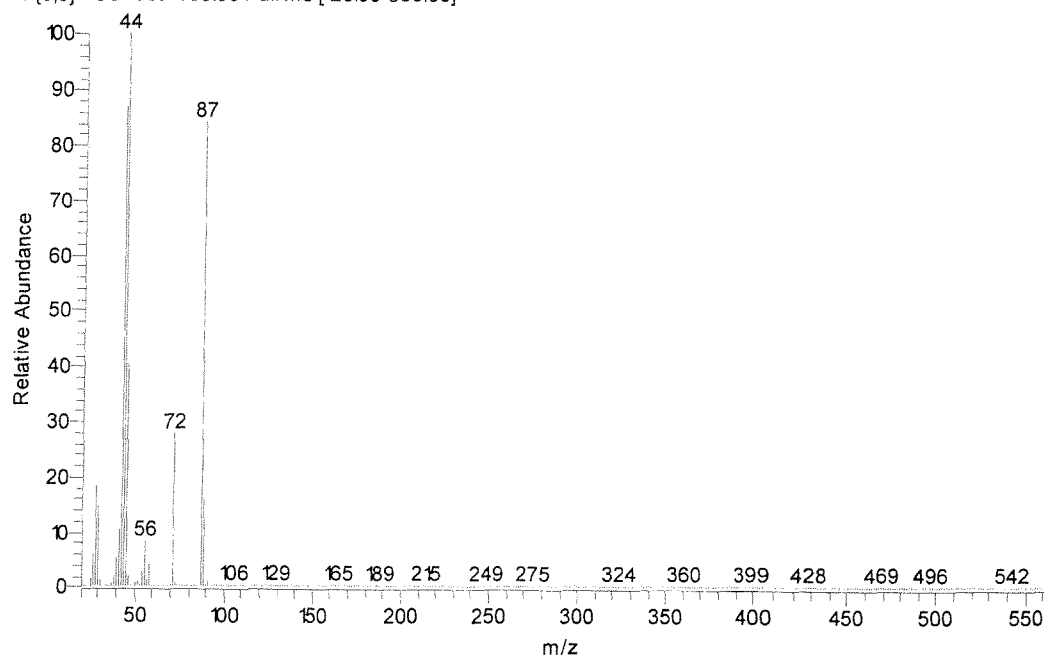
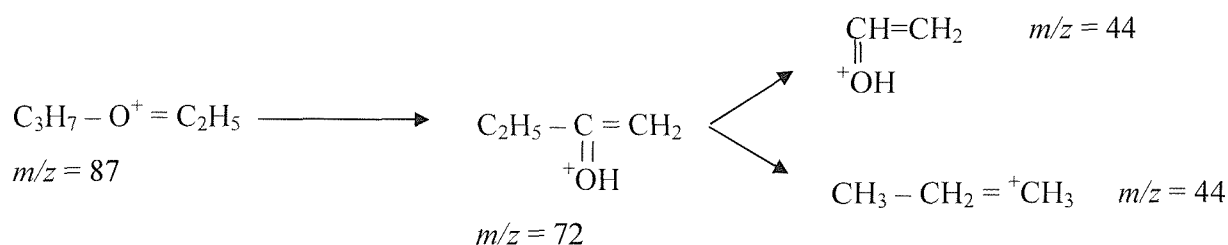


Figure 2-17 Mass spectrum of SF extracted from CrI and MnI
at retention time 6.10 min

The highest mass m/z is 87 and is likely to correspond to an ether and the ion formula would be: $C_3H_7 - O^+ = C_2H_5$.

The degradation sequence would then be:



If this hypothesis is true, the ether probably comes from the phenolic resin contained in the polymer base.

05230017_150412#882 RT: 10.37 P: + NL: 4.89E6
T: {0,0} +c EI det=350.00 Full ms [20.00-560.00]

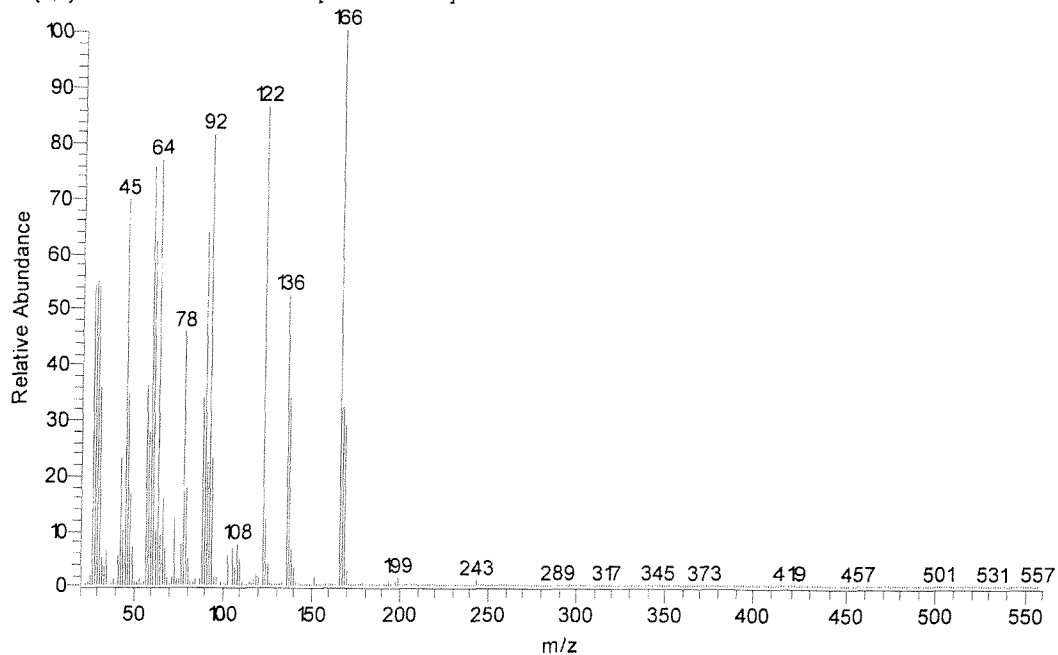
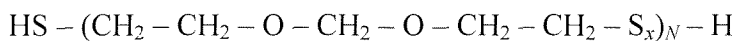


Figure 2-18 Mass spectrum of SF extracted from Cr1 and Mn1
at retention time 10.38 min

At this retention time, the highest mass m/z is 166. This is most likely to be the liquid polysulfide polymer which was extracted by the fuel. The liquid polymer used in these sealants, is based on the following formula:

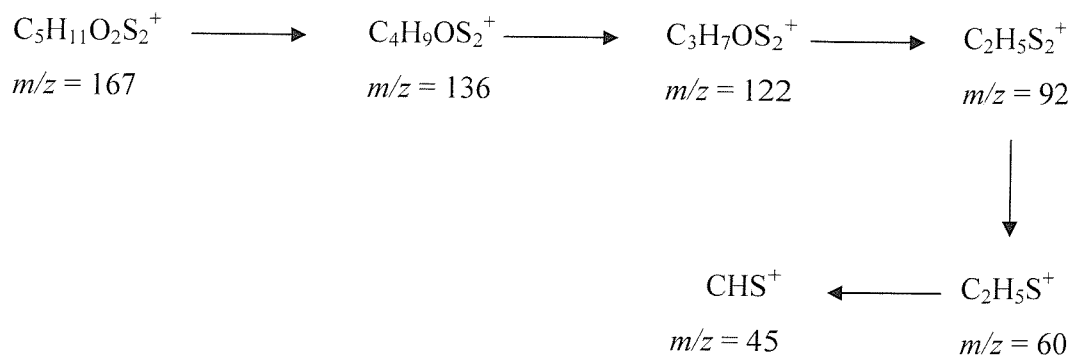


Where $x = 2.1$

$N = 22$

The ion would then be: $\text{CH}_3 - \text{CH}_2 - \text{O} - \text{CH}_2 - \text{O} - \text{CH}_2 - \text{CH}_2 - \text{S} - \text{S}^+$

and the degradation sequence:



Thus, the liquid polymer, which is the backbone of the sealant, is extracted by the Synthetic Fuel during the extraction process.

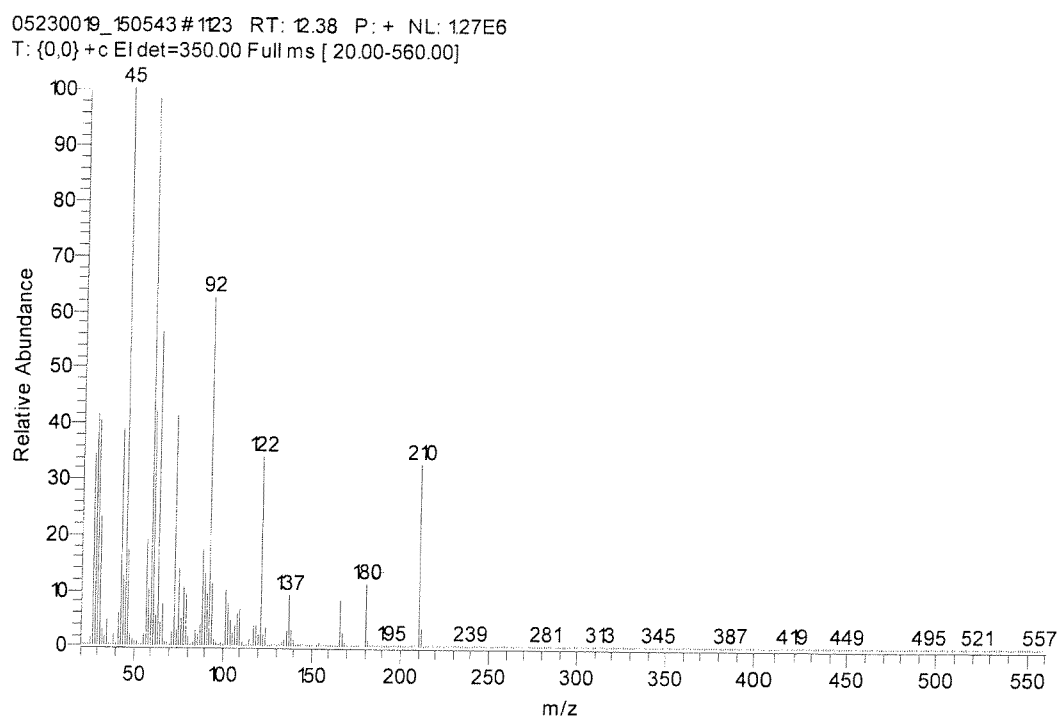


Figure 2-19 Mass spectrum of SF extracted from CrI and MnI at retention time 12.38 min

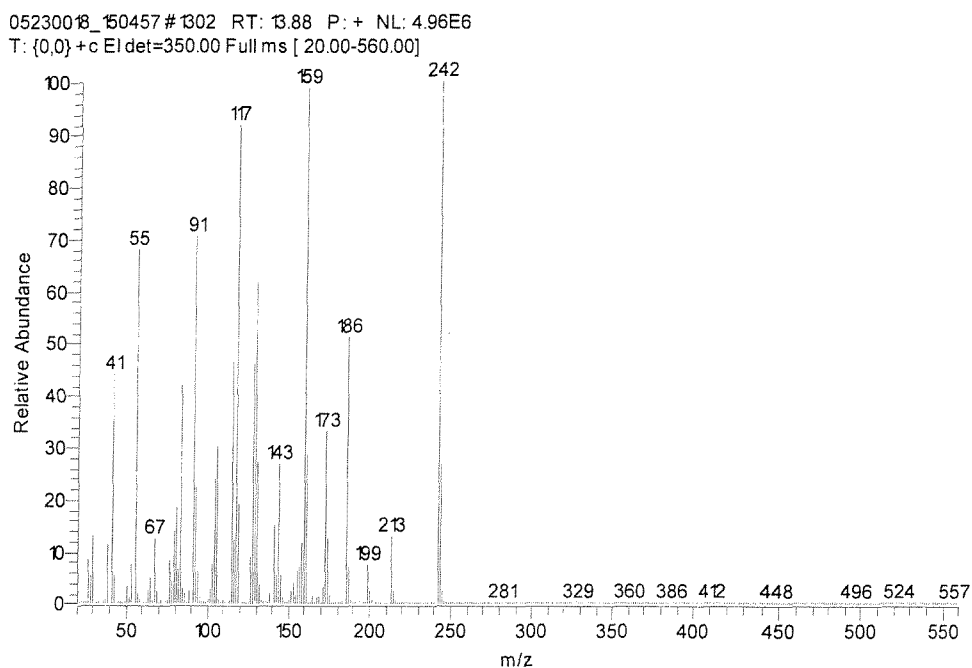
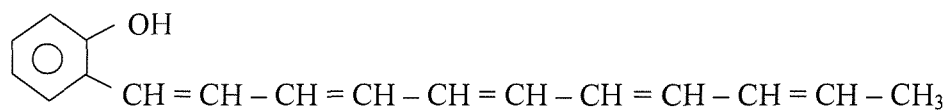


Figure 2-20 Mass spectrum of SF extracted from Cr1 and Mn1 at retention time 13.89 min

As before, the ion fragment analysed at this retention time, could come from the phenolic resin, including a long unsaturated chain of aliphatic carbons such as:



05230018_150457 #1702 RT: 17.21 P: + NL: 176E6
T: {0,0} +c EI det=350.00 Full ms [20.00-560.00]

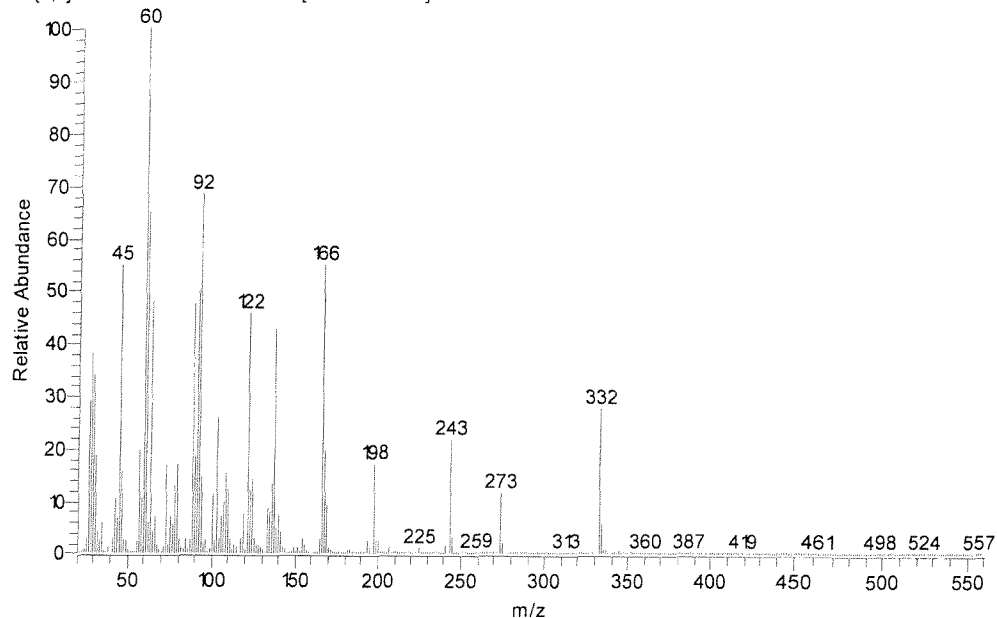
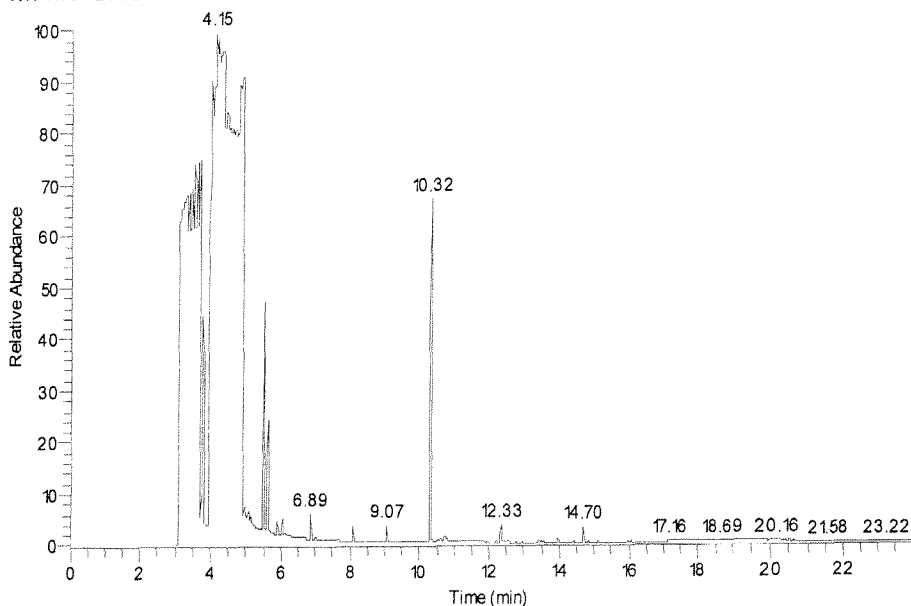


Figure 2-21 Mass spectrum of SF extracted from Cr1 and Mn1
at retention time 17.22 min

At this time, the first part of the spectrum is very similar to the spectrum at 10.38 and the heaviest ion has a mass of 332 g (=166 g x 2). Thus, this species may be a dimer of the liquid polymer extracted before.

RT: 0.00 - 23.99 SM: 1G



NL:
1.09E8
TIC MS
07240009
_114553

Figure 2-22 Gas Chromatography of Water and Ethylene Glycol extracted from
Cr1, Mn1 and Mn2

05230017_150412#882 RT: 10.37 P: + NL: 4.89E6
T: {0,0} +c EI det=350.00 Full ms [20.00-560.00]

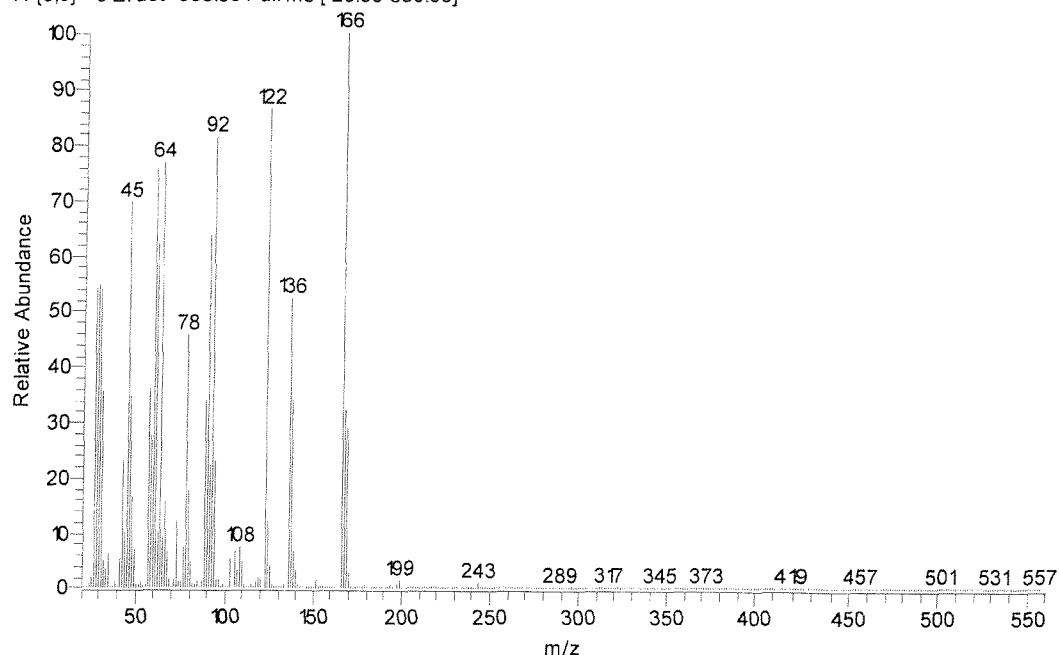


Figure 2-23 Mass spectrum of Water extracted from Cr1, Mn1 and MN2 at retention time 10.32 min

The GC/MS spectra of Cr1, Mn1 and Mn2 extracted with water and ethylene glycol all look the same, except for the peak intensity. An example is displayed in Figure 2-22. This result highlights the hypothesis that water and the mixture water/ethylene glycol have the same effect on sealants and thus only water really acts as a degrading agent. The only peak present in these spectra appears at the retention time 10.32 min and the associated mass spectrum is shown in Figure 2-23. This spectrum is identical to the one in Figure 2-18 for a retention time of 10.38 min but in synthetic fuel. This peak has been associated with the extraction of the liquid polymer from the sealant. Thus, the ageing effect of water on the sealants only affects the backbone of it, the polymer.

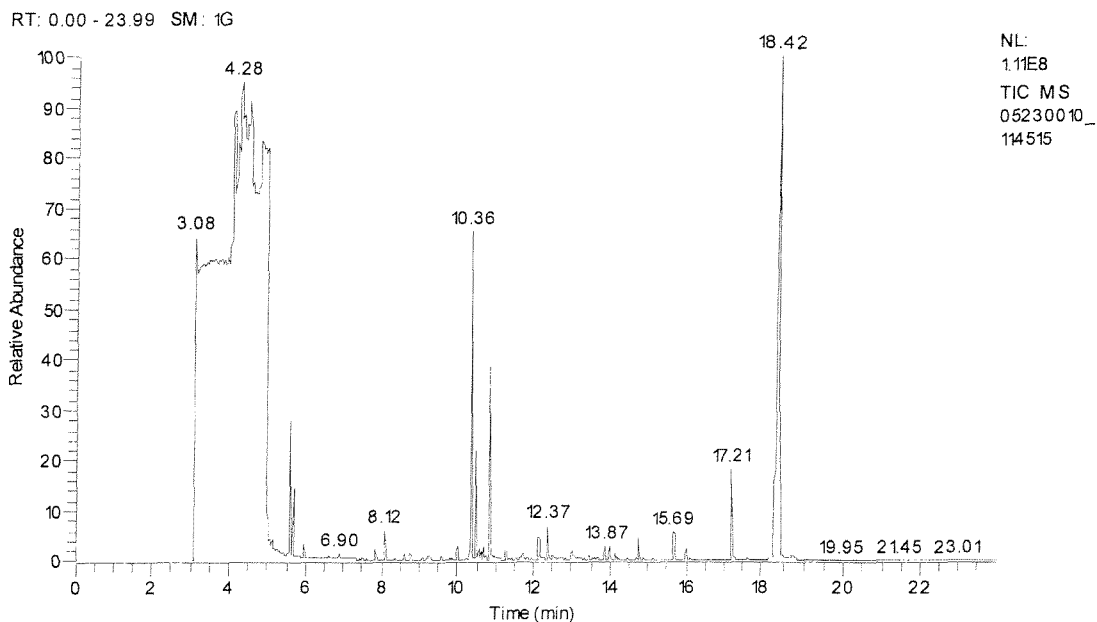


Figure 2-24 Gas Chromatography of Synthetic Fuel extracted from Mn2

The mass spectra of Synthetic Fuel extracted from Mn2 at retention times 10.36 min and 17.21 min are the same as Mn1 and Cr1

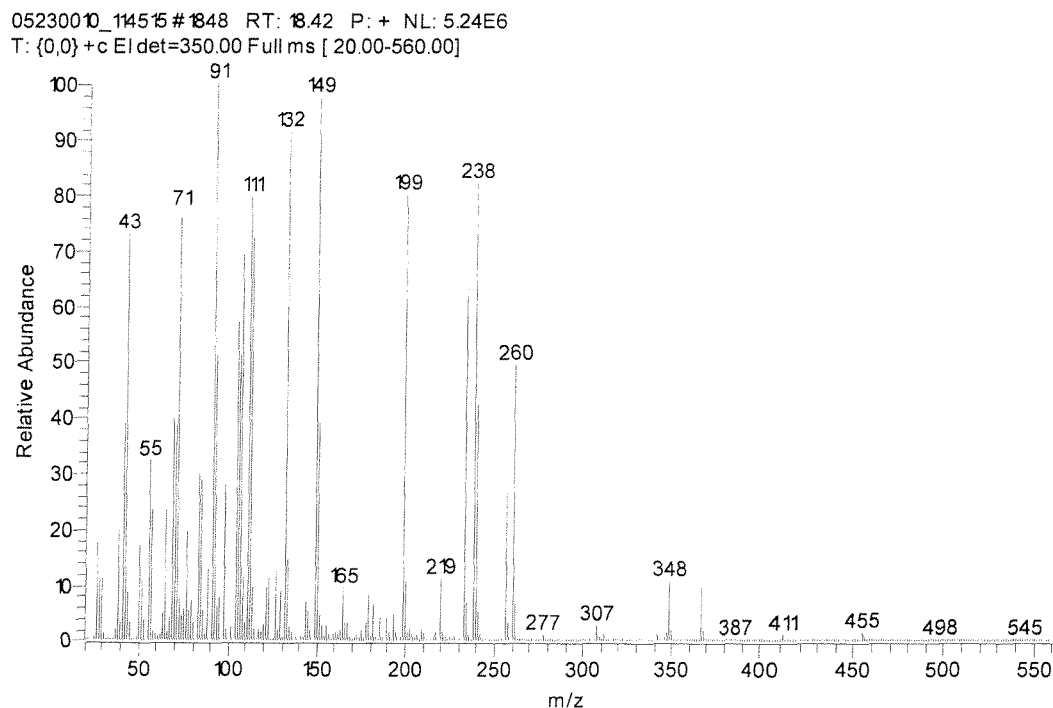
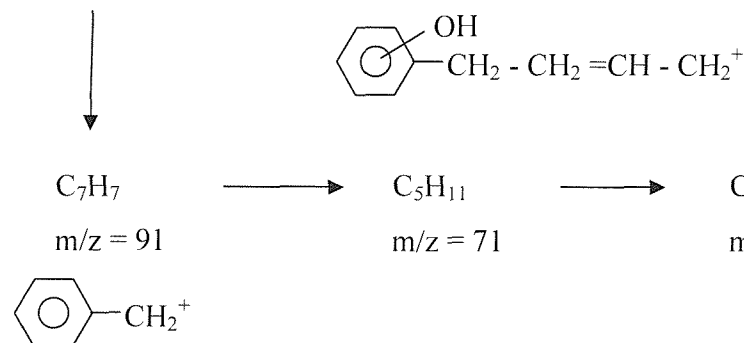


Figure 2-25 Mass spectrum of SF extracted from Mn2 at retention time 18.42 min

$$\begin{array}{ccccc} \text{C}_{21}\text{H}_{32}\text{O}_4 & \longrightarrow & \text{C}_{17}\text{H}_{24}\text{O}_2 & \longrightarrow & \text{C}_{17}\text{H}_{18}\text{O} \\ m/z = 348 & & m/z = 260 & & m/z = 238 \end{array}$$


Analysing the extracted solvents by GC/MS helps to understand how the sealants degrade under the action of these solvents. However, this study should not be carried out on its own in an ageing experiment but alongside the other analyses presented in this report.

3.3. Mini-peel results

3.3.1. Measurements

All the mini-peel tests have been carried out at room temperature. The results, first given in kilogram force (kgf) then in Newtons (N), have been corrected from the chart recorder values with the calibration curve detailed below.

3.3.2. Calibration

As the tensile stage was not calibrated, results from a previous experiment comparing the tensile stage and INSTRON values was used to correct the recorded data.

The materials used for the correction were as follows:

- Cu wire, 1.0 mm \varnothing (99.9 % pure, annealed) – Goodfellow CU005290/9
- Fe wire, 0.9 mm \varnothing (99.5 % pure, annealed) – Goodfellow FE005170/2
- Ni wire, 1.0 mm \varnothing (99.0 % pure, as drawn) – Goodfellow NI005160/4
- Cu wire, 0.5 mm \varnothing (99.98 % pure, as drawn) – Goodfellow CU005282/1
- Cu-Be wire, 1.0 mm \varnothing (hard temper) – Goodfellow CU075150/3

Approximately 4 mm length of wire was cut and then the ends were bent round into a “staple” shape to prepare each test specimen. The grips were set to about 10 mm apart. The results are shown in the following table. The experiment was carried out by C.C. Figure from BAe Systems.

Table 2-3 Calibration results

Material	Peak chart recorder value (kgf)	Average chart recorder value (kgf)	Average chart recorder value (N)	Calibrated INSTRON values (N)
Cu 0.5 mm Ø	7.92	8.1	79.5	77.3
	8.03			
	8.35			
Cu 1.0 mm Ø	25.45	24.15	236.9	213
	24			
	23			
Fe 0.9mm Ø	27.75	28.58	280.4	263.1
	28.7			
	29.3			
Ni 1.0 mm Ø	46.3	45.67	448	400.6
	43.7			
	47			
Cu-Be 1.0 mm Ø	92.12	92.12	903.7	807.3

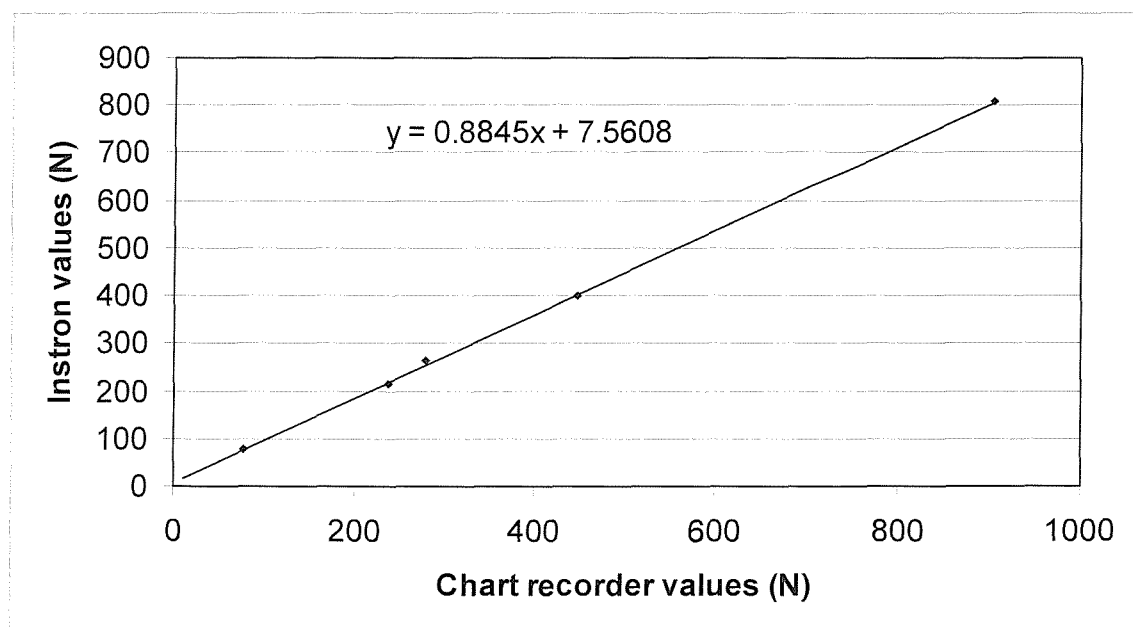


Figure 2-26 Calibration graph

3.3.3. Results and Discussion

The following table lists the samples that have been studied with the mini-peel technique.

Table 2-4 Samples studied with the mini-peel technique

Sealant	Cure	Solvent
Cr1	Normal	Non Aged, SF, W, EG
Cr1	Short	Non Aged, SF, W, EG
Mn1	Normal	Non Aged, SF, W, EG
Mn1	Short	Non Aged, SF, W, EG
Mn2	Normal	Non Aged, SF, W, EG
Mn2	Short	Non Aged, SF, W, EG

While recording the force needed to peel the sample off the plate, the sealants have also been monitored during the test to check whether the failure was cohesive, in which case the sample would pass the test, or adhesive, which would correspond to a failed sample. Examples of the two types of shearing are displayed in Figure 2-27 and Figure 2-28.

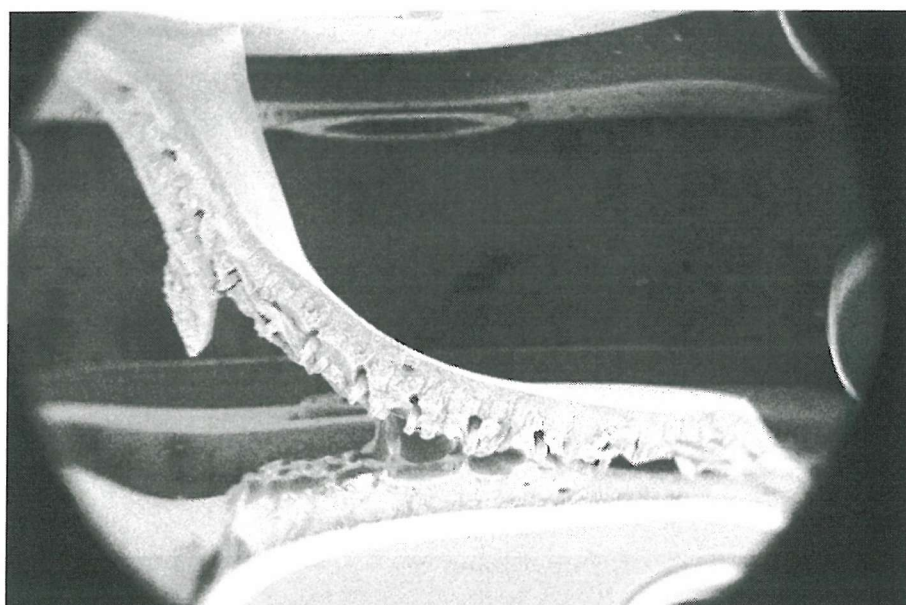


Figure 2-27 Cohesive failure (pass)

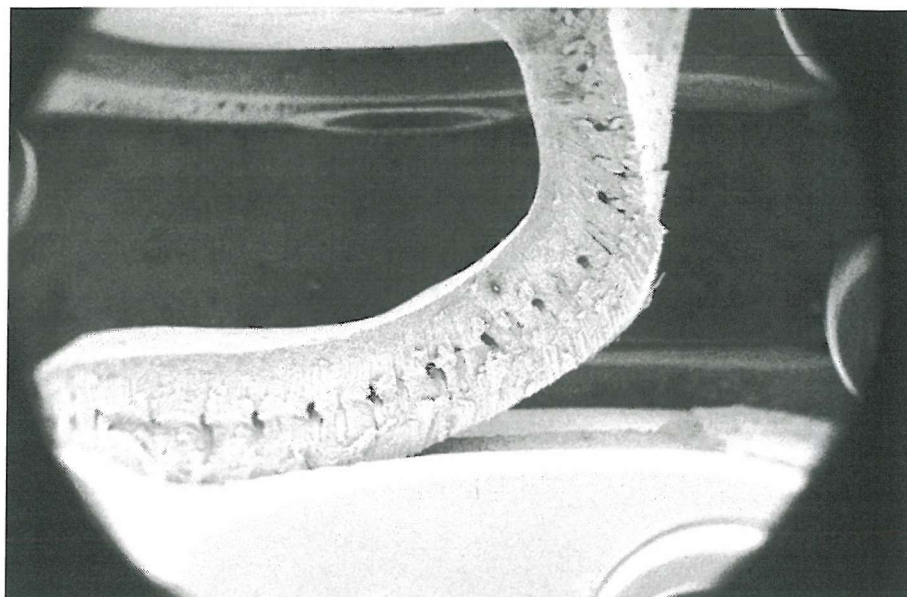


Figure 2-28 Adhesive failure (fail)

The results of the mini-peel tests are displayed in Table 2-5

Table 2-5 Mini peel results (a peel width of 3.5 mm was used throughout)

Sealant / Cure / Solvent	Corrected Value of the force (N)	Cohesive (✓) or Adhesive (✗) failure
Cr1 / Normal / Non Aged	11.38	✓
Cr1 / Normal / SF	17.45	✓
Cr1 / Normal / W	17.80	✓
Cr1 / Normal / EG	21.62	✓
Cr1 / Short / Non Aged	14.85	✓
Cr1 / Short / SF	18.32	✓
Cr1 / Short / W	16.32	✓
Cr1 / Short / EG	17.80	✓
Mn1 / Normal / Non Aged	21.01	✓
Mn1 / Normal / SF	19.10	✓
Mn1 / Normal / W	10.51	✗

Table 2-5 Mini peel results (carried over)

Sealant / Cure / Solvent	Corrected Value of the force (N)	Cohesive (✓) or Adhesive (✗) failure
Mn1 / Normal / EG	16.76	✓
Mn1 / Short / Non Aged	16.41	✓
Mn1 / Short / SF	23.35	✓
Mn1 / Short / W	22.22	✓
Mn1 / Short / EG	18.49	✓
Mn2/ Normal / Non Aged	16.32	✓
Mn2/ Normal / SF	19.53	✓
Mn2/ Normal / W	13.81	✓
Mn2 / Normal / EG	18.67	✓
Mn2/ Short / Non Aged	18.67	✓
Mn2/ Short / SF	17.28	✓
Mn2/ Short / W	13.11	✓
Mn2/ Short / EG	17.63	✓

Only one sealant failed this test: PR1779 B2 after a normal cure and aged in Water. As demonstrated before, the manganese cured sealants have a very poor resistance to water immersion. Thus, the literature reports [9,20] have been proved right when they say that a prolonged water immersion of manganese cured sealants ends in the attack on the sealant – primer interface causing adhesion failure

Although it seems that when the hardness has increased, after the drying period, the force to peel off the sealant increases as well, it is very difficult to establish a standard behaviour for the samples studied. A suggestion would be to obtain the results of the normal peeling on the studied samples and to try to correlate them with the mini-peel results.

The mini-peel results are very useful for the Aerospace industry where the adhesion properties are of primal importance. However, the peel test values are very difficult to

reproduce and to correlate to the other results. This test should then only be carried out to study the adhesion loss of the new formulations of sealants.

3.4. UV-Visible spectroscopy

3.4.1. Instrument

The spectrometer used was a Hewlett Packard 8452A UV-Visible Instrument with a diode array lamp. The resolution of the instrument is 2 nm

3.4.2. Results and Discussion

The spectra that have been recorded are similar for all the samples that have been extracted with synthetic fuel. The results are also independent of the cure. For all the displayed UV-Visible spectra, the background sample used was the pure solvent. An example of Synthetic Fuel absorption spectrum is displayed in Figure 2-29.

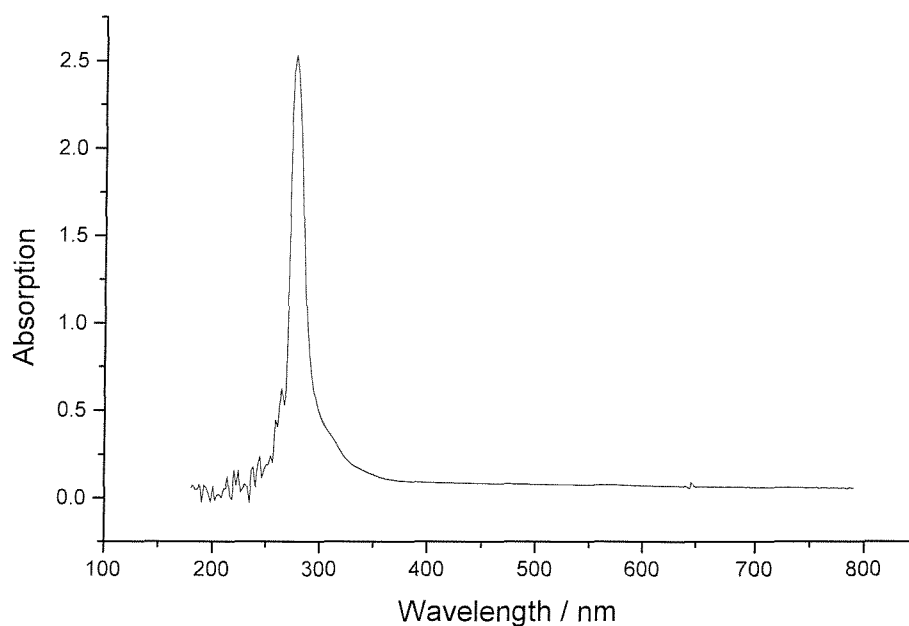


Figure 2-29 Absorption spectrum of synthetic fuel extracted by Cr1, Mn1 and Mn2

The UV-Visible spectra of the Synthetic fuel are the same for the sealants and for LP2C[®]. Thus this band characterises the polysulfide. According to the literature, Hydrogen Sulfide exhibits strong absorption at wavelengths just below 300 nm [22]. We can then conclude that the absorption band around 280 nm is due to the thiol end of the polysulfide which was extracted during the ageing process.

The same phenomenon occurred with Water and Ethylene Glycol, i.e. all the spectra are similar. One of them is then shown in Figure 2-30.

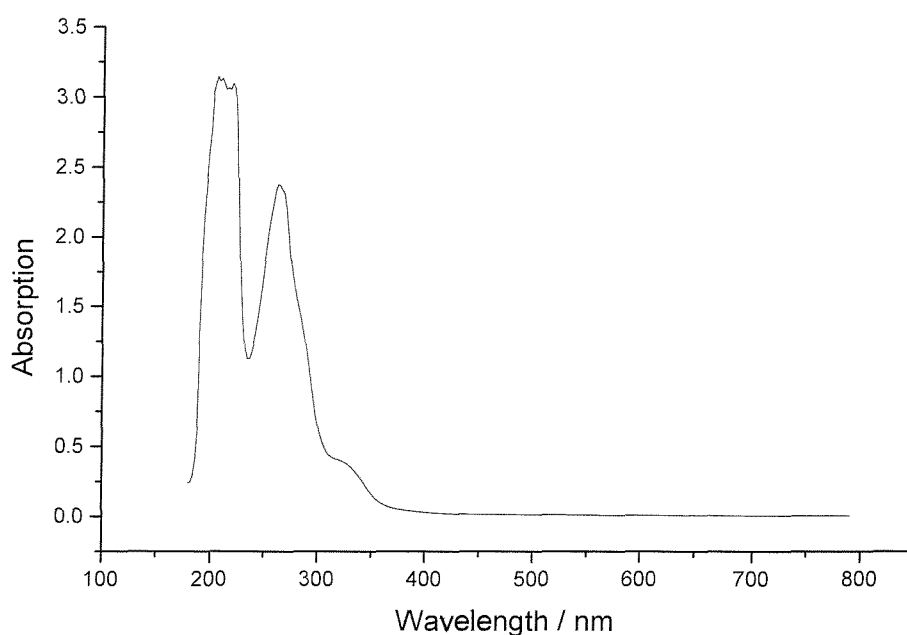


Figure 2-30 Absorption spectrum of Water and Ethylene Glycol extracted by Cr1, Mn1 and Mn2

To be able to interpret these spectra, the same extraction process has been applied to an uncured Liquid Polymer (LP2C[®]) sample. The resulting spectra are displayed in Figure 2-31 and Figure 2-32 below.

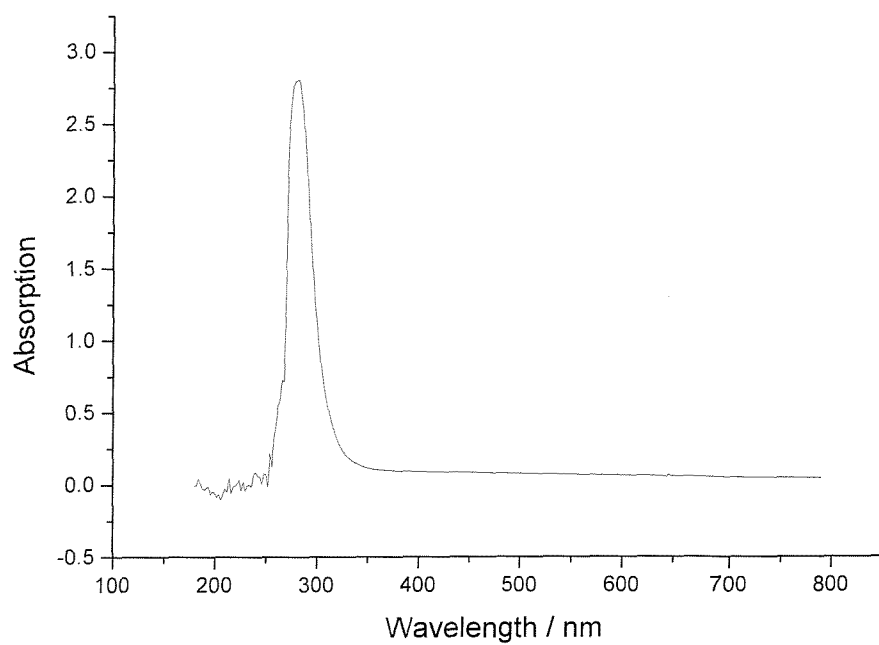


Figure 2-31 Absorption spectrum of Synthetic Fuel extracted by LP2C[®]

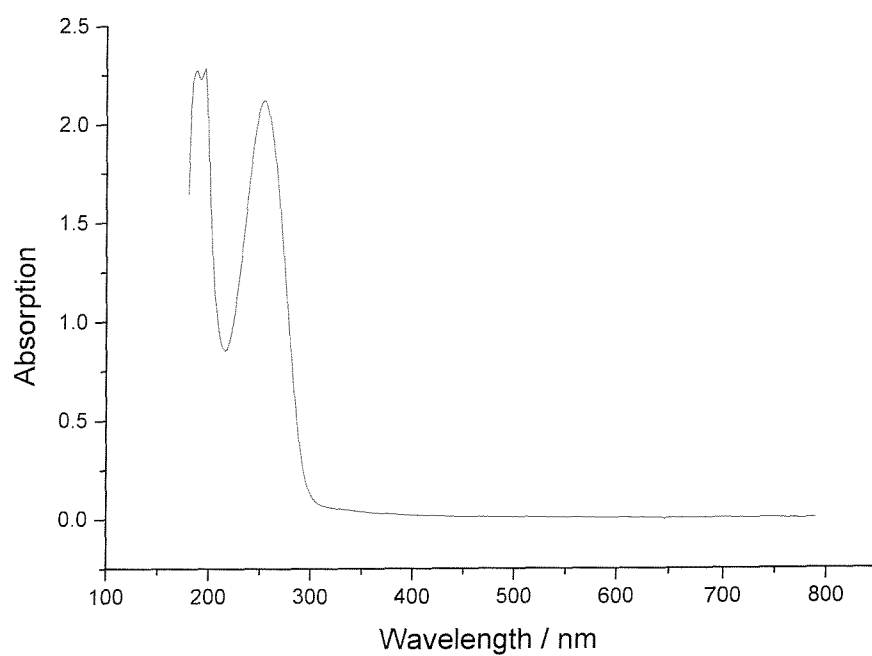


Figure 2-32 Absorption spectrum of Water and Ethylene Glycol by LP2C[®]

The spectra of Water and Ethylene Glycol exhibit the same band around 290 nm that we attributed to the -SH group in the polysulfide. However, two other bands are also present in the spectrum. Gauduel *et al* did some research about the absorption of dimethyl sulfide (CH₃)₂S. They came to the conclusion that dimethyl sulfide was absorbing at the wavelength of 210 nm [23]. In the spectra of Water (Figure 2-30 and Figure 2-32) our band is centered on 212 nm. The slight shift in wavelength is probably due to the difference of environment around the CH₂S group in our molecule. However, this band can be associated with the CH₂S group.

The last band present in the spectrum of the extract following exposure of the sealant to water does not appear in the LP2C[®] extract spectrum. The peak is centered on 326 nm. Guenther *et al* discussed the same kind of effect in their article about the absorption of Hydrogen Sulfide [22]. They attributed a bump at 260 nm to dissolved organic carbon. The mass spectrometry results showed the presence of phenols extracted (coming from the phenolic resins). By analogy, the peak at 326 nm can be associated to these species that were extracted during the ageing process of the sealants. That would also explain the absence of this peak in the LP2C[®] spectrum.

Once again this technique gives useful information about the degradation of the sealants during the ageing process. However, this technique alone will not provide enough information and must be associated with some of the other ones described before.

4. Conclusion

The aim of this project was to develop an ageing system to study the new formulation of sealants. After disregarding the Soxhlet extraction system which was not effective because of the re-condensation problems, the ultrasonic heating bath was adopted. It proved to be an effective system. No re-condensation was required, the sealants are always in contact with the extracting solvent and the ultrasonic system provides good agitation around the sample. These conditions tend to recreate the real conditions that sealants endure during their life in the fuel tanks of the aeroplane. Associated with this ageing process, several techniques have been used to try to facilitate understanding of how the sealants degrade and behave during the ageing process. Hardness testing, Mass uptake, Mass Spectrometry, UV-Visible spectroscopy, have all been proved to give useful information. However, none of these techniques provide conclusive evidence on their own. They all give clues to the behaviour of the sealants and when put together they help in drawing a pattern and maybe predict a good or a bad behaviour for a new formulation. One technique described before, the mini-peel test, did not prove itself to be of great utility. The data could not be correlated with that from the other techniques values. However, the mini-peel test can still be used to test failure mechanism, either cohesive or adhesive.

From all these techniques, it appears that mainly uncured parts are extracted from the sealants, such as ending chains of liquid polysulfides or parts of the phenolic resins. However, no part from the curing agents (i.e. the plasticiser) has been proved to be extracted during the ageing process.

Finally, to test new formulations of sealants, using the extraction system on the new sealant alone is not recommended. Testing the new sealant in parallel with a sealant whose behaviour is well known (a good one and a bad one for example) will help the researcher to rate this sealant.

5. References

- [1] Stout, R. J. Service sensitivity of polysulfide sealants. In *13th National SAMPE Technical conference*, 1981; Vol. 13; pp 64.
- [2] Barber, J. W.; Hanhela, P. J.; Huang, R. H. E.; Paul, D. B. *Polymer Testing* **1990**, 9, 291.
- [3] Shephard, N. E.; Wightman, J. P. An analysis of the 180 ° peel test for measuring sealant adhesion. In *Science and Technology of Building Seals, Sealant, Glazing and Weatherproofing*; American Society for testing and materials, 1996; Vol. 5th volume.
- [4] Carre, A.; Schultz, J. *Journal of Adhesion* **1984**, 18, 171.
- [5] “Military Specification - Sealing Compound, Temperature-Resistant, Integral Fuel Tanks and Fuel Cell Cavities, High Adhesion,” US Army, report no MIL - S - 8802F 80, 1980, pp. 40.
- [6] Amstock, J. S. High Performance Sealants. In *The Construction Specifier*, July 1995; pp 61.
- [7] Karpati, K. K. *Durability of Building Materials* **1987**, 5, 35.
- [8] Karpati, K. K. *Journal of Paint Technology* **1973**, 45, 49.
- [9] Hanhela, P. J.; Huang, R. H. E.; Paul, D. B.; Symes, T. E. F. *Journal of Applied Polymer Science* **1986**, 32, 5415.
- [10] Stargel, S. *Journal of Elastoplastics* **1971**, 3, 222.
- [11] Bertozzi, E. R. *Rubber Chemistry and Technology* **1968**, 41, 114.
- [12] Ennis, B. C.; Pearce, P. J.; Morris, C. E. M. *Journal of Applied Polymer Science* **1989**, 37, 15.
- [13] Watts, J. F. *Surface and Interface Analysis* **1988**, 12, 497.
- [14] Allen, K. W.; Hutchinson, A. R.; Pagliuca, A. *International Journal of Adhesion and Adhesives* **1994**, 14, 117.
- [15] Ramaswamy, R.; Achary, P. S. *Journal of Applied Polymer Science* **1985**, 30, 3569.

- [16] Lacasse, M. A. Advances in test methods to assess the long-term performance of sealants. In *Science and Technology of Building Seals, Sealant, Glazing and Weatherproofing*; American Society for testing and materials, 1994; Vol. 3rd volume.
- [17] Mood, A. M.; Graybill, F. A.; Boes, D. C. *Introduction to the Theory of Statistics*, 3rd ed.; McGraw-Hill International Book Company: Singapore, 1984.
- [18] Chapman, S.; Cowling, T. G. *The Mathematical Theory of Non-Uniform Gases; an Account of the Kinetic Theory of Viscosity, Thermal Conduction, and Diffusion in Gases*, 3rd ed.; Cambridge University Press: Cambridge, 1970.
- [19] Paul, D. B. *Abstracts of Papers of the American Chemical Society* **1987**, 193, 109.
- [20] Hanhela, P. J.; Huang, R. H. E.; Paul, D. B. *Industrial & Engineering Chemistry Product Research and Development* **1986**, 25, 321.
- [21] Choi, S. S. *Bulletin of the Korean Chemical Society* **2000**, 21, 628.
- [22] Guenther, E. A.; Johnson, K. S.; Coale, K. H. *Analytical Chemistry* **2001**, 73, 3481.
- [23] Gauduel, Y.; Marignier, J. L.; Belloni, J.; Gelabert, H. *Journal of Physical Chemistry A* **1997**, 101, 8979.

Chapter 3. Investigation on the polysulfides bonding

1. Introduction

The field of self-assembled monolayers (SAMs) has witnessed a tremendous growth over the past 20 years. However, the field began much earlier: in 1946, Zisman published the preparation of a monolayer by adsorption (self-assembly) of a surfactant onto a clean metal surface [1]. At that time, the potential of self assembly was not yet recognised. More recently, Nuzzo and Allara showed that SAMs of alkanethiolates on gold can be prepared by adsorption of di-*n*-alkyl disulfides from dilute solutions [2]. Many self-assembly systems have since been investigated, but monolayers of alkanethiolates on gold are probably the most studied SAMs to date.

In nature, self-assembly results in supramolecular hierarchical organisations of interlocking components. SAMs offer unique opportunities to increase fundamental understanding of self-organisation, structure – property relationships and interfacial phenomena. The ability to tailor both head and tail groups of the constituent molecules makes SAMs excellent systems for a more fundamental understanding of phenomena affected by competing intermolecular, molecular – substrates and molecule – solvent interactions like ordering and growth, wetting, lubrication, corrosion and adhesion [3].

SAMs of alkanethiols are of interest in a various range of disciplines apart from chemistry: in biology and biochemistry where they are used to study large molecules, viruses and proteins in membrane cells [4], in nanotechnology and semi-conductors [5].

They also have been studied with a wide range of techniques, such as: X-ray Photoelectron spectroscopy [5-10], Infrared spectroscopy [6,8-14], Microscopic techniques (SEM, AFM...) [4,15], Ellipsometry [13,16], computational chemistry [14] and Time of Flight – Second Ion Mass Spectrometry [6,17].

In parallel, the SERS technique has also been widely used to study SAMs and in particular SAMs of alkanethiols and polysulfides [18-21]. However, no published article dealt with a molecule containing both a thiol and a disulfide group. This technique is very useful for the study of interfaces because of the adsorption process induced by the use of SAMs and because of the sensitivity of the technique at the molecule – metal interface.

As seen in chapter 2, alkanethiols also comprise the backbone of the polymers used to seal aircraft fuel tanks. It was thus of interest to study the adsorption process of these thiol molecules as they also contain disulfides. This chapter will deal with the adsorption process of different model molecules and the real molecules used in Aerospace industry as well as their SERS spectra. Finally, a model will be proposed relative to the geometry that the molecule adopts on the metal surface.

2. Experimental

As seen in Chapter 1, the SERS effect needs a roughened substrate to give a fully enhanced spectrum. There are several substrates that can be used to do so, such as a roughened electrode surface, the use of colloids [22] or a roughened metal foil [23]. The aim of this chapter is to study the adsorption mode of the polysulfides used in aerospace industry. These polysulfides are designed to be adsorbed at the surface of a metal surface, thus this work ought to be as much reproductive of the technique used by the industry as possible. For this reason, the choice of using colloids was eliminated straight away. Both roughened electrodes and roughened metal foil were considered. As a potential control was not needed for this work, the roughened electrode system could be eliminated as well.

Various metals are SERS active. According to the literature [24], Cu, Ag, Au, Li, Na, K, In, Pt and Rh have been demonstrated to show a SERS effect. Most commonly, Gold, Silver and Copper are used for their enhancement properties. However, to obtain the best SERS signal the operator has to match the metal used with the laser wavelength.

When an incident radiation hits the metal surface, an energy transfer occurs and some electrons of the valence band are excited to the conduction band. This process is associated with the vibration of the metal atoms, this vibration is called plasmon. This plasmon has an energy that should be matched with the laser wavelength to obtain the best enhancement process. Provided that a red excitation is used, Moskovits calculated that for a Ag sphere with a surface plasmon at ca. 380 nm, the enhancement associated with modes normal and tangential to the surface will be ca. 500:1 [25].

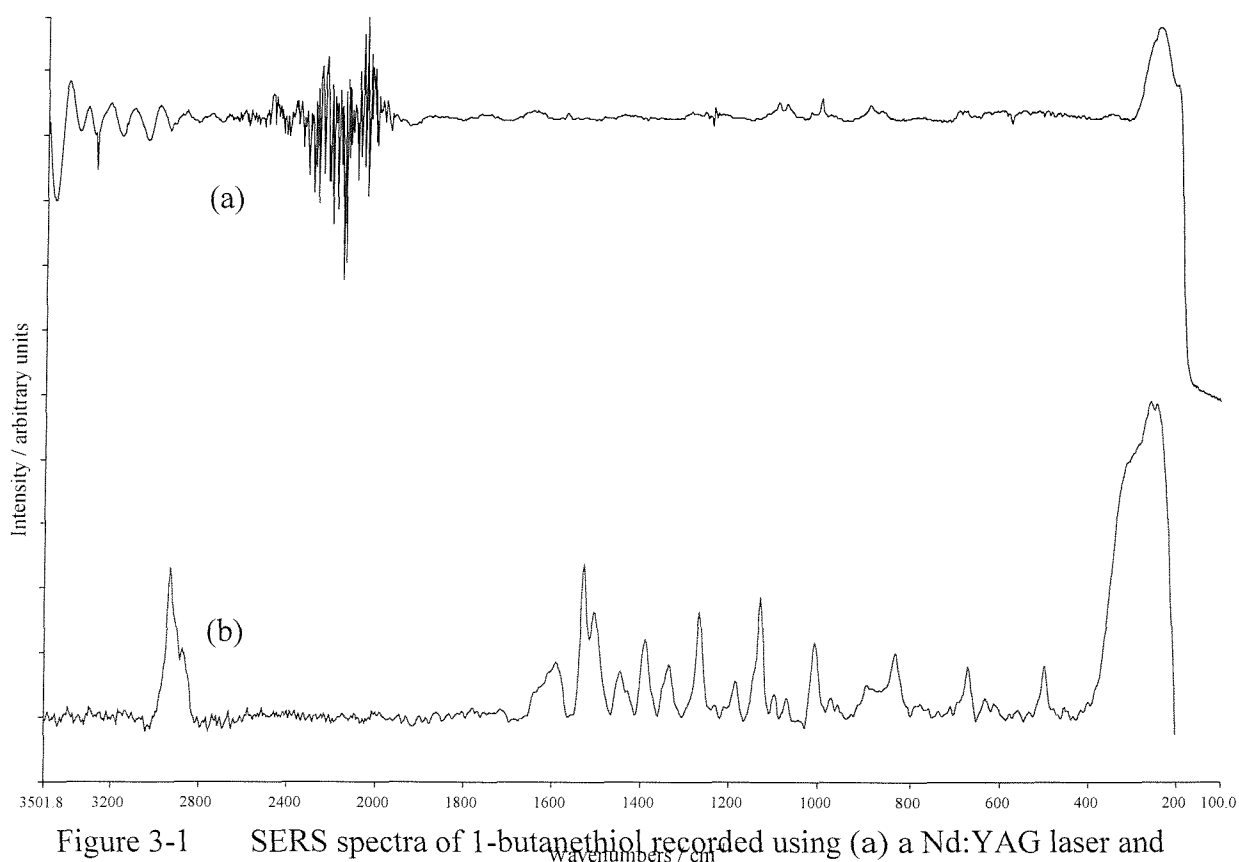


Figure 3-1 SERS spectra of 1-butanethiol recorded using (a) a Nd:YAG laser and (b) a He-Ne laser. The spectra are offset vertically for display purposes.

For real surfaces used in SERS measurements, such as roughened silver foil, the plasmon has been reported to be further in the red [26]. Thus, the closest match for the use of roughened silver foil is a Helium Neon laser that emits at $\lambda=632.8$ nm. An example of the effect of laser wavelength is shown in figure 3.1. The SERS spectrum of 1-butanethiol on AG using a Nd:YAG laser ($\lambda=1064$ nm) and a He-Ne laser ($\lambda=632.8$ nm) are displayed. The Nd:YAG laser is associated with a Perkin Elmer 2000 series FT-Raman spectrometer using an InGaAs detector at room temperature.

One can see that the level of detail is much greater when using the red He-Ne laser. Moreover, the noise induced by the roughening of the foil in the region of 2500 – 2000 cm^{-1} present in the spectrum 2-1 (a) completely disappears when the He-Ne laser is used. Finally, the time factor between both spectra is relatively high; i.e. to record a SERS spectrum using the Nd:YAG laser, 15 hours of scanning are needed, whereas the recording of the same spectrum with the He-Ne laser only used 15 minutes of scanning.

Another reason for using the He-Ne laser is that Raman intensities are proportional to the frequency to the power of 4 (see Equation 1-16 in Chapter 1). Thus, the red laser emitting at $\lambda = 632.8$ nm having a higher frequency than the near infrared one ($\lambda = 1064$ nm), its cross-section is higher and intensities are then enhanced. This might not be noticeable with bulk liquids or solids, but when using a fairly low number of molecules, every little bit helps.

2.1. Roughening process

The process followed to roughen the silver foil was as described in the literature [23]. The silver used was 99.9 % pure and 0.025 mm thick, it was purchased from Aldrich. A solution of HNO_3 (of specific gravity 1.42, 70 % from Fisher) of concentration higher than 3.5 M was prepared. The silver foil was cut into small pieces of 1x1 cm and dipped into the nitric solution for about 10 minutes, until the silver changed from metallic to a milky colour. The pieces of silver were then taken out and rinsed with plenty of water to stop the etching process. They were then dried using absorbing paper and compressed air. They were kept in polyethylene bags until used.

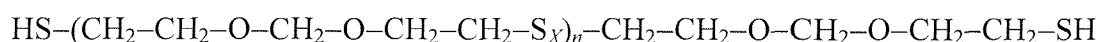
2.2. Molecule adsorption

Once again, the literature process was followed to adsorb the molecules onto the surface of the roughened silver [23]. As only a monolayer of molecule was required to do this study, low concentration solutions have been used. In 1994, Xue *et al* discussed the concentration-dependence of SERS for organic disulfides adsorbed on metals from solutions [27]. They found that the spectral qualities are inversely proportional to the concentration of the applied solutions. Excellent SERS spectral enhancement and perpendicular orientation could be achieved for the sample adsorbed from a 0.0001 M

solution rather than that from a 0.001 M solution. Hence, all the solutions that have been used in this study were of concentration 10^{-4} M or below. As in the etching process the silver was dipped into the studied molecule solution; because of the strong specific interaction between the sulphur atom and the silver surface, the assembly of an adsorbed monolayer at the silver-solution interface was almost spontaneous. Therefore, the silver foil was left in the solution no more than 5 minutes, knowing that, according to Joo et al [28], multiple layers of thiols are rarely formed on a silver surface, contrary to gold surface. After that, the piece of silver was rinsed with the same solvent used in the solution to remove all the physisorbed molecules present on the surface of the silver. Thus, only the chemisorbed molecules were analysed in the SERS experiment.

2.3. Studied molecules

The purpose of this chapter is to study how the sealants used in the aerospace industry bond to the metal surface. These sealants are mainly composed of polysulfides (see Chapter 2) of formula:



Where,

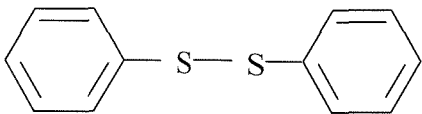

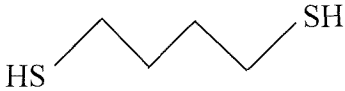


X = average polysulfidity factor and can vary from 1 to 2.2

n = can vary from 6 to 42

This kind of molecule is rather complex and to be able to compare its behaviour when adsorbed, model molecules have also been used in this study. The first model molecule is called diphenyl disulfide and is represented in Table 3-1.

It has been chosen in the first instance for its disulfide group but also because it has been well studied in the literature and its behaviour when adsorbed onto silver is well known. The other model compounds chosen were 1-butanethiol (see below) and a collection of dithiols (see Table 3-1).

Table 3-1 Molecule studied as model molecules

Diphenyl Disulfide	
1-butanethiol	
1,4-butanedithiol	
1,6-hexanedithiol	
1,8-octanedithiol	

1-Butanethiol was an interesting molecule to study because it is terminated by a thiol group, whereas the dithiol contains two thiol groups at each end of the molecule just as in the liquid polysulfide.

For the study of the real molecules, a various range of samples was available. Nine different liquid polymers, courtesy of Morton Thiokol, were on offer as well as the base parts of the sealants used by BAe Systems. In the following table, the details of the liquid polysulfides are displayed:

Table 3-2 Liquid Polysulfides details

Polymer	Molecular Weight / g.mol ⁻¹	Viscosity / Pa.s	Repeat unit <i>n</i> value	Polysulfidity <i>X</i>
LP-31	8000	11.25	42	2.63
LP-2C	4000	4.65	23	2.01
LP-32C	4000	4.65	23	2.01
LP-980C	2600	1.25	15	1.88
LP-3	1000	0.115	6	1.14
LP-33	1000	0.175	6	1.14

As several of these polysulfides have the same degree of polysulfidity, only LP2C and LP33 have been used so they could represent a monosulfide and a disulfide. In addition to these two polysulfides, the base of the sealant, coded Mn1 (see chapter 2 for details) has also been chosen. The polysulfide that is used in this base is not known, because of commercial confidentiality, but is “very likely” to be LP2C or at least a disulfide.

Because the liquid polymers and the sealant base are semi-liquid or even thicker, an extraction process was used to prepare the solutions. About 2 ml of the polysulfide was placed into vials and topped with 20 ml of toluene. To accelerate the process, the vials have been placed into an ultrasonic bath for ~20 minutes. A GC/MS spectrum was then run to check that the dissolution had occurred. These solutions were then diluted, to obtain a low concentration of the analyte in solution [27].

2.4. Spectral conditions

All the spectra displayed in this chapter have been recorded with the Renishaw 2000 System. The laser wavelength was $\lambda=632.8$ nm (He-Ne laser), the objective used for the microscope was a x50 and the system was in confocal mode. The spectra have been recorded in extended condition on a 20 s exposure basis and 2 accumulations, i.e. the grating was exposed to the Raman scattering light for 20 s. The grating used represents 520 cm⁻¹ across the CCD, it thus took about 6 min 30 s to scan the whole spectral range of interest. The spectral range is 3600 to 200 cm⁻¹.

Concerning the reproducibility of the results, several spectra were taken on each plate and the most representative of the others is displayed in this thesis.

3. Results and Discussion

3.1. Diphenyl Disulfide

The adsorption of Diphenyl Disulfide (DDS) studied by SERS is well-known and has been widely reported in the literature [18,29-31]. In Figure 3-1 are displayed the spectra of DDS free and adsorbed on roughened silver.

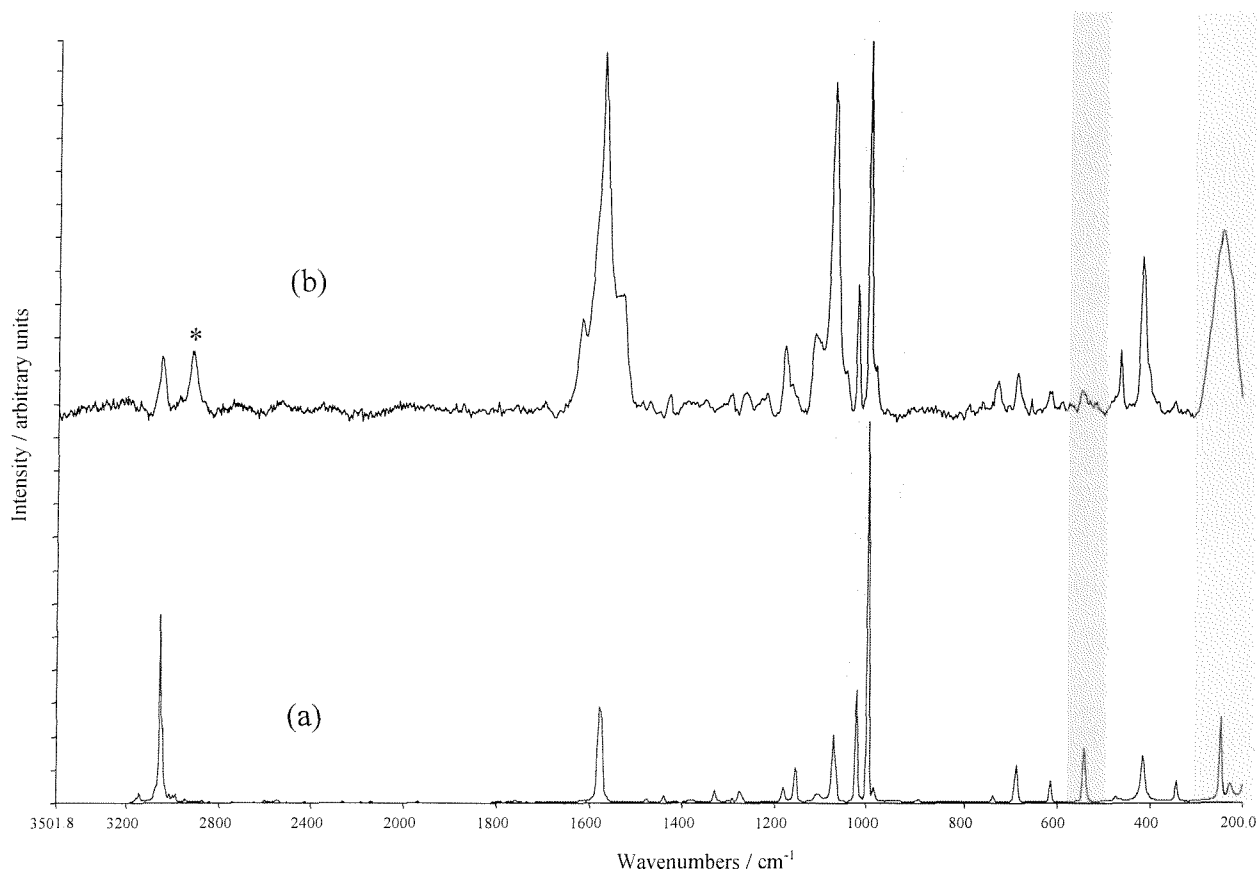


Figure 3-2 Raman spectra of Diphenyl Disulfide (a) free and (b) adsorbed on silver

The SERS spectra presented in figure 3-2 and in the rest of this thesis have been background corrected. An example of the raw and corrected spectrum is displayed in Figure 3-3.

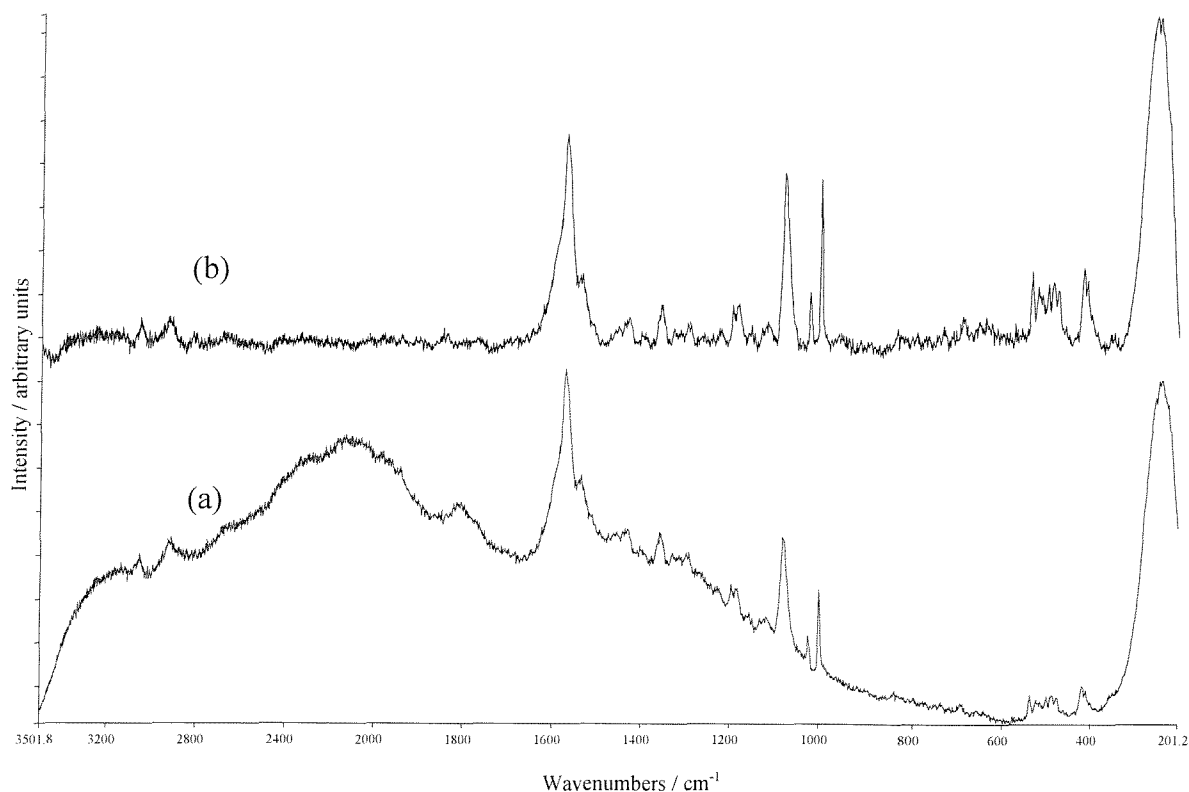


Figure 3-3 Raw (a) and background corrected (b) SERS spectra of diphenyl disulfide.

The first interesting region is centered at 1000 cm^{-1} . The intense Raman lines at 996 and 1576 cm^{-1} are due to the phenyl ring vibrations. The lines at 1070 and 1020 cm^{-1} are characteristic of the Ph – S stretching. When the DDS is adsorbed on silver, the relative intensities of these lines change considerably. The line at 996 cm^{-1} decreases as the peak at 1070 cm^{-1} increases. This implies big changes in the Ph – S bonding when the DDS is deposited on silver.

These changes are confirmed by the peak at 540 cm^{-1} . Present in the free molecule spectrum, this peak almost completely disappears in the SERS spectrum. This band is known to be due to the S – S stretching vibration. Its disappearance means that when the molecule is adsorbed, the S – S bond is broken to allow both sulphur atoms to link with the surface of the metal [32].

The last region of interest for this spectrum is around 200 cm^{-1} . The broad band produced in the SERS spectrum is due to the vibration of the silver atoms. However, a small shoulder is present at 248 cm^{-1} and is due to the stretching of the S – Ag bond.

The band at $\sim 1590\text{ cm}^{-1}$ is also greatly enhanced when the DDS is adsorbed onto the surface. This band corresponds to the C = C stretches in the benzene ring and as a result of the adsorption, it is easily understandable that these modes are greatly disturbed, and hence enhanced.

To summarise, when the diphenyl disulfide is adsorbed on a metal, the S – S bond breaks to allow both of the sulphur atoms to bond with the metal surface, hence the important changes in intensities in the SERS spectrum.

The band marked with a star on the SERS spectrum was, at first, thought to be due to some impurities in the solution. However, after some literature research, the same effect seemed to happen in the SERS spectra of molecules treated with styrene oxide. Dai and co-workers [33] attributed the band at 2930 cm^{-1} to the CH stretching of $-\text{CH}_2-\text{O}-\text{CH}_2$. The DDS studied here was dissolved in acetone at a relatively low concentration (typically 10^{-4} M), it is then not unlikely that some DDS molecules interacted with some molecules of the solvent and hence the new band in the spectrum. However, in terms of the development of our understanding of the bonding of the DDS to the silver surface, this interaction and the resulting band can be largely ignored.

3.2. 1-Butanethiol

As in the case of DDS, alkanethiols have been extensively studied in the literature [6,7,14,31,34-36] and especially butanethiols [19,37-39]. The free and adsorbed spectra of 1-butanethiol are displayed in Figure 3-4.

In their article, Joo and co-workers [38] explain extensively the SERS spectrum of 1-butanethiol. The vibrational assignment of 1-butanethiol is relatively complicated due to the possible presence of several conformational isomers around the C(1) – C(2), C(2) – C(3) and S – C(1) bonds; i.e. since the rotational isomers with trans and gauche conformations are possible for each bond, various kind of spectroscopically distinct conformers may be present in the liquid and adsorbed states. The spectrum of the liquid state gives an average fingerprint of all the molecules present in this state because of the freedom of movement. However, when adsorbed, the molecules cannot move anymore

and different conformations can be adsorbed at the same time. This is the reason why the following SERS spectrum is rather complex.

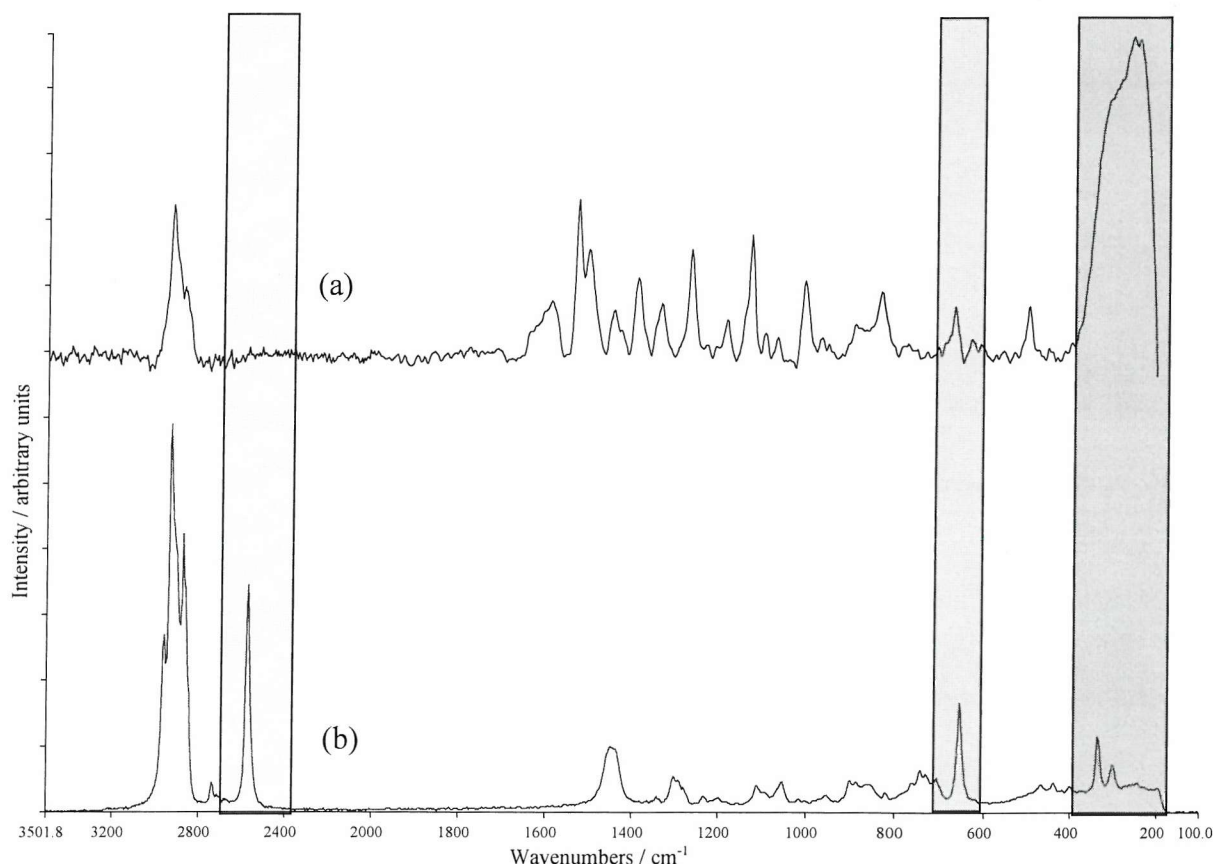


Figure 3-4 SERS (a) and neat (b) spectra of 1-butanethiol

The bands between 1600 and 1000 cm^{-1} are all associated with the vibrations of various CH modes either in a *trans* or in a *gauche* conformation. Nevertheless, three regions of the spectrum are interesting. The first region contains the S – H stretching vibration. This particular vibration occurs around 2570 cm^{-1} . This band, which is present and intense in the neat spectrum, completely disappears in the adsorbed spectrum. This is due to the adsorption process; i.e. the hydrogen atom is removed (probably hydrolysed in solution) to allow the sulphur atom to bond with the surface, hence, the disappearance of the S – H vibration in the adsorbed spectrum.

The spectral region between 700 and 600 cm^{-1} , contains the C – S stretching vibration. Present at 655 cm^{-1} in the neat spectrum, it is shifted down to 626 cm^{-1} . This shift can be explained by the adsorption process and the disruption of the associated electronic cloud.



Finally, the broad band at 210 cm^{-1} in the adsorbed spectrum corresponds, as for the DDS, to the silver atom vibrations. However, this time the shoulder emerging at 250 cm^{-1} can be easily observed and associated with the S – Ag stretching vibration, as explained in the DDS section.

To summarise, when the 1-butanethiol is adsorbed on the silver surface, the ending –SH group loses the hydrogen to allow the sulphur atom to bond with the surface of the metal. This bonding creates a disruption of the electronic cloud (see the SERS effect in chapter 1) and hence the line associated with the stretching of the C – S bond is shifted.

3.3. Dithiols collection

In Figure 3-6 to Figure 3-9, the spectra of 1,4-butanedithiol, 1,6-hexanedithiol and 1,8-octanedithiol are displayed. They all show the spectrum of the compound free (liquid) at the bottom and adsorbed on silver foil at the top.

The first highlight of the spectra below is the S – H stretching region ($\sim 2570\text{ cm}^{-1}$). In the case of 1-butanethiol, the molecule was bonding to the metal through the sulphur atom. In this case, two sites are available for the linking of the molecule to the metal surface. In their article, Joo et al [28] report the case of 1,4 benzenedithiol. They used both gold and silver surfaces to adsorb the molecule. When adsorbed on gold the molecule adopts a tilted conformation on the surface, whereas with silver, the molecule adsorbs via both sulphur atoms and is parallel to the surface (see Figure 3-5).

In this study reported in this chapter, however, the band at $\sim 2570\text{ cm}^{-1}$ does not disappear when the dithiols are adsorbed onto the silver surface. See the following figures (3-6 to 3-8).

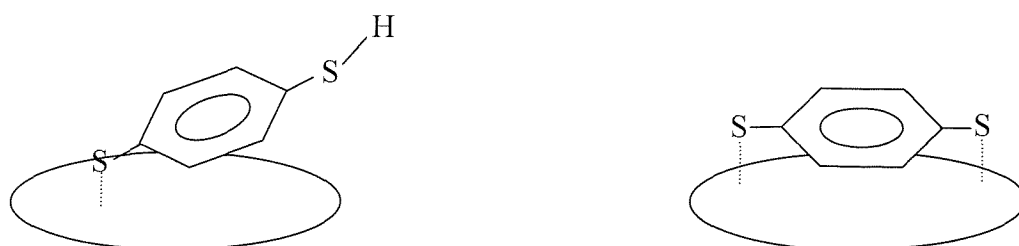


Figure 3-5 Plausible adsorbate structures of 1,4-benzodithiol on Gold (a) and on silver (b), according to Joo et al [28].

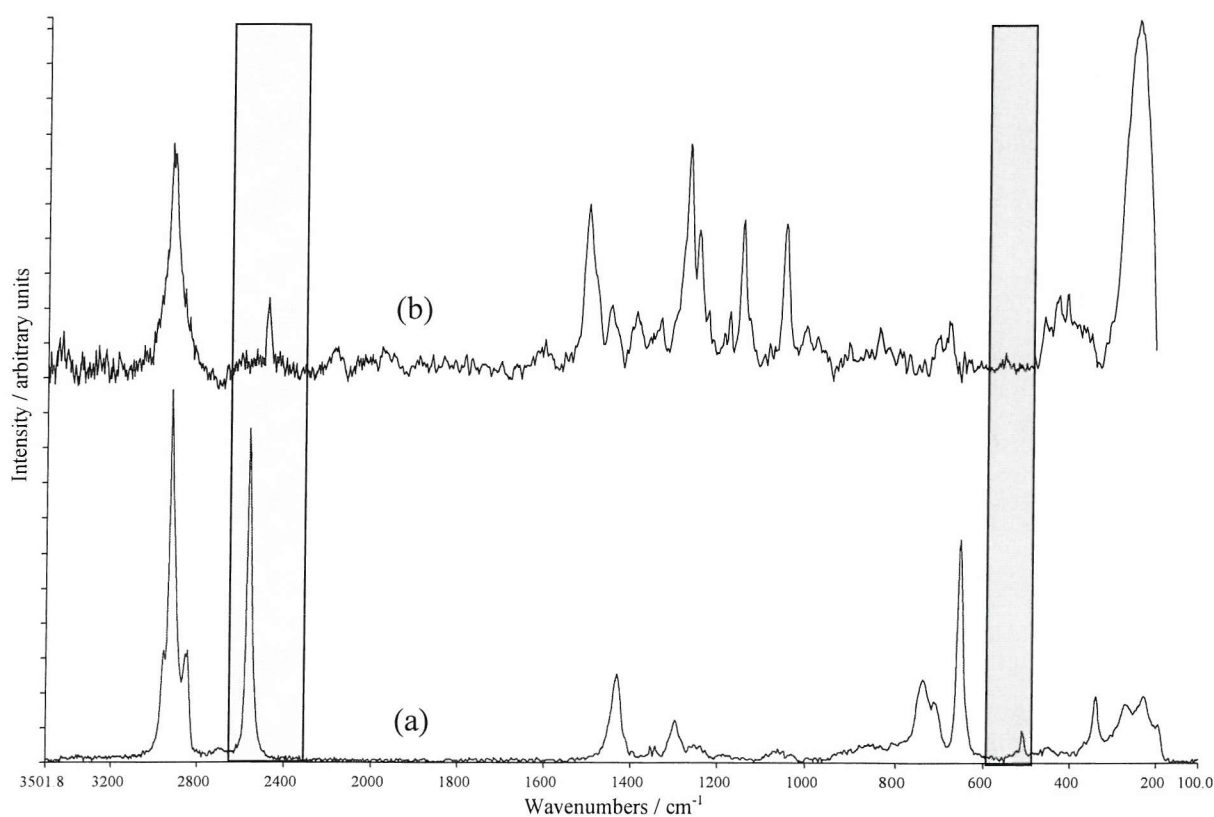


Figure 3-6 Spectra of 1,4-butanedithiol, neat (a) and adsorbed on silver (b)

The S – H peak intensity decreases with the number of carbon atoms in the chain. This could be due to two different effects. The first one is in the limit that the molecule are close packed and standing on the surface of the metal slightly tilted ($\sim 20^\circ$) from the normal to the surface, as described before in the literature [10]. In this hypothesis, one hydrogen atom disappears to allow the S atom to bond with the metal surface and the other \sim SH group is then further from the surface and thus with the number of carbons increasing, it benefits less and less from the SERS effect.

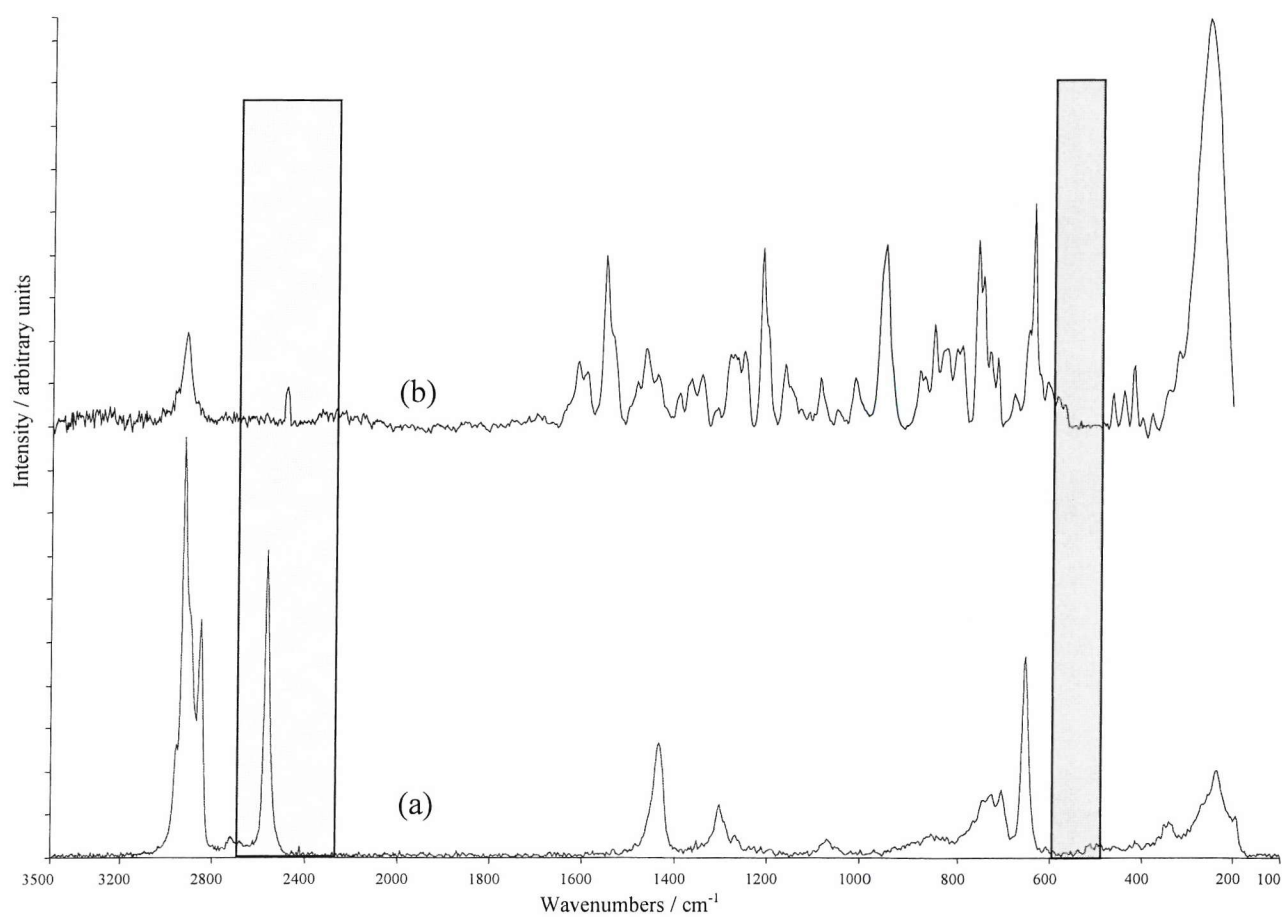


Figure 3-7 Spectra of 1,6-hexanedithiol, neat (a) and adsorbed on silver (b)

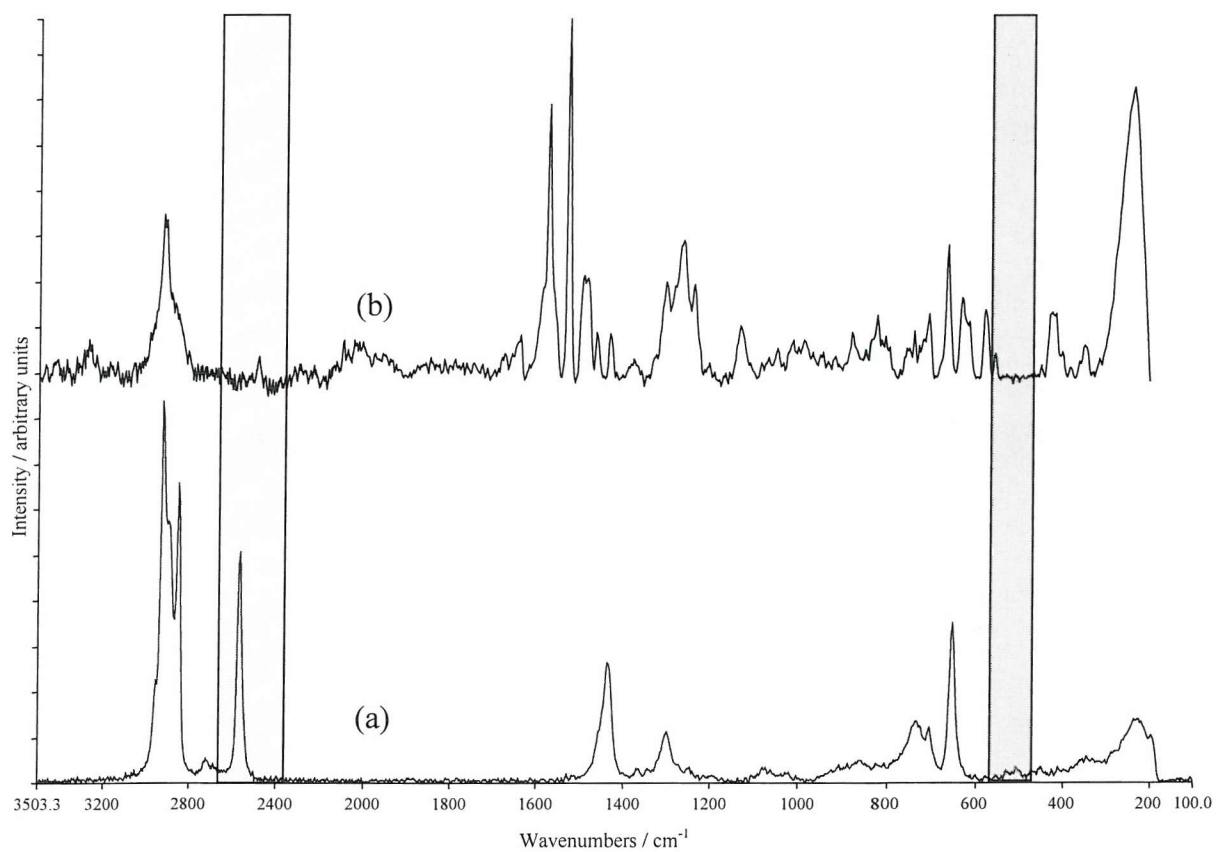


Figure 3-8 Spectra of 1,8-octanedithiol, neat (a) and adsorbed on silver (b)

In their article, Tsen and Sun [40], discuss the distance dependence of SAM of thiols in SERS. They first report the calculated theoretical model from Gertsen and Nitzan [41](GN model), which is displayed below:

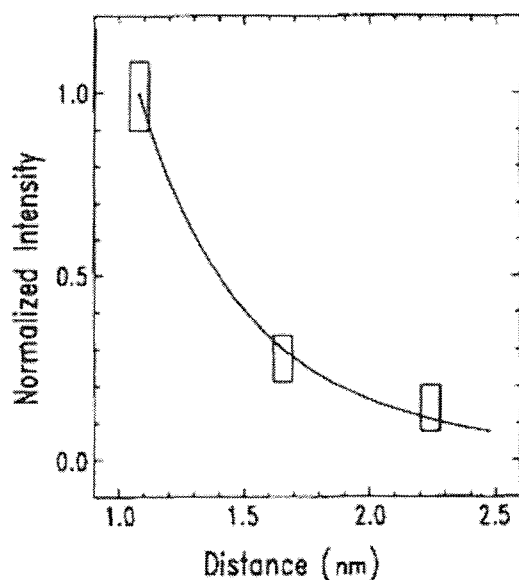


Figure 3-9 Normalised SERS enhancement factor on silver vs. distance plot. Reproduced from Tsen and Sun [40].

This curve shows that at a distance greater than 2.5 nm the SERS enhancement is almost equal to zero and it is decreasing exponentially with the distance from the surface. The authors conclude, according to their results, that the decay could be at a rate 10 times larger than those reported before. However, they also state that their conclusion needs to be verified with more data points. Unfortunately, these authors have not published further work in this area. However, in 1999, Kenedy et al. [42] published an article that confirms the theory of Gertsen and Nitzan. However, the curve used in Figure 3-9 is not representative of the surface that has been used in this work. Thus, it has been decided to make the same kind of graph, using the data presented here. The intensity of the S – H vibration will be ratioed to the silver peak taken as the internal reference. The results are presented in Table 3-3 and in Figure 3-10.

Table 3-3 Ratio of the S – H peak height over the silver peak height

Compound	S – H peak height	Silver peak height	Ratio
Butanedithiol	313.41	720.92	0.44
Hexanedithiol	412.21	1873.70	0.22
Octanedithiol	250.53	1500.74	0.14

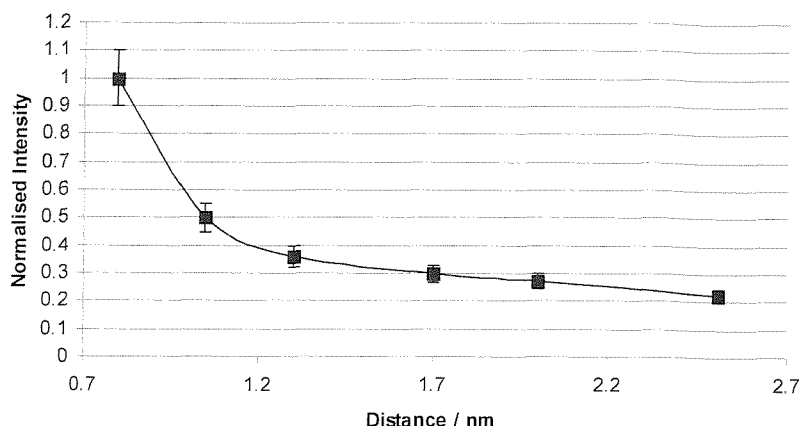


Figure 3-10 Normalised Intensity of the SERS effect on the surface used in this project as a function of the distance from the surface. (The first three values are calculated from the spectra whereas the three others have been extrapolated).

In the following table, the chain length of the different thiol used for this study are listed (see Table 3-3). The bond length used to calculate the total length have been found in the CRC handbook [40] of chemistry and are as follow: $l(\text{C-C}) = 154 \text{ pm}$, $l(\text{C-S}) = 179 \text{ pm}$. The assumption was also made that the molecule was stretched on the surface, with an angle between each atom of 109.28° .

Table 3-4 Bond length of the various thiols used in this study

Compound	Number of Carbons	Chain length in nm
Butanethiol	4	0.649
1,4-butanedithiol	4	0.795
1,6-hexanedithiol	6	1.047
1,8-octanedithiol	8	1.298

In all the cases, the total length of the chain is smaller than the limit of 2.5 nm.

However, as can be seen in picture 6-9, the difference of intensity between 1 nm and 1.3 nm is dramatic and can easily explain the decrease of intensity of the S-H peak in the SERS spectra.

The second idea is still within the close packed monolayer hypothesis, but in this case, instead of standing straight, the longest molecules would loop to allow both $\sim\text{SH}$ groups to bond with the silver atoms. Hence the decreasing in relative intensity of the S – H stretching peak. This hypothesis would join the theory of Joo et al [28], but in all the literature, alkanedithiols stand upright on the surface of metals. The molecule studied by Joo et al contains a benzene ring as the alkane chain. However, benzene is known to be an electron donor (nucleophile) where Silver with its $4d^{10} 5s^1$ electronic structure is an acceptor (electrophile). Hence, they are likely to attract each other and force the molecule to lie parallel to the surface, making ideal conditions to create a second S-Ag bond.

In the figure 3-11 is summarised the two hypotheses explained above.

To conclude on this part of the spectrum, the first hypothesis is the most plausible. The thiol and dithiol molecules are closely packed on the surface, probably with an angle of $\sim 20^\circ$. The decrease of the SH bond vibration intensity is probably due to the distance effect in SERS spectroscopy.

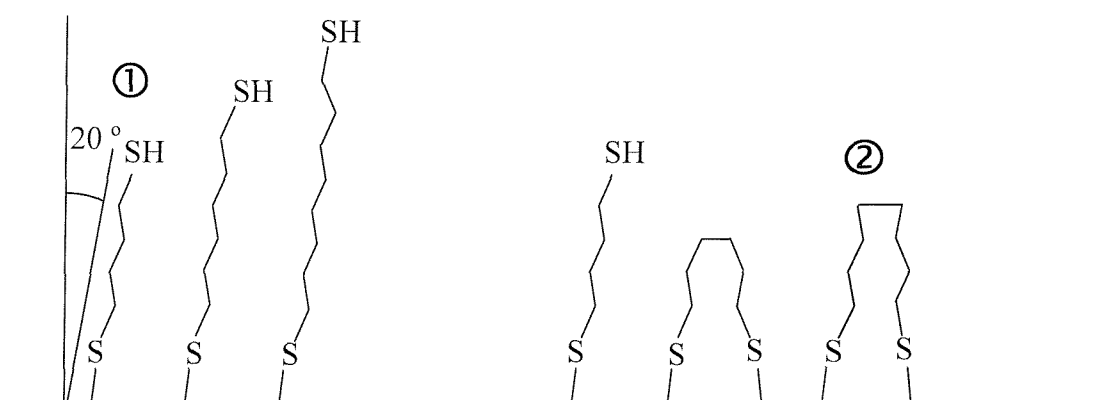


Figure 3-11 The first hypothesis (molecule close packed tilted from the normal) is represented in part ① and the second hypothesis (longer molecules looping) is in part ② of the figure

The other highlighted region in these spectra corresponds to the S – S stretching region ($550 - 500 \text{ cm}^{-1}$). This region has been brought forward because of the absence of a peak in the SERS spectra. According to Joo, Han and Kim [35], over-exposure of the substrate to the solution can lead to the formation of a multilayer of disulfide. However, they report that it is very likely that disulfides would form some polysulfides forms when adsorbing on the substrate in a multilayer frame. The absence of peak in the spectra displayed above proves that only a monolayer had been adsorbed on the surface of the metal, as the distance of a first S – S bond would still be in the range of the SERS effect (see table 3-3).

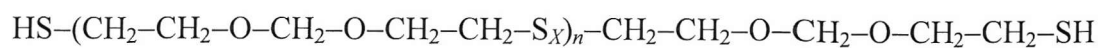
Finally, the rest of the SERS spectrum is quite complicated and a lot of bands that do not appear in the neat spectrum are present. As explained before, alkanethiols show several conformational isomers. The neat spectrum is an average picture of the bulk in which the thiols are present in a liquid state. When the molecules are adsorbed at the surface of the metal, no one can predict which isomer is going to be adsorbed at which place. The size of the laser spot is approximately 2.5 micron in diameter, hence an area of 4900 nm^2 . A full monolayer coverage of alkyl thiol represents $\sim 10^{14}$ molecules / cm^2 . Hence, about 4900 molecules are illuminated during the process. Therefore, a lot of different conformations are possibly illuminated by the laser spot and the result is a complex spectrum.

To summarise, the first hypothesis in which the molecules are close packed on the surface, tilted with an angle of $\sim 20^\circ$ from the normal has been adopted. Also, only one monolayer of dithiol is adsorbed onto the surface of silver. But a lot of different conformations are adsorbed and the arbitrary illumination by the laser gives a complex spectrum of the adsorbed species.

3.4. The sealant molecules

Three molecules have been studied, as stated before. The first one is LP2C, a liquid polysulfide containing an average of 2 sulphur atom in the monomer. The second is LP33, another liquid polymer containing an average of 1 sulphur atom in the monomer. The last molecule is the backbone of the base used for the sealant Mn1.

The molecule is represented below:



Where,

X = polysulfidity factor and can vary from 1 to 2.2

n = can vary from 6 to 42

The spectra displayed below show each molecule neat as a liquid polymer and adsorbed on silver.

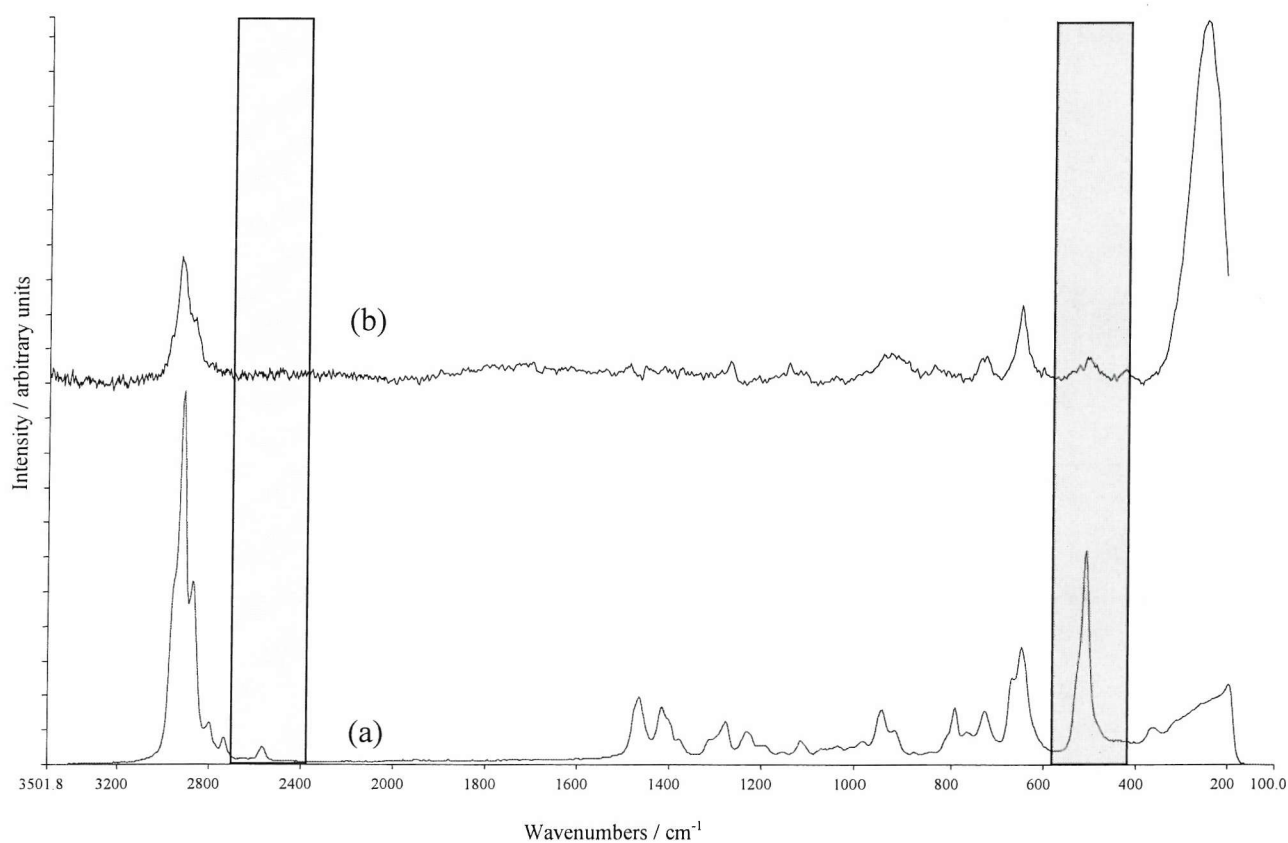


Figure 3-12 Neat (a) and SERS on silver (b) spectra of Liquid Polymer LP2C

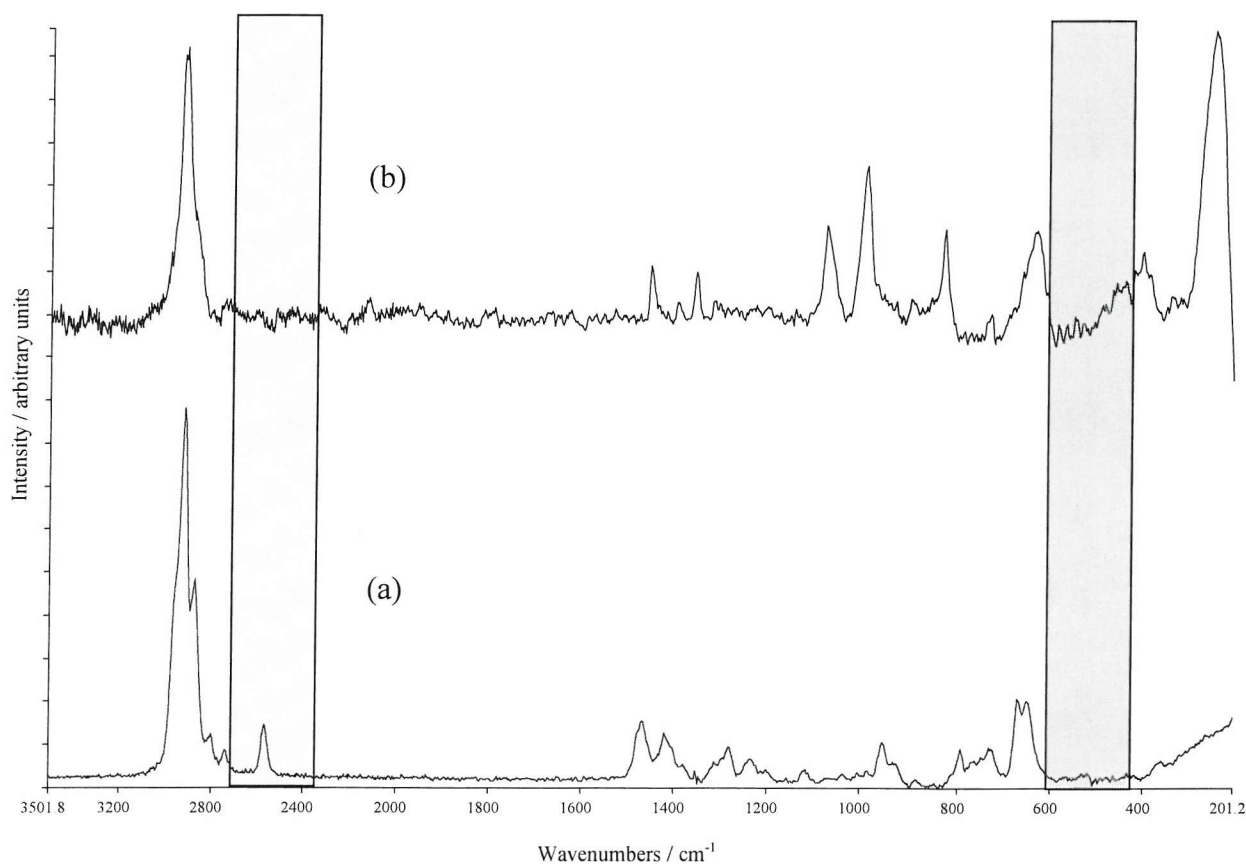


Figure 3-13 Neat (a) and SERS on silver (b) spectra of Liquid Polymer LP33

The main features of the two spectra above are as follows:

- When adsorbed on the metal surface, both of the liquid polymers adsorb dissociatively, i.e. one or both of the hydrogen atoms is removed to allow the corresponding sulphur atom to bond with the surface of the metal. This can be observed in the total disappearance of the \sim SH stretching peak in the SERS spectrum.
- The other interesting feature of these spectra is the S – S stretching peak around $550 - 500 \text{ cm}^{-1}$. It is present in both neat and adsorbed spectra of LP2C. However, totally absent in the LP33 spectra. This is due to the polysulfidity factors of both these polymers: LP2C contains an average of 2 sulphur atoms in the middle of the monomer, whereas LP33 contains an average of ~ 1 .

- As usual, in both spectra the silver – sulphur stretching band around 260 cm^{-1} is present.

The backbone of the sealant is contained in the base of the two part mix (see Chapter 2) and because it contains more than the polysulfide itself, the other components could have masked the interesting peaks. Therefore, the base has been mixed in toluene to extract the polysulfide. The spectrum of the resulting solution would have been dominated by the peaks of toluene, thus the solvent was removed by rotary evaporation so that only the polysulfide remained. The spectrum of the remaining oil has then been taken and is presented as the neat spectrum in Figure 3-14.

Once again, two major features arise from this last spectrum:

- No band is present in the S – H stretching region ($\sim 2570\text{ cm}^{-1}$).
- A strong band can be observed in the S – S stretching region ($500 - 550\text{ cm}^{-1}$).
- The Ag – S band is seen at $\sim 260\text{ cm}^{-1}$.

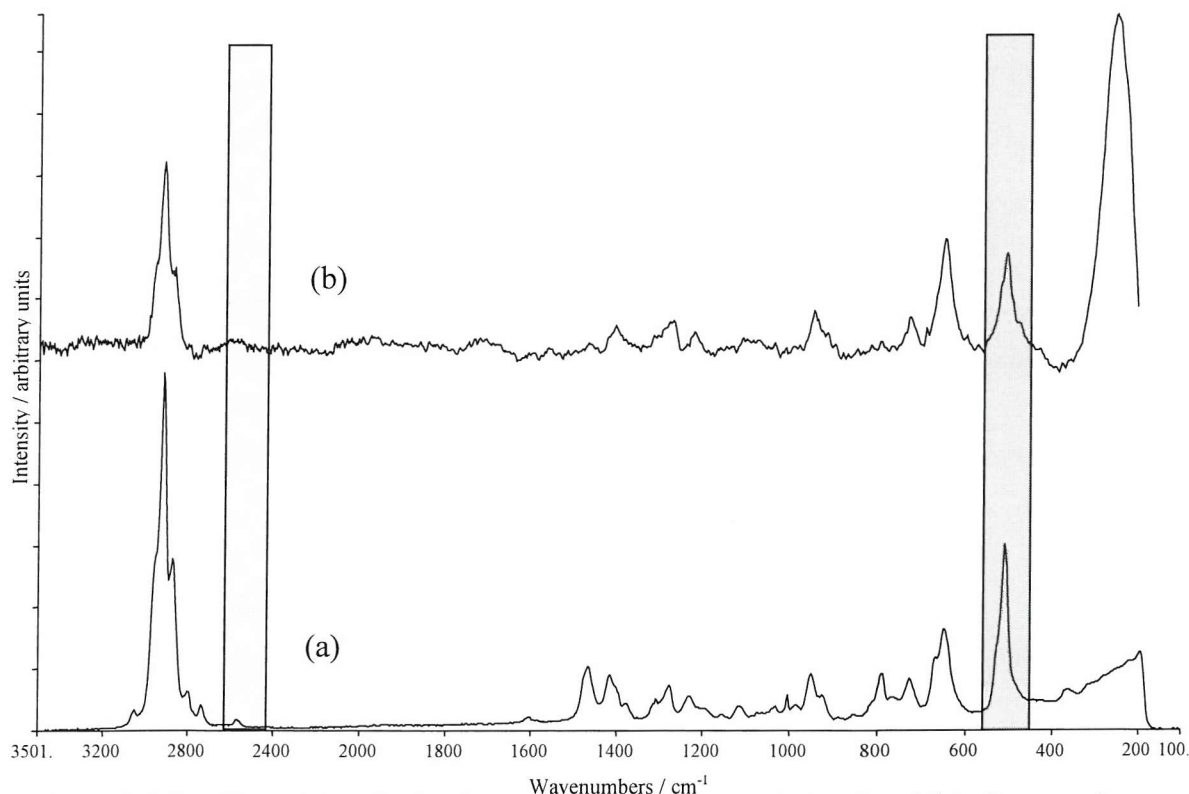


Figure 3-14 Neat (a) and adsorbed (b) spectra of extracted polysulfide from sealant base coded Mn1

As described before, several possibilities can occur when adsorbing a thiol or a disulfide on silver foil. In the case of the thiols, they adsorb dissociatively; the hydrogen atom is removed (passing into the solution) to allow the sulphur atom to bind with one metal atom. For the dithiols, two phenomena can occur: either only one S – H bond is broken and the molecule is standing straight in a close pack monolayer at the surface of the metal, or both hydrogen atoms are removed to allow the sulphur atoms to bind and thus bending the molecule to make a loop. When studying the diphenyl disulfide, the conclusion that could be drawn was that the S – S bond was breaking and the two remaining parts of the molecule were binding to the surface via the sulphur atom.

In the study of the sealants, the molecule contained two terminal ~SH groups and a S – S group. The two process described above were then competing to bind the molecule to the surface of the silver metal. When looking at the dissociation energies [43], the S – H bond is easier to break than the S – S bond;

$D_{298}^0(\text{S-H}) = 344.3 \pm 12.1 \text{ kJ.mol}^{-1}$ and $D_{298}^0(\text{S-S}) = 425.01 \pm 0.04 \text{ kJ.mol}^{-1}$. This is confirmed when observing the SERS spectra. For LP2C and LP33 (containing respectively 2 and 1 sulphur atoms in the middle of the monomer), it is clear that the molecule is not breaking any S – S bonds but binds to the surface via the S – H group. In effect, the two liquid polymers show no sign at all of S – H stretching vibrations remaining in the SERS spectra but an Ag – S stretching vibration is present in both. However, the S – S bond remains in the SERS spectrum of adsorbed LP2C.

The spectra of the liquid polymer contained in the Mn1 base displays the same kind of results: the S – H vibration is absent in the SERS spectrum and the S – S stretching vibration is present and stronger than in the spectra of LP2C. However, as discussed in chapter two, several species were extracted when the base is in contact with the toluene. The most important one is: $\text{CH}_3\text{CH}_2\text{OCH}_2\text{OCH}_2\text{CH}_2\text{SSH}$, present at a retention time of 10.36 min in the GC spectra. This species can explain the high intensity of the S – S stretching band in the spectrum. The species is once again adsorbed on the surface via the S – H group: the molecule loses the hydrogen atom and a covalent bond is then created between the metal surface and the sulphur atom, hence the disappearance of the S – H stretching vibration and the emergence of the

Ag – S vibration. However, the S – S group is now positioned very close to the surface of the metal and the bond intensity is greater because of the SERS effect. Therefore, the S – S stretching vibration is amplified comparatively to the LP2C SERS spectra in which the S – S group is further away from the surface (see table 3-4)

Table 3-5 Distance of the S-S bond to the surface for different compounds

Compound	Distance of the S-S bond from the surface (nm)
LP2C	1.242
Extracted base	0.208

According to Figure 3-10, the decrease in SERS effect between those two compounds would be of a factor of ~70 %, which confirms the experimental details.

The process of adsorption of the Liquid Polymers and disulfides onto a metallic surface is now clear. However, the SERS results presented in this chapter do not give enough information about the orientation of the molecule on the surface. It has been shown previously that the S – H vibration disappeared from the adsorbed molecule spectra. This could be due to two different effects:

- First, the molecule is bonding via its two ends, creating two Ag – S bonds. In this case, No S – H vibration would then occur in the SERS spectrum.
- The second hypothesis is that the molecule is adsorbed in a close packed monolayer and standing straight on the surface of the metal. If the molecule was standing straight on the surface, the second SH group would be at a distance of 2.736 nm, which is too far to benefit from the SERS effect.

The following figure (Figure 3-15) shows the two hypotheses represented.

These two hypotheses are both possible. In 1992, Pemberton *et al.* proposed a simple method for determination of orientation of adsorbed organics of low symmetry using

SERS [44]. They used a curve fitting program on the CH_3 and CH_2 stretching vibration bands to determine the relative positioning of these groups in the molecule.

Nevertheless, this kind of technique requires a nice, smooth and highly resolved spectrum. Thus, this could not have been applied to the spectra recorded for this study, because, as explained before, it was not possible to accumulate the spectra due to the luminescence effect that creates an increase of the background noise but not of the peaks themselves.

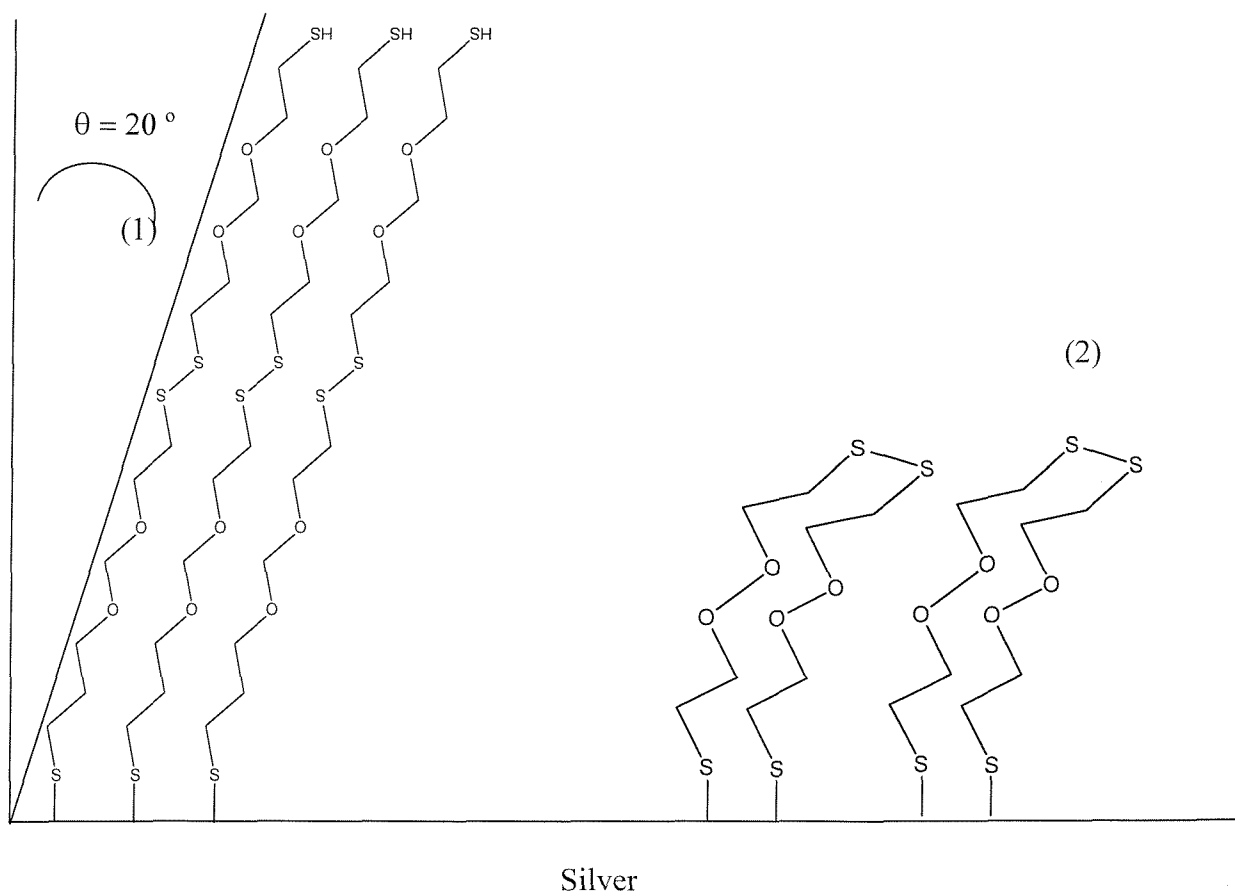


Figure 3-15 The two hypotheses presented above, (1) a close packed monolayer of polysulfides standing straight and (2) a monolayer of bent polysulfide, binding via both sulphur ending atoms.

Another option to try to determine the geometry of the molecules is to run a simulation program. With the help of this kind of software, it is possible to calculate the energy required by both the straight and the curved molecules. This has been done using a software called Macromodel. The molecule was entered into the program using the sketch pad. The AMBER* [45,46] force field was used. The

molecule was stretched using a restraint, and then minimised in the absence of the restraint. The results are the following: the total energy required for the molecule to stand straight is $E = 82.97 \text{ kJ.mol}^{-1}$. For the folded form, the ends of the molecule were restrained to a short distance (5 \AA) apart, minimised, and then molecular dynamics was performed at 600 K for 10 ps to relax the structure. The restraint was then removed, and the molecule minimised to yield the following total energy $E = 41.82 \text{ kJ.mol}^{-1}$. Both of these calculations have been made as a gas phase environment, hence no neighbouring molecules were included. However, against all odds, the looped molecule seems to be more stable than the straight one. One could think that the steric encumbrance due to the folding of the molecule on itself would make the energy increase dramatically. Nonetheless, the molecule contains two oxygen atoms and four sulphur atoms. These atoms present in the group 16 of the periodic table have the ability of creating hydrogen bonding. There are also numerous of Van der Waals interactions created because of the folding of the molecule that stabilises its energy.

As the results of the calculation have been conducted in a gas phase environment, some conjectures should be made on the monolayer packing. When considering the molecule standing straight on the surface of the metal, closed packed, the same kind of interactions (hydrogen bonding and Van der Waals) will appear between the molecules. This will reduce the energy of the molecule. However, another important factor is the energy that the molecule will gain by linking the second sulphur atom to the surface. In effect, the typical enthalpy of a silver – sulphur bond is $\Delta H_{298}^0 = 217.1 \text{ kJ.mol}^{-1}$ [47]. Considering this and all the interaction intra-molecular happening when the molecule is folding, it becomes clear that the energy gain and the stabilisation eventually acquired by the molecule makes the looped conformation more favourable.

4. Conclusion

The aim of this chapter was to study the adhesion process of the polysulfide sealants used in Aerospace industry. These sealants are composed of two ending thiol groups and a middle disulfide group. The SERS technique has been chosen for this study because it gives information about the interface between the molecule and the metal surface.

After considering several model molecules composed of disulfides, thiols and dithiols, it was established that the bonding was happening through the sulphur atom, either through the breaking of the S – H or the breaking of the S – S bond. In any case, a silver – sulphur bond was created. However, the liquid polysulfide contains two ~SH group and a ~SS~ group. Thus, the SERS technique helped in deciding that the molecule was not breaking in the middle but was bonding via the terminal sulphur atoms.

Finally, one unknown was remaining: the orientation of the molecule onto the metal surface. The SERS spectra showed no S – H vibration. This could have been a distance effect due to the molecule standing straight on the metal or to the linking of both ending sulphur atoms. Some recent publications also showed that it was likely that the alkanethiols would lay on the surface of silver and stand on the surface of gold. Nevertheless, the molecule used in this study was an aromatic thiol that was probably laying on the surface because of the affinity between the benzyl ring and the silver. However, the calculation showed that the energy required for the molecule to stand straight was greater than the of the folded molecule. Thus it is very likely that the molecule is folding and has both sulphur ending atoms linked to the surface of metal.

These results will be useful for the aerospace industry as they wish to improve the new formulation of sealants. The strength of the sealant joint is given by the cross-linking factor. This cross-linking is very likely to happen at the S – S bond. On the other hand, the percentage of ~SH ending groups is thus also important to reinforce the adhesion of these joints to the metal wing.

Nonetheless, other methods are used to increase the adhesion of the sealants. The most important one is the use of adhesion promoters: they are coupling agents that promote the adhesion of the joint. The way they really act on the polysulfide to reinforce the adhesion is still not completely understood. Some think that the coupling agent works as a retardant that slows down the curing of the sealant and that this increases the cross-linking ratio. Others think it actually bonds with the sealant. These assumptions will be discussed in the next chapter.

5. References

- [1] Bigelow, W. C.; Pickett, D. L.; Zisman, W. A. *Journal of Colloid Interface Science* **1946**, *1*, 513.
- [2] Nuzzo, R. G.; Allara, D. L. *Journal of American Chemical Society* **1983**, *105*.
- [3] Ulman, A. *Chemical Reviews* **1996**, *96*, 1533.
- [4] Kumar, A.; Abbott, N. L.; Enoch, K.; Biebuyck, H. A.; Whitesides, G. M. *Accounts of Chemical Research* **1995**, *29*, 219.
- [5] Bain, C. D.; Troughton, E. B.; Tao, Y.-T.; Evall, J.; Whitesides, G. M.; Nuzzo, R. G. *Journal of American Chemical Society* **1989**, *111*, 321.
- [6] Beulen, M. W. J.; Huisman, B. H.; vanderHeijden, P. A.; vanVeggel, F.; Simons, M. G.; Biemond, E.; deLange, P. J.; Reinhoudt, D. N. *Langmuir* **1996**, *12*, 6170.
- [7] Troughton, E. B.; Bain, C. D.; Whitesides, G. M.; Nuzzo, R. G.; Allara, D. L.; Porter, M. D. *Langmuir* **1988**, *4*, 365.
- [8] Zhong, C. J.; Brush, R. C.; Anderegg, J.; Porter, M. D. *Langmuir* **1999**, *15*, 518.
- [9] Nuzzo, R. G.; Dubois, L. H.; Allara, D. L. *Journal of American Chemical Society* **1990**, *112*, 558.
- [10] Tour, J. M.; Jones, L.; Pearson, D. L.; Lamba, J. J. S.; Burgin, T. P.; Whitesides, G. M.; Allara, D. L.; Parikh, A. N.; Atre, S. V. *Journal of American Chemical Society* **1995**, *117*, 9529.
- [11] Zhang, M. S.; Anderson, M. R. *Langmuir* **1994**, *10*, 2807.
- [12] Troughton, E. B.; Bain, C. D.; Whitesides, G. M. *Langmuir* **1988**, *4*, 365.
- [13] Porter, M. D.; Bright, T. B.; Allara, D. L.; Chidsey, E. D. *Journal of American Chemical Society* **1987**, *109*, 3559.
- [14] Ulman, A.; Eilers, J. E.; Tillman, N. *Langmuir* **1989**, *5*, 1147.
- [15] Schonherr, H.; Vancso, G. J.; Huisman, B. H.; vanVeggel, F.; Reinhoudt, D. N. *Langmuir* **1997**, *13*, 1567.
- [16] Whitesides, G. M.; Laibinis, P. E. *Langmuir* **1990**, *6*, 87.

- [17] Hagenhoff, B.; Benninghoven, A.; Spinke, J.; Liley, M.; Knoll, W. *Langmuir* **1993**, *9*, 1622.
- [18] Bandyopadhyay, K.; Vijayamohanan, K.; Venkataramanan, M.; Pradeep, T. *Langmuir* **1999**, *15*, 5314.
- [19] Bryant, M. A.; Pemberton, J. E. *Journal of the American Chemical Society* **1991**, *113*, 3629.
- [20] Merklin, G. T.; He, L. T.; Griffiths, P. R. *Applied Spectroscopy* **1999**, *53*, 1448.
- [21] Li, F. T.; Lu, Y.; Xue, G. *Applied Spectroscopy* **1997**, *51*, 804.
- [22] Sutherland, W. S.; Winefordner, J. D. *Journal of Raman Spectroscopy* **1991**, *22*, 541.
- [23] Lu, Y.; Xue, G.; Dong, J. *Applied Surface Science* **1993**, *68*, 485.
- [24] Moskovits, M. *Reviews of Modern Physics* **1985**, *57*, 783.
- [25] Moskovits, M.; Suh, J. S. *Journal of Physical Chemistry* **1984**, *88*, 5526.
- [26] Bryant, M. A.; Pemberton, J. E. *Langmuir* **1990**, *6*, 751.
- [27] Xue, G.; Lu, Y.; Gao, J. *Applied Surface Science* **1994**, *78*, 11.
- [28] Joo, S. W.; Han, S. W.; Kim, K. *Journal of colloid and interface Science* **2001**, *240*, 391.
- [29] Dong, J.; Sheng, Z. H.; Xue, G. *Spectrochimica Acta Part a-Molecular and Biomolecular Spectroscopy* **1995**, *51*, 1031.
- [30] Huang, F. K.; Horton, R. C.; Myles, D. C.; Garrell, R. L. *Langmuir* **1998**, *14*, 4802.
- [31] Szafranski, C. A.; Tanner, W.; Laibinis, P. E.; Garrell, R. L. *Langmuir* **1998**, *14*, 3570.
- [32] Cymerman, J.; Willis, J. *Journal of the Chemical Society* **1951**, 1332.
- [33] Dai, Q. P.; Xue, C. C.; Xue, G.; Jiang, L. X. *Journal of Adhesion Science and Technology* **1995**, *9*, 1465.
- [34] Bain, C. D.; Biebuyck, H. A.; Whitesides, G. M. *Langmuir* **1989**, *5*, 723.
- [35] Joo, S. W.; Han, S. W.; Kim, K. *Journal of Physical Chemistry B* **2000**, *104*, 6218.
- [36] Joo, S. W.; Han, S. W.; Kim, K. *Langmuir* **2000**, *16*, 5391.
- [37] Joo, T. H.; Kim, M. S.; Kim, K. *Journal of Molecular Structure* **1987**, *160*, 81.

- [38] Joo, T. H.; Kim, K.; Kim, M. S. *Journal of Molecular Structure* **1987**, 158, 265.
- [39] Sobocinski, R. L.; Bryant, M. A.; Pemberton, J. E. *Journal of the American Chemical Society* **1990**, 112, 6177.
- [40] Tsen, M.; Sun, L. *Analytica Chimica Acta* **1995**, 307, 333.
- [41] Gersten, J. J.; Nitzan, A. *Journal of Chemical Physics* **1980**, 73, 3023.
- [42] Kennedy, B. J.; Spaeth, S.; Dickey, M.; Carron, K. T. *Journal of Physical Chemistry B* **1999**, 103, 3640.
- [43] *CRC Handbook of Chemistry and Physics*, 58th ed.; CRC Press, Inc.: Cleveland, 1978.
- [44] Pemberton, J. E.; Bryant, M. A.; Sobocinski, R. L.; Joa, S. L. *Journal of Physical Chemistry* **1992**, 96, 3776.
- [45] Weiner, S. J.; Kollman, P. A.; Case, D. A.; Singh, U. C.; Ghio, C.; Alagona, G.; Profeta, S.; Weiner, P. *Journal of the American Chemical Society* **1984**, 106, 765.
- [46] Weiner, S. J.; Kollman, P. A.; Nguyen, D. T.; Case, D. A. *Journal of Computational Chemistry* **1986**, 7, 230.
- [47] <http://www.webelements.com>.

Chapter 4. Study of Adhesion Promoters

Introduction

When a polymer is deposited on a surface, the formation of an interphase results from the reaction when two substrates are in contact. However, for such a reaction to occur, it is necessary that each surface contains functional groups accessible for bonding. It is therefore often desirable to modify one of the surfaces to increase reactivity, which, in macroscopic terms, would imply a modification of the surface energy. This is schematically depicted in Figure 4-1 (part B). In contrast to case A, where an interfacial region develops as a result of chemico-physical interactions, in case B, a polymeric coating is deposited on a pre-treated substrate. As a result, thicker interfacial region, or interphase, is created. [1]

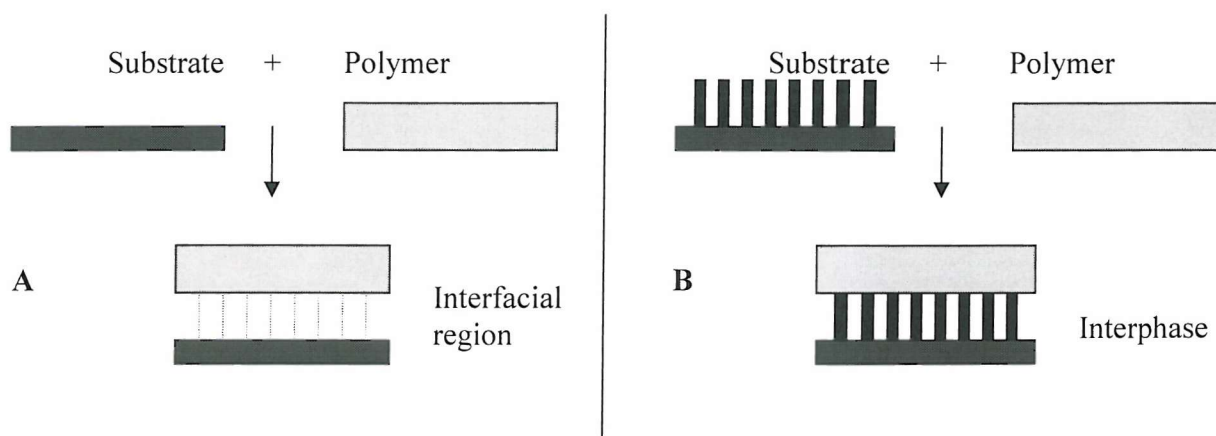


Figure 4-1 The process of interphase without (A) and with (B) surface pre-treatment.

A coupling agent, a product added to the coating formulation or used in surface treatment which improves adhesion by creating stronger interfacial interaction between the coating and the substrate, is usually considered as an adhesion promoter.

The adhesive bond strength of a coating to the substrate can be increased by:

- (i) mechanical alteration of the substrate;
- (ii) polar interactions with the bonding agent; or
- (iii) chemical bonding facilitated by an adhesion promoter [2,3]

Mechanisms (i) and (ii) are effective in improving adhesion to some extent, however, more useful additives promote adhesion between coating and the substrate by enhancing the bond strength, either by reacting chemically with both the phases or by altering the critical surface tension; some of them perform both actions.

Additives like coupling agents form molecular bridges at the interface between an inorganic surface and the organic polymer matrix. Gent [4] classifies them as adhesion promoters, which make adhesive joints between the coating and the substrate (metal or glass) able to withstand variations in the temperature and humidity. They interlock the two phases by reacting with free radicals and atoms at the interface. A coupling agent not only improves the total adhesive strength, but also the durability of the adhesive joint [5]. The functional groups of a coupling agent react with and form chemical bonds between the inorganic substrate and the organic coating / adhesive. They form a zone at the resin – substrate interface with a modulus intermediate between the high modulus substrate and the low modulus resin as well as tightening up the polymer structure and provide groups for bonding to the mineral surface [6].

The following adhesion promoters are used in organic coating formulations or in surface pre-treatment [7]:

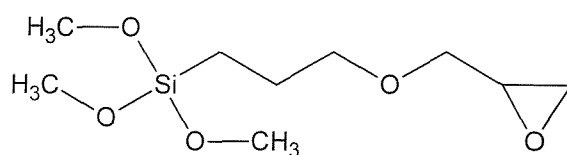
- Organosilanes used in coating formulations
- Silanes used as additives
- Organotitanates used as adhesion promoters
- Silicones and silicone modified polymers
- Siloxanes

In the aerospace industry, the two major adhesion promoters used are organosilanes and organotitanates. These are applied as coatings.

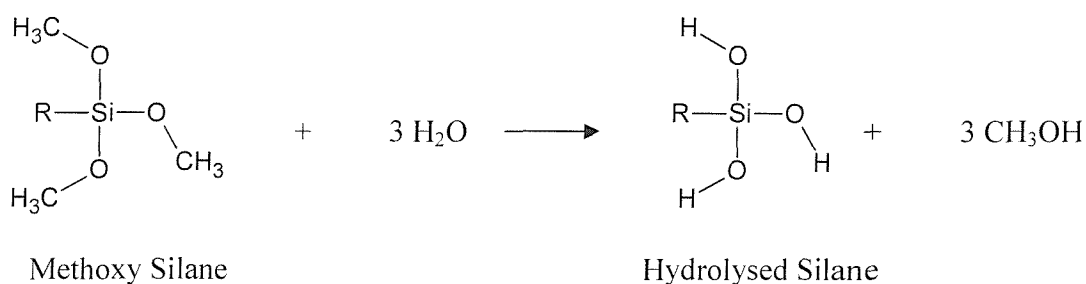
1.1. Organosilanes

Organosilanes have been used for over 30 years, initially in reinforced plastics and later in adhesives and organic coating. Silane compounds have performance advantages, such as adhesion promoting or improving the thermal stability of metal to metal adhesive bonds [8]; nonetheless, they have certain limitations such as their high cost, severe hydrolytic instability, and non-optimal performance on siliceous substrates [7].

The generic formula of silanes is $R' - Si(OR)_3$ where R' represents an organic functional group tailored to react with radicals, such as amino, mercapto, vinyl, epoxy and methacryloxy, etc., and (OR) is the hydrolysable alkoxy group. Silane coupling agents have two functional ends, one promotes adhesion to metals and inorganic substrates, the other is chemically reactive [9]. A typically silane coupling agent is represented below:



In use, the silane end gets hydrolysed in the presence of water and forms a bond after application

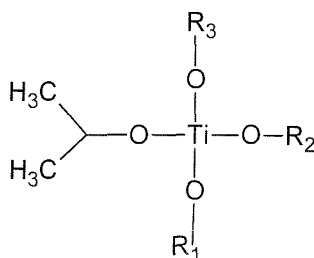


The hydroxyl silane forms strong chemical bonds with metal, glass and other inorganic substrates. Polymeric materials get copolymerised with the organic end of the silane. Optimum adhesion is achieved with one to three layers of coupling agents on the surface.

1.2. Organic Titanates

During recent years, organic titanates have been used as surface active materials for adhesion promotion, pigment surface modification, dispersion improvements and rheology aids [7].

The generalized structural formula for the organic titanates is:



R₁, R₂ and R₃ are the organic substituents.

These compounds work similarly to the silanes and offer certain advantages. The Cleveland Society for Coatings Technology [10] studied a series of organic titanates as adhesion promoters for steel surfaces. Their findings indicate that titanates with certain organic moieties are superior in promoting adhesion. It is also shown that the favourable or adverse effects of titanates on the adhesion of an acrylic thermoset or thermoplastic coating depends on the position of the organic radicals substituted to the titanium atom.

Experimental

1.3. Experimental details

As in Chapter 3, the SERS technique seems to be very appropriate to study this type of sample. As their role is to promote the adhesion between the sealant and the substrate, and as SERS allows the study of adsorbed species, it should be possible to study the chemical reaction between the coupling agent and the polysulfide molecules.

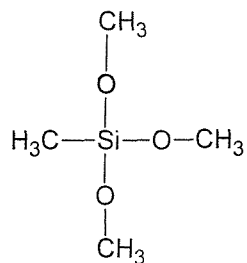
As before, the experimental conditions are as follows:

- The solutions prepared are diluted to 10^{-4} M to allow only one monolayer to build up onto the metal surface
- The metal used is roughened silver foil (see technical details in chapter 3)
- The metal and solution are left in contact for about 10 minutes (time required to build a full monolayer)
- The spectrometer used was the Renishaw 2000 System
- The laser was the HeNe laser emitting at $\lambda = 632.8$ nm
- The microscope objective was the x50
- The confocal mode was used
- The spectra have been recorded on a 20 s and two accumulation basis between 3600 and 200 cm^{-1} .

1.4. Molecules studied

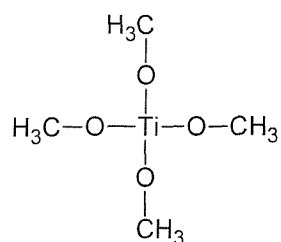
Like in the polysulfide case, the adhesion promoters used by the aerospace industry are protected because of trading purposes. However, it was possible to know what kind of family they belong to: two types of coupling agents are used, organosilanes and organotitanates. Because the real adhesion promoters used are a mixture of the coupling agents, volatile organic compounds and dyes, it was then decided to choose two model molecules in addition of the real adhesion promoters. They are as follows:

The first molecule belongs to the organosilane group. It is called trimethoxymethylsilane and is represented below:



A relatively simple molecule was deliberately chosen to limit the number of isomers and hence display spectra that will be easier to analyse. It includes three hydrolysable groups (methoxy) and one functional group (methyl).

The second molecule that has been chosen is an organotitanate: titanium(IV) methoxide. The molecule is represented below:



The titanate was purchased in a powder form with a very poor solubility. It was however possible to dissolve it in toluene (0.1 g per 100 mL [11]). The silane came as a liquid, it was then possible to dilute it to obtain a low concentration solution. Both compounds were purchased from Aldrich.

The real adhesion promoter used by BAe Systems has also been used. It is coded ADP in this chapter and is a red liquid. To adsorb it, it was diluted using toluene. As the formula is unknown, the exact concentration of the solution is not known but it was diluted at a 1000:1 toluene:adhesion promoter v/v ratio.

1.5. Interactions

As well as the spectra of neat and adsorbed adhesion promoters, it was interesting to study the interactions they have with the polysulfides. Thus, they have been combined with the molecules studied in chapter 3. Diphenyl disulfide, 1,4 butanedithiol, and LP2C have been used. The preparation of such samples was as follows:

- The adhesion promoter was adsorbed on roughened silver foil by immersion in a low concentration solution
- A SERS spectrum was taken to check it was adsorbed correctly
- The foil was then dipped into the second molecule solution to adsorb a second monolayer of compound on the top of the adhesion promoter.

The SERS spectra were then recorded as usual.

Results and Discussion

1.6. The model molecules

1.6.1. Organosilane

The following spectra (Figure 4-2) display the neat (bottom) and adsorbed (top) on roughened silver foil response of trimethoxymethylsilane.

Various changes occurred when adsorbing the molecule on silver. The first dramatic change is the almost total disappearance of the Si – O symmetric stretching peak at 640 cm^{-1} . A peak is still present in the SERS spectrum but very low in intensity and shifted towards the higher frequencies at 675 cm^{-1} .

The other important change occurs in the $1140 - 1100\text{ cm}^{-1}$ zone. The peak corresponding to the CH_3 rocking is shifted towards higher wavenumbers, when the molecule is adsorbed onto the metal surface. However, Colthrup *et al.* [12] used the RAIRS technique to assign a band at 1135 cm^{-1} to an Si – O – Si asymmetric stretching.

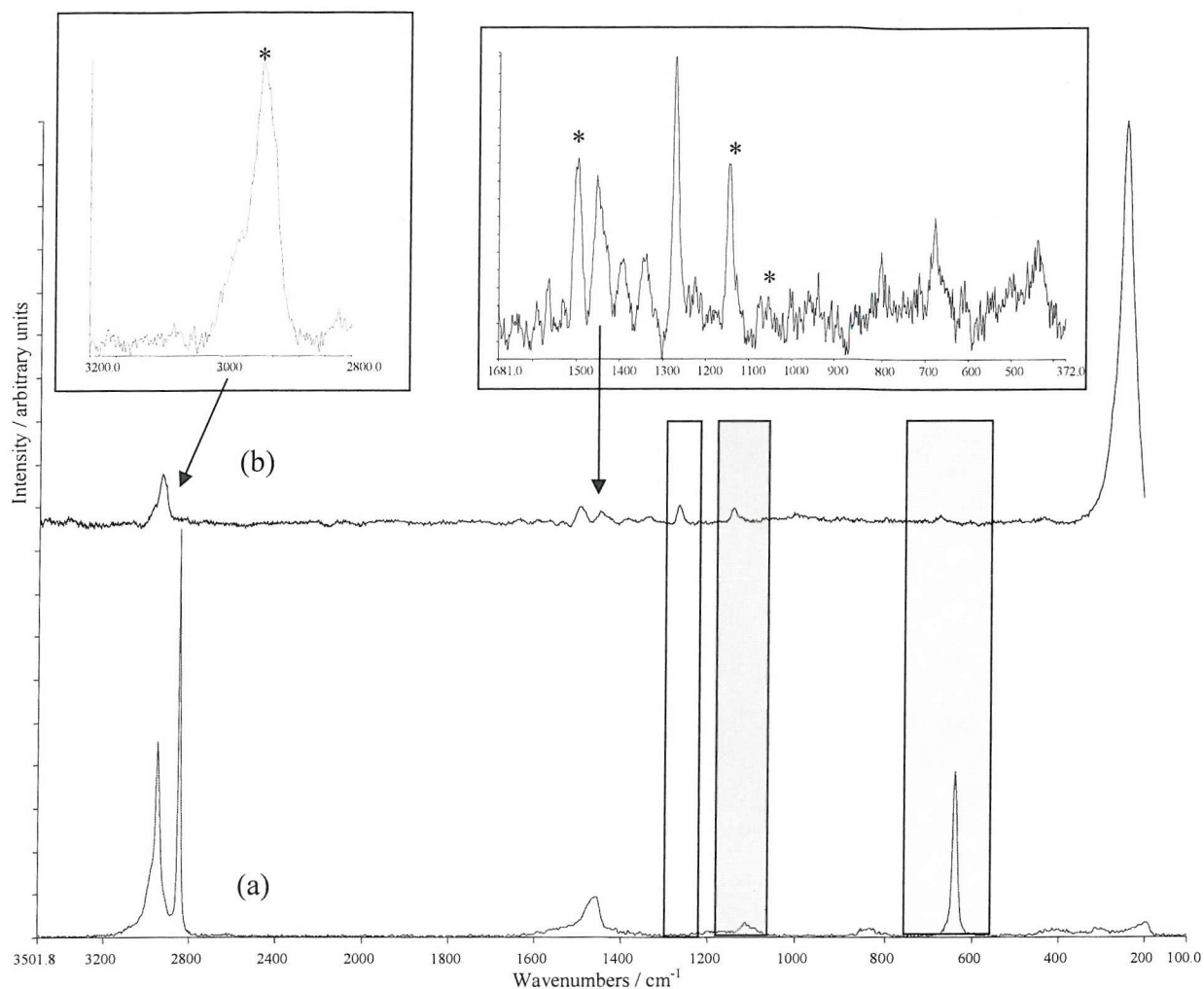


Figure 4-2 Neat (a) and adsorbed (b) spectra of trimethoxy methyl silane. The insets are the expanded region as indicated by the arrows.

Bearing in mind that the silanes are hydrolysed when in solution, Walker [13] proposes that one hydroxyl group would be used to bond with the metal surface, while the other two would be used to link with the neighbours, creating a chain of silanes onto the surface.

Figure 4-3 gives a schematic of Walkers' theory:

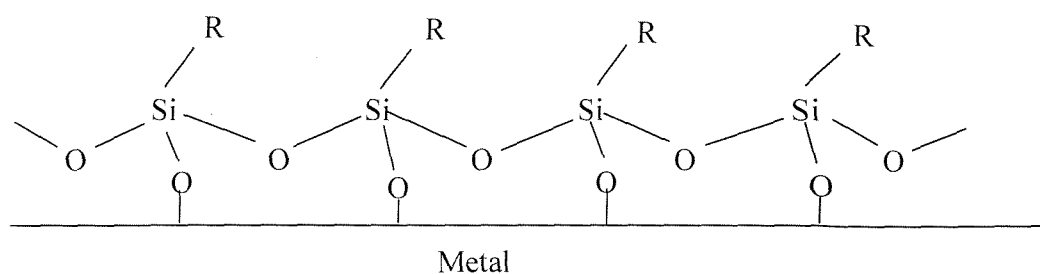


Figure 4-3 Silane network onto the metal surface according to Walker.

Walker's theory took into account that the original silanes are methoxy silane species and that they are hydrolysed when in contact with the solvent. However, they did not take into account that methoxy groups are present in the solvent and can be also be adsorbed onto the surface along with the silane. To prove this, a spectrum of sodium methanolate, species in which all the methoxyl groups are ionised, such as in the case of the silane, has been recorded:

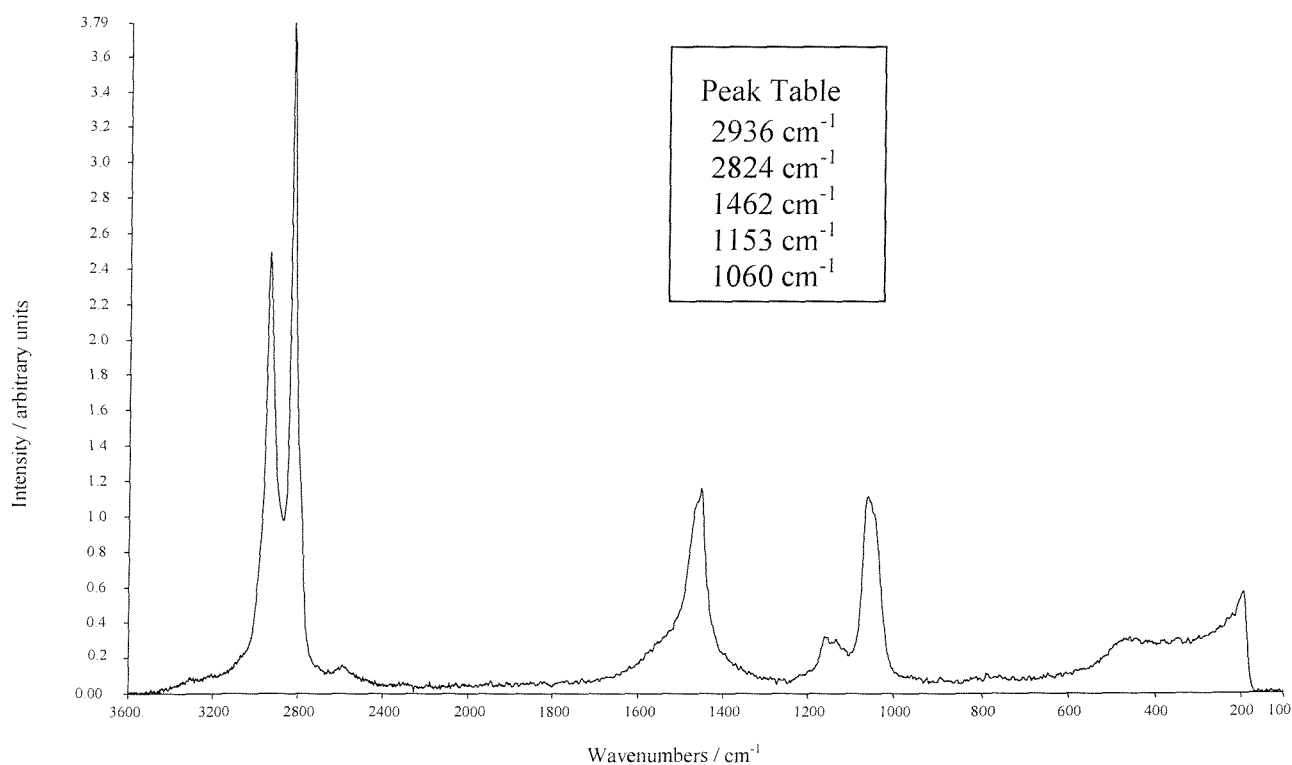
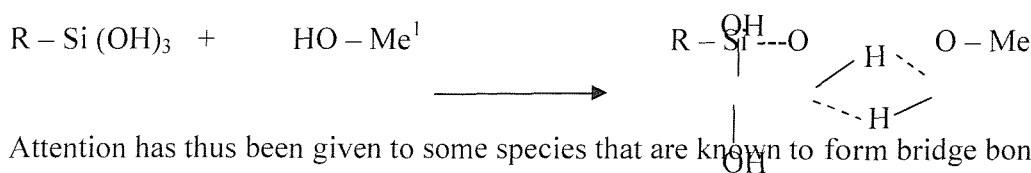
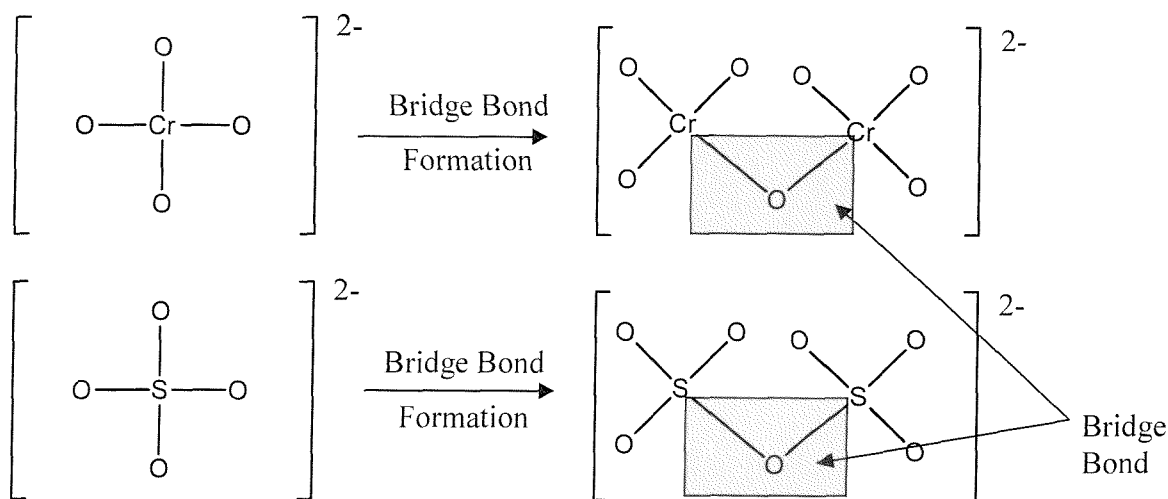


Figure 4-4 Raman spectrum of Sodium methanolate in a liquid state.

Most of the peaks present in the methanolate spectrum are also in the adsorbed silane spectrum (marked with a * in the SERS spectrum). This can mean only one thing: as well as the silane species, methanolate is also adsorbed. Thus, Walker's theory does not fully agree with the results presented above. There is little evidence for the existence of a bond between the silane and the surface other than that presented by Gettings and Kinloch [14] who detected an ion mass 100 assigned to FeSiO^+ , in the SIMS spectrum of a steel surface treated with an aqueous solution of 3-glycidoxypolytrimethoxysilane. These authors claim that this is a strong evidence for the formation of a chemical bond, probably $-\text{Fe}-\text{O}-\text{Si}-$ between the metal oxide and polysiloxane primer. Walker [13], also describes how the silane can easily bond with the oxide on the metal surface by hydrogen bonding:



Attention has thus been given to some species that are known to form bridge bonding, such as CrO_4^{2-} or SO_4^{2-} (see diagram below). The chromium atom is too electronically different from the silicon. However, the Sulphur atom is interestingly close to the silicon. In 1972, Ross *et al.* assigned the bands in the Raman spectrum of $\text{K}_2\text{S}_2\text{O}_7$ and $\text{Na}_2\text{S}_2\text{O}_7$ [15]. Their findings are reported in Table 4-1.



¹ In this case, Me stands for Metal

Table 4-1 Bridge vibrations of $\text{S}_2\text{O}_7^{2-}$ species [15]

	$\text{Na}_2\text{S}_2\text{O}_7 / \text{cm}^{-1}$	$\text{K}_2\text{S}_2\text{O}_7 / \text{cm}^{-1}$	$\text{K}_2\text{S}_2\text{O}_7 (\text{melt}) / \text{cm}^{-1}$	Type
Bridge Stretching	793	-	790	Antisymmetric
Bridge Stretching	741	743	730	Symmetric
Bridge Bending	346	321	320	-

Clearly, three vibrations have been assigned to the bridge bond stretching. Looking at the silane SERS spectrum, three bands at 800, 680, and 345 cm^{-1} are also present and can be attributed to the bridge stretching and bending vibrations according to the previous literature results. Moreover, various articles report the Si – O – Si stretching vibration, in the infrared, between 900 and 1100 cm^{-1} [16,17]. This could correspond to the small peak at 960 cm^{-1} . These results confirm that the silanes are bridging over the surface when adsorbed onto the metal.

Finally, a strong band appears at 1270 cm^{-1} . In 1985, Withnall and Andrews reported this band and attributed it to a Si = O stretching vibration [18,19]. The enthalpy of formation of a Si = O bond is roughly -102 kJ.mol^{-1} [20]. Unfortunately, the change of entropy could not be found, but looking at similar species, it is very likely to be a positive number. Hence, the change of free enthalpy for the formation of a Si = O will be negative, which makes the reaction very likely to happen.

Looking at the conformation proposed before, one H_2O molecule is removed for two silanes to create the Si – O – Si bond. Knowing that in practice, silane films, on both glass and metal, are discontinuous and consist of discrete islands or agglomerates [13] and according to the Walker's theory, the place where the double bond is most likely to be created is at the end of the islands. The following schematic (Figure 3-5) could represent what is likely to happen at the surface of the metal. It was not however possible to represent the Si = O as it is not possible for it to occur as an ending.

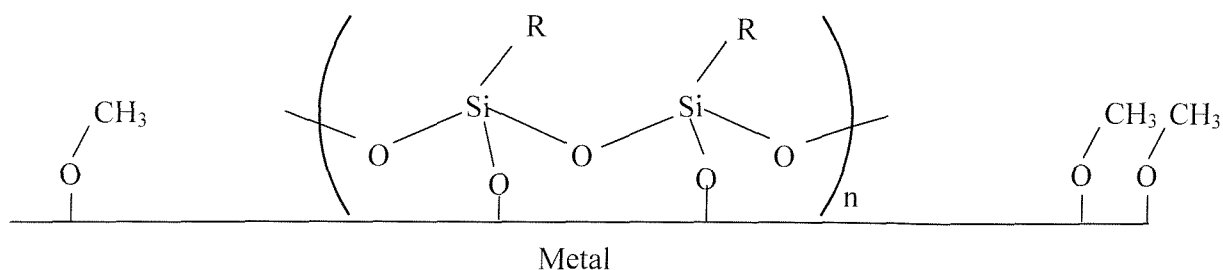


Figure 4-5 Silane network onto the silver substrate

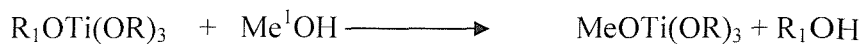
This schematic is only a two dimensional representation of what could really happen in 3D.

1.6.2. Organotitanate

The Figure 4-6 displays the free (bottom) and adsorbed spectra of tetramethoxy titanate (top).

The neat spectrum presents several characteristic vibrations. Two Ti – O stretching vibrations, one has a very low intensity and is the asymmetric one around 1010 cm^{-1} [21]. The second one, the symmetric vibration situated around 600 cm^{-1} [22] is, in contrast, very intense. The C – H vibrations appear, as usual, around $3000 - 2800\text{ cm}^{-1}$ and the CH_3 deformation around 1450 cm^{-1} . The peak at 1150 cm^{-1} can be attributed to the C – O stretching vibration. This vibration should normally occur at higher frequency but the titanium atom with its $4s^2 3d^2$ electronic structure significantly disturbs the electronic cloud around the C – O bond.

According to Walker [9,13], titanate coupling agents are unique in that their reaction with the free protons on the substrate results in a monomolecular layer on the surface. The reaction proceeds according to the following equation:



The adsorbed spectrum is once again very different from the neat one. As in the case of the silane coupling agent, the vibrations of methanolate group can be retrieved from the spectrum. They are shown with a * in Figure 4-5. The details of the Methanolate spectrum have been presented in the previous section and the spectrum is displayed in Figure 4-4. In the previous section, the $S_2O_7^{2-}$ species have been used as a comparison and to prove that a bridging was occurring. In the case of titanate, the chromium species, $Cr_2O_7^{2-}$, will be used as the electronic structure of chromium is very close to the structure of titanium. In their article, Brown and Ross [15] showed that the bridge vibrations for $K_2Cr_2O_7$ and are displayed in Table 4-2.

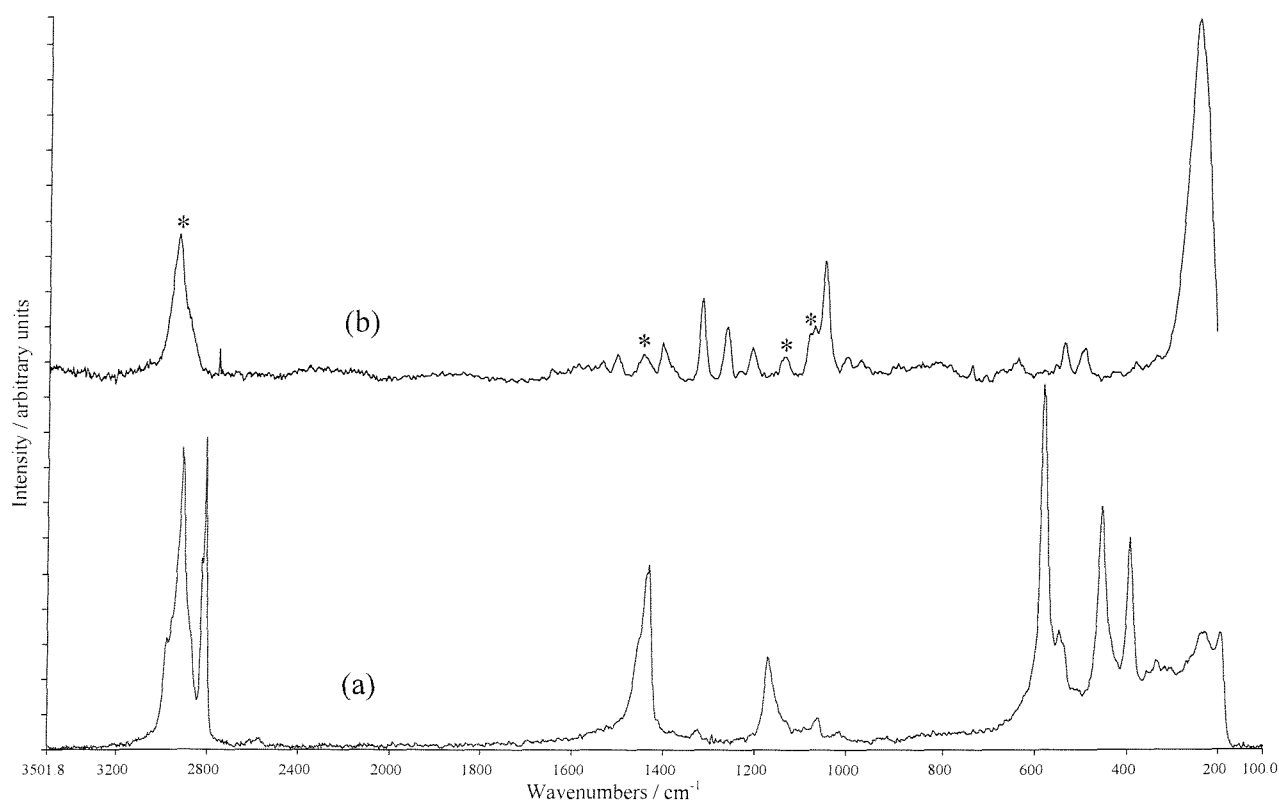


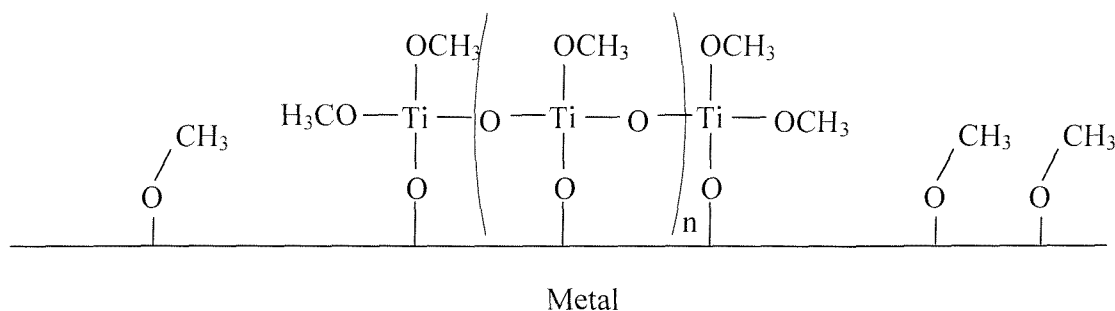
Figure 4-6 Neat (a) and adsorbed spectra (b) of tetramethoxytitanate.

^I Me stands for Metal

Table 4-2 Raman shifts of $K_2Cr_2O_7$ [15]

	Frequencies observed / cm^{-1}	Frequencies calculated / cm^{-1}
Bridge Stretching (asymmetric)	755 - 770	764
Bridge Stretching (symmetric)	550 - 570	560
Bridge bending	218 - 230	225

In the SERS spectrum of the titanate, two bands at 770 and 560 cm^{-1} are present. The third band that could correspond to the bridge bending ($\sim 220\text{ cm}^{-1}$) can be present but is probably masked by the huge peak corresponding to the etched silver. Therefore, the presence of methanolate groups and the bridging evidences lead to the following conclusion that the titanates polymerise when adsorbed onto the surface of the metal. Considering what happened in the case of the silanes, a structure like the one presented in the schematic below, is therefore proposed:



1.7. Real adhesion promoter

The next figure displays the neat and adsorbed on rough silver spectra of the adhesion promoter used by BAe systems and coded ADP1.

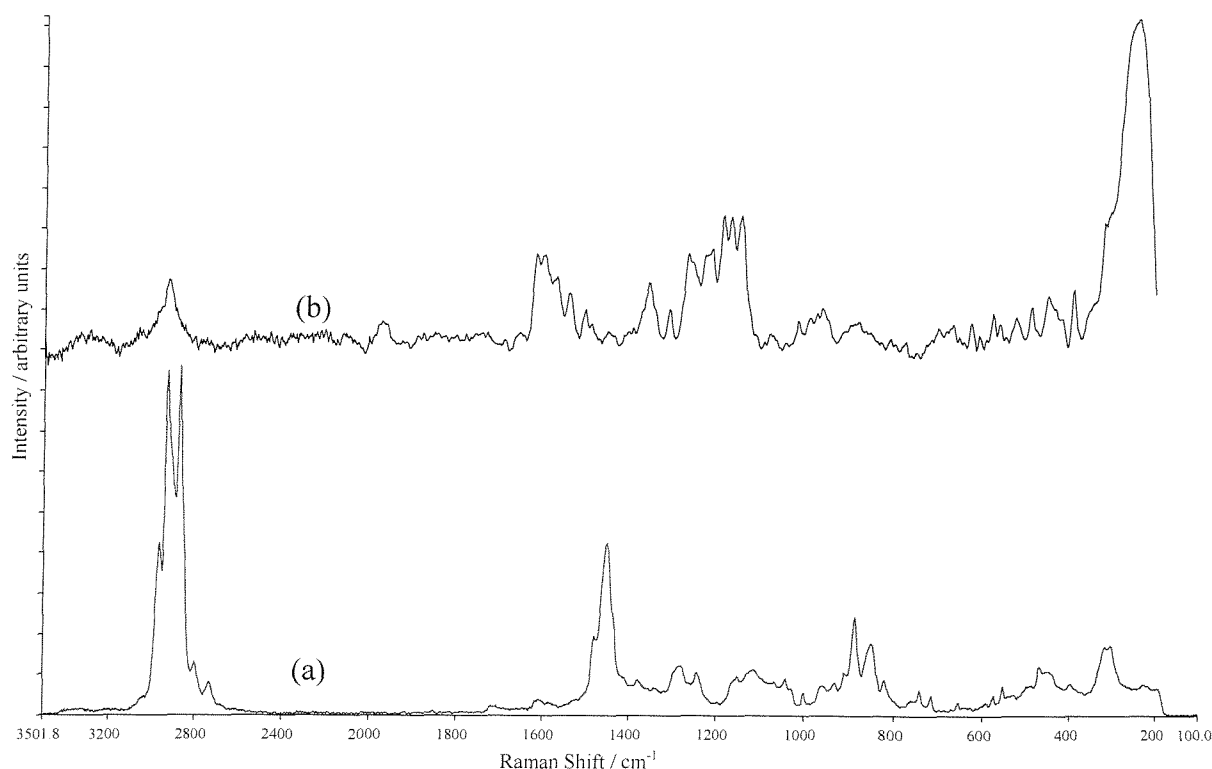


Figure 4-7 Free (a) and adsorbed (b) spectra of ADP1.

As can be observed in the above figure, the spectrum of the real adhesion promoter is much more complicated than the silane or titanate only. This is due to all the additives added to the active molecules as well as the reactive group of the molecule itself, which remains unknown. This coupling agent is probably a mix of titanate and silane but also contains solvents and dyes (red) that may mask the interesting peaks but also make the compound fluoresce when exposed to the red laser light.

However, some features of the organosilane are present in the spectra presented above. A small peak at 670 cm^{-1} corresponding to the Si – O stretching vibration can be seen in the free spectrum of ADP1. Unfortunately, the noise intensity in the SERS spectrum is too high to distinguish if the peak is still present or not.

A peak at 1270 cm^{-1} in the SERS spectrum could also be assigned to the Si = O band as described before and the peak at 1140 cm^{-1} could be associated with the Si – O – Si asymmetric stretching.

Some characteristics of the organotitanate species can also be observed in the spectrum of ADP1. For example, the vibrations at 600 and 1010 cm^{-1} are present in the adsorbed spectrum. They do not really appear in the neat spectrum because of the other compounds present in the solution. However, when adsorbed on the metal surface, mainly the ‘active’ molecules are present and detected, hence enhanced because of the SERS effect.

Although quite small, the peaks of the adsorbed methanolate are present in the SERS spectrum: they appear at 1470, 1150 and 1050 cm^{-1} along with the CH_3 vibrations around 2900 – 2800 cm^{-1} .

It is difficult to conclude much about this compound because of its complexity. However, as in the case of the silane and the titanate, it is probably hydrolysed when it is in contact with the solvent and the active molecules of silane and titanate are adsorbed along with the methanolate. Other molecules are also adsorbed onto the metal surface, but they are almost impossible to identify because of the commercial sensitivity of this mixture.

1.8. Interactions

1.8.1. *Organosilane and DDS*

The first interaction to be examined was between the organosilane (trimethoxy methyl silane) and the diphenyl disulfide studied in Chapter 3.

The following figure (4-8) shows the adsorbed spectra of the organosilane (bottom), the DDS (middle) and the interaction of both (top).

Major changes appear between the SERS spectra of DDS with and without a silane monolayer. First, some characteristics of the organosilane spectrum appear in the combined one: the peak at 1270 cm^{-1} assigned to the $\text{Si} = \text{O}$ stretching vibration and the $\text{Si} - \text{O} - \text{Si}$ vibration, situated at 680 cm^{-1} in spectrum (a), which is shifted to 711 cm^{-1} in the combined spectrum (c).

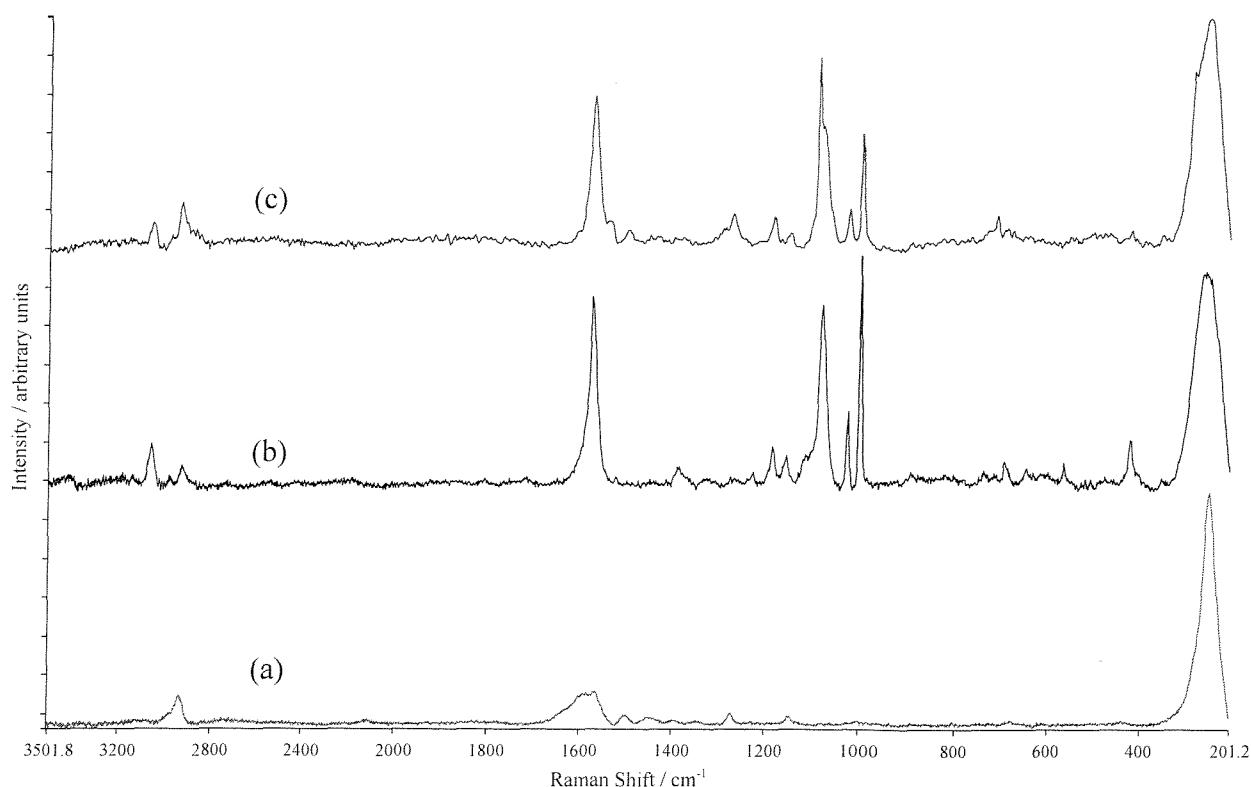


Figure 4-8 SERS spectra of trimethoxy trimethyl silane (a), diphenyl disulfide (b) and the interaction of both on the same plate (c).

The other differences may be attributed to the DDS. The most dramatic one occurs in the region between 1000 and 1100 cm^{-1} and involves the band due to the ring breathing (1000 cm^{-1}) and the S – Phenyl stretching (1020 and 1070 cm^{-1}). It can be seen in the combined spectrum (c) that the band at 1077 cm^{-1} is even more enhanced than in the case of a simple adsorption. Also, a peak at 1084 cm^{-1} , stronger than the S – Phenyl adsorption arose.

Variations are also observed in the low wavenumbers region, specifically the profile of the peak at 200 cm^{-1} . In the spectra of coupling agents on their own, the band is relatively narrow and does not show a shoulder indicating the presence of sulphur – silver bonding. However, in the combined spectrum, this band is broader, which shows an Ag – S stretching vibration. Also to be noticed, there is no peak in the 540 cm^{-1} region, indicating that there is no S – S bond in the molecule, hence the DDS is still adsorbed dissociatively.

The last change in the interaction spectrum, is the peak at 2930 cm^{-1} . This has been assigned to the CH stretching in $\text{CH}_2 - \text{O} - \text{CH}_2$ groups adsorbed on the surface and is due to the interaction between the acetone and the DDS. In the combined spectrum, this vibration appears to be much smaller than in the normal DDS SERS spectrum, probably due to the high coverage of silane islands on the surface of silver.

Finally, as described in chapter 3, the broadening of the peaks, compared to the neat spectra, is once again due to the tilting of the molecules on the surface of the metal.

An easy interpretation of these phenomena could be that a monolayer of silane is adsorbed onto the surface of the metal then a second monolayer of DDS is then formed above the silane. This would be a good explanation in a world ruled by order. Unfortunately, in the real world chaos/entropy is governing. In their article, Sockalingum *et al.* [23] describe the competitive adsorption of benzotriazole and tolyltriazole. They conclude that instead of having two nice and ordered monolayers, some molecules of the first monolayer are removed to allow the second type of molecule to be adsorbed onto the surface of the metal in a completely chaotic way. Hence, the SERS spectrum appears like the spectrum of one molecule with added features of the other one. This is very similar to what appears to be happening in this case, the combined spectrum strongly looks like the DDS spectrum with some features of the silane. This is probably due to the removal of some of the silane from the surface by the DDS molecules.

There is evidence, in the combined spectrum, that the DDS is bonding to the surface of the metal. The most evident one is the appearance of the shoulder at 260 cm^{-1} , proof of an Ag – S stretching. On the other hand, the spectrum is also showing most of the features of the adsorbed Si species.

At this stage, another experiment has then been carried out. A monolayer of silane has been adsorbed on rough silver and after drying, the piece of silver has been immersed in the diluted solution of DDS, but this time for a longer period of time. In the initial experiment (see chapter 3), the piece of silver was left in contact with the solution for no more than 5

minutes. The exposure was extended to 8 minutes. The spectrum recorded then showed exactly the same characteristics of the SERS spectrum of DDS on its own. Thus, it is clear that the DDS had removed the silanes from the surface. This probably comes from two facts:

- The affinity of silver for the DDS is greater than with the silane.
- This simpler form of silane was not designed to promote the adhesion of this kind of disulfide, unlike the “real” system.

It is important to keep in mind that adhesion promoters are coupling agents that help slow down the curing of the sealant. In the “real” system the removal of the silane probably takes longer than the curing process.

1.8.2. Organosilane and LP2C

The second interaction investigated was the interaction of the organosilane modified surface and the liquid polymer. The figure 4-9 displays the SERS spectra of silane, LP2C and both silane and LP2C on the same plate.

As in the case of the DDS/organosilane interaction described above, the interaction spectrum for the LP2C and organosilane (Figure 4-9 c) shows many of the features of the individual components. Bands related to the silane are present at 1270 cm^{-1} , the Si = O stretch, and at 960 cm^{-1} , the Si – O – Si bridging species. As in the spectrum of adsorbed LP2C (Figure 4-9 b) no peak attributable to the terminal S – H, thiol, is observed. As described in Chapter 3, the absence of this peak may be attributed to either the long distance of the –SH group from the surface if the LP2C molecule is standing upright, or to a cleavage of the S – H bond if the molecule loops back to form two bonds with the surface.

The significant differences between the simple adsorption (b) and interaction (c) spectra are all related to S bonding. The intensity of the peak at 510 cm^{-1} , assigned to the S – S

vibration, is significantly enhanced in the interaction spectrum (c). The C – S stretch at 640 cm^{-1} is also enhanced, although to a lesser degree. A peak related to the Ag – S stretch is observed in both spectra.

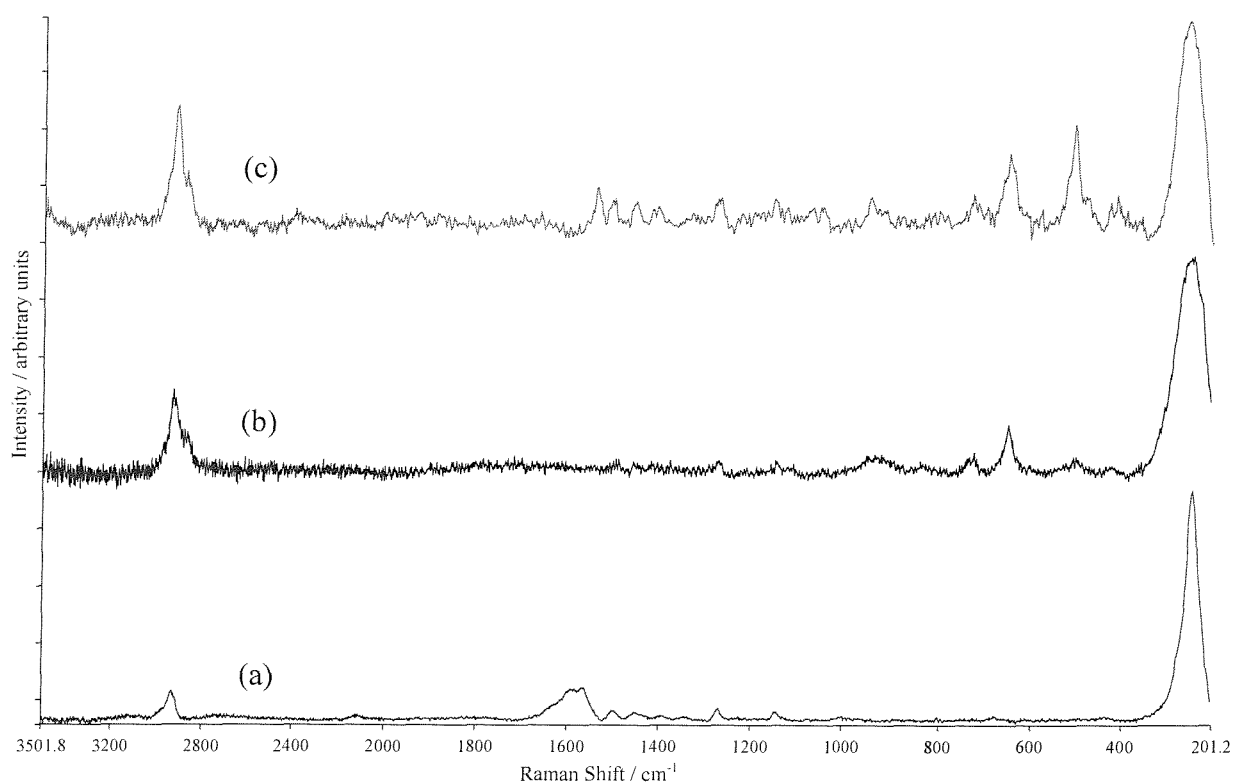


Figure 4-9 SERS spectra of Silane (a), LP2C (b) and combined silane and LP2C (c).

The enhancement of the S – S and the C – S vibrations may be accounted for by two explanations. First, the electron cloud around these bands could be disturbed by the interaction with the organosilane, giving a greater change in the polarisability of the vibration. Secondly, the functional group(s) may be situated closer to the metal surface as a result of the interaction with the organosilane. The presence of the Ag – S stretching vibration in the interaction spectrum indicated that the LP2C molecule is displacing some of the organosilane molecules from the silver surface as was observed for the DDS. The presence of the organosilane, however, creates a more hydrophobic/hydrocarbon surface than the bare Ag surface. Thus, isolated LP2C molecules, surrounded by bound organosilane molecules may lie more parallel to the metal surface, rather than standing upright. This would have the effect of bringing the S – S and C – S functional groups closer

to the surface where the SERS effect is stronger. This second explanation seems more reasonable than the first.

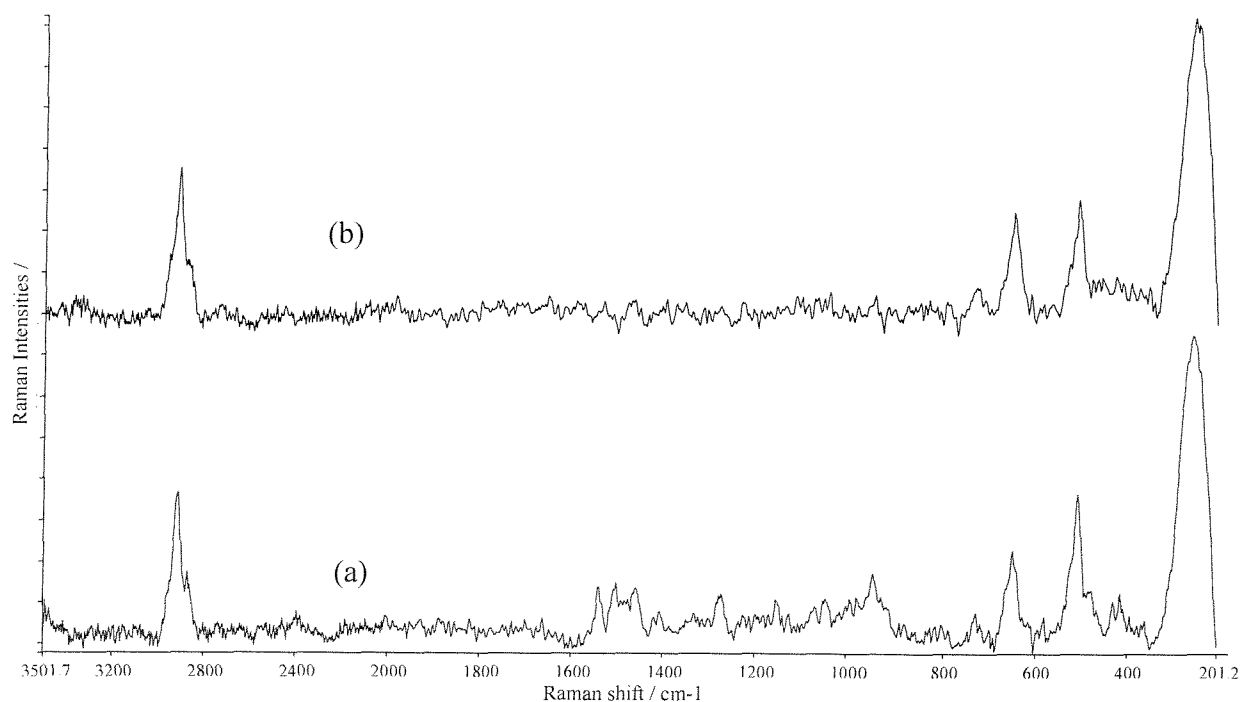


Figure 4-10 SERS spectra of silane an LP2C combined on the same plate. (a) normal exposure time to LP2C (b) longer exposure time to LP2C.

As discussed above, the LP2C molecule with its terminal thiol groups appears to displace the pre-adsorbed organosilane species. The effect of exposure time was, therefore, also investigated for this pair of adsorbate species, the results are shown in figure 4-10. After 8 minutes exposure to the LP2C containing solution, all features related to the organosilane are once again removed.

1.8.3. Organotitanate and DDS

The investigation of the organotitanate and diphenyl disulfide, DDS, was then investigated. Figure 4-11 displays the SERS spectra on rough silver foil of tetramethoxy titanate, DDS and both the organotitanate and DDS adsorbed on the same plate.

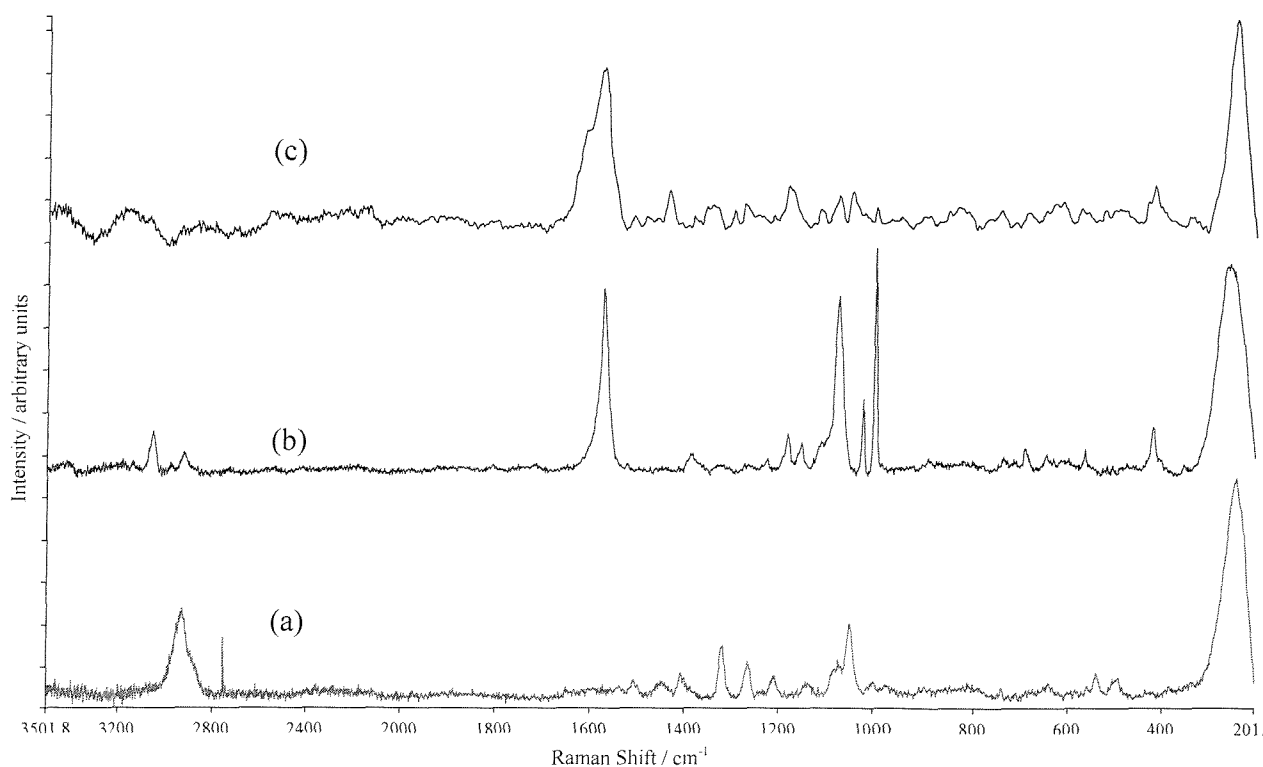


Figure 4-11 SERS spectra of Titanate (a), DDS (b) and both titanate and DDS on the same plate (c)

As in the case of the silane, an experiment was conducted using a longer exposure to the DDS than normal, to observe any changes in the combined spectrum. The result observed was different from the silane results as the exposure time did not have any effect on the spectrum. According to Sockalingum *et al.*[23], both adsorbates will compete to bind to the surface and the result would be the winner's spectrum with some of the features of the defeated adsorbate. However, in the presented combined spectrum, none of the adsorbate seems to have taken the lead.

Unlike the interaction spectra obtained with the organosilane, that with the organotitanate (Figure 4-11 c) is not simply the sum of the two simple adsorption spectra a + b. Several new features / bands are observed in the interaction spectrum. The differences will be discussed starting at the low wavenumber end of the spectrum.

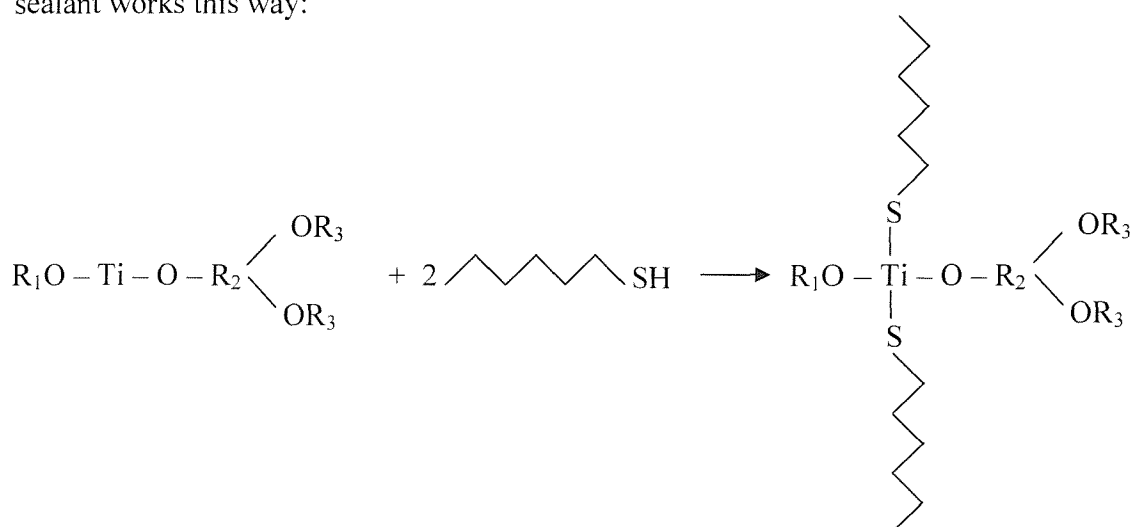
As discussed previously, the width of the band in the $200 - 280 \text{ cm}^{-1}$ region is related to the presence of an Ag – S bond. As can be seen in the interaction spectrum (4-10 c), the band remains narrow, revealing that there is no Ag – S interaction. Thus the DDS does not rapidly displace the organotitanate.

When looking at the $1100 - 1000 \text{ cm}^{-1}$ region of both DDS and titanate spectra, some peaks are overlapping each other. When comparing the silane + DDS spectrum and the titanate + DDS spectrum one can remark that the enhancement in this region is much more intense when using the silane. It is also quite difficult to find any titanate correspondence in the mixture spectrum, apart from the asymmetric Ti – O stretching (1045 cm^{-1}).

Examining the ring modes of the DDS molecule, there is a dramatic effect of the interaction with the organotitanate modified surface. The ring modes in the $1000 - 1120 \text{ cm}^{-1}$ region are suppressed, whilst the C = C stretching modes at 1600 cm^{-1} remains strong. This latter feature is also broadened.

Finally, no CH_3 stretching vibration can be observed in this spectrum in the region around 2900 cm^{-1} .

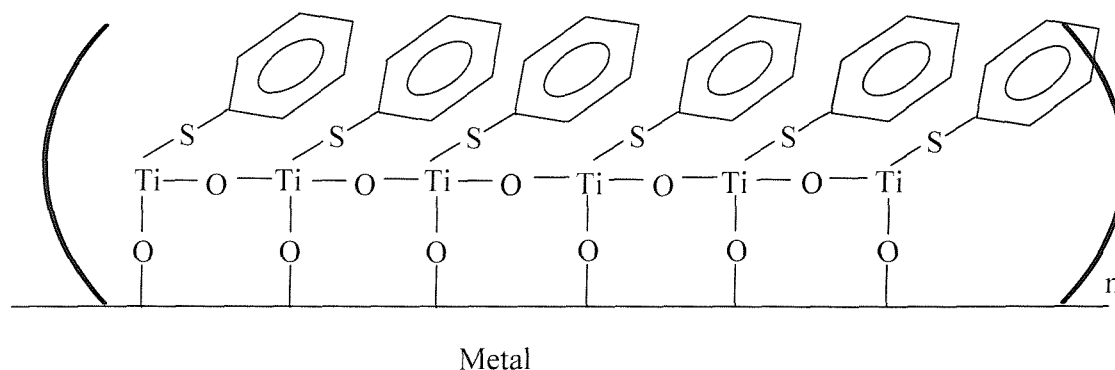
According to Usmani *et al* [24], the reaction between a titanate primer and a thiol ended sealant works this way:



They also state that the role of the titanate is to slow the curing of the sealant, a slower curing leading to an improved adhesion.

It is a bit difficult to discuss the orientation and adsorption site of the DDS molecule on this surface. The only bond clearly identifiable as belonging to the DDS is that at 1600 cm^{-1} . Therefore, it is almost impossible to speculate about the geometry of DDS, as the important bands are normally smaller than the phenyl ones. However, as described before, the silver band is narrower than when sulphur bonds to the surface, it is thus possible that none, or a very small amount, of the sulphur atoms bonded to the metal surface.

As discussed above, the S – S bond of DDS is broken upon adsorption, giving two S – Phenyl groups. Thus, a reasonable explanation of what is happening is described in the schematic below:



In this eventuality, no CH_3 group is left, and only aromatic CH could give rise to a vibration peak in the 3000 cm^{-1} region. The methoxyl group is removed upon the adsorption of the sulphide group. This is possible, due to the second contact of the adsorbed layer to the acetone used to dilute the diphenyl disulfide.

1.8.4. Organotitanate and dithiol

The following figure shows the SERS spectra of tetramethoxy titanate, 1,4 butanedithiol and both of them on the same silver roughened plate.

Once again, the combination of both adsorbates gives a very perturbed spectrum. However, in this case, the interaction spectrum is more well represented by the sum of the individual components.

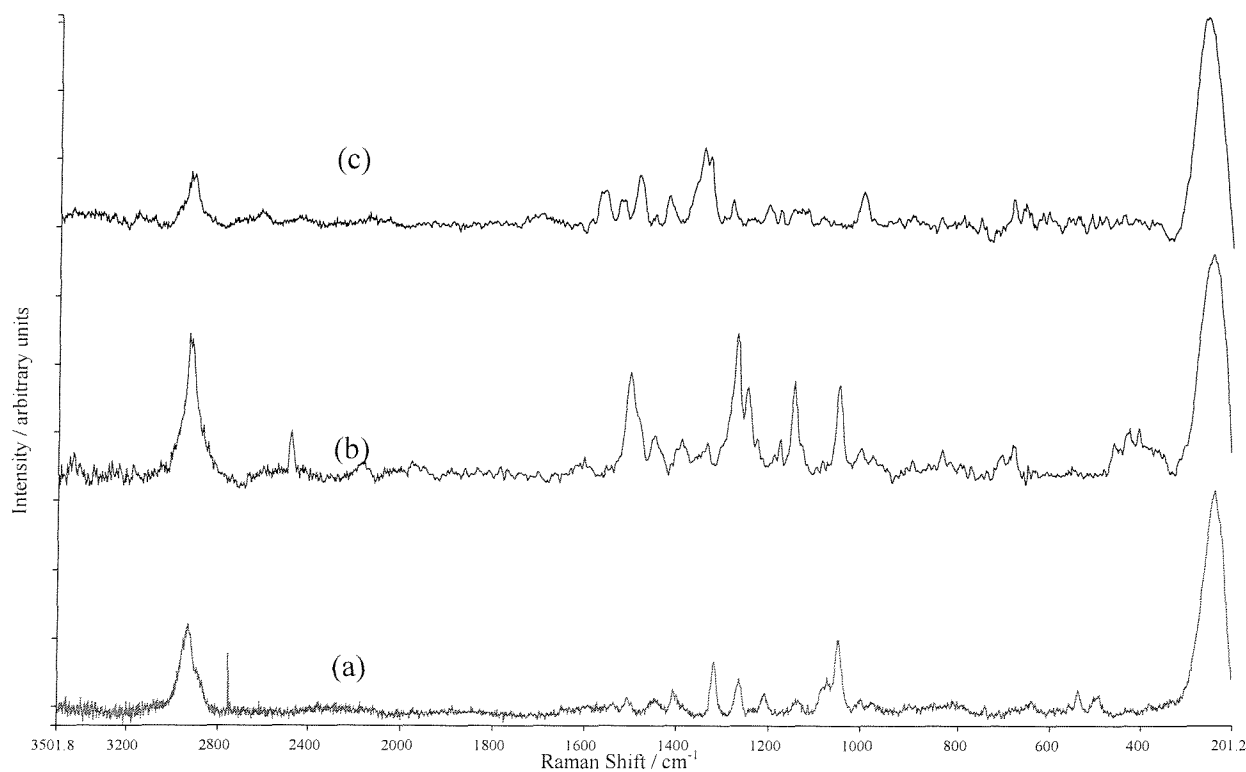


Figure 4-12 SERS spectra of tetramethoxy titanate (a), 1,4 butanedithiol (b) and both titanate and dithiol on the same slide (c).

As described before, Sockalingum *et al.* [22] proposed that a competition occurs between the adsorbates and thus the resulting spectrum would display the SERS spectrum of the winning adsorbate with some features of the loser.

One should also keep in mind the results discussed in Chapter 3: because of the high number of conformational isomers of the 1,4-butanedithiol, it is therefore impossible to predict what isomer will adsorb at a specified point, and especially where the laser spot is illuminating. Thus the SERS spectrum of thiols / dithiols may be different every time. In the above combined SERS spectrum, most of the peaks are situated in the 1600 –

1200 cm^{-1} region, the precise region where the different trans and gauche stretching vibrations occur. Moreover, the broad band at 200 cm^{-1} shows an S – Ag vibration. Finally, some of the peaks from the titanate spectrum can be observed in the interaction spectrum.

The same experiment as before has also been conducted, i.e. leaving the sample exposed longer to the thiol. As in the case of the silane, the resulting spectrum had no features of the titanate after prolonged exposure to the thiol containing solution.

1.8.5. *Organotitanate and LP2C*

In figure 4-13 are represented the SERS spectra of tetramethoxy titanate (bottom), LP2C (middle) and both the titanate and LP2C combined on the same plate.

Once again, features from the individual adsorption spectra can be seen in the interaction spectrum.

The two major features of the LP2C SERS spectrum are the band at 650 cm^{-1} , the C – S stretching vibration and the S – S stretching one at 500 cm^{-1} . Both of these features are represented in the combined SERS spectrum as well, with the difference that they are both more enhanced.

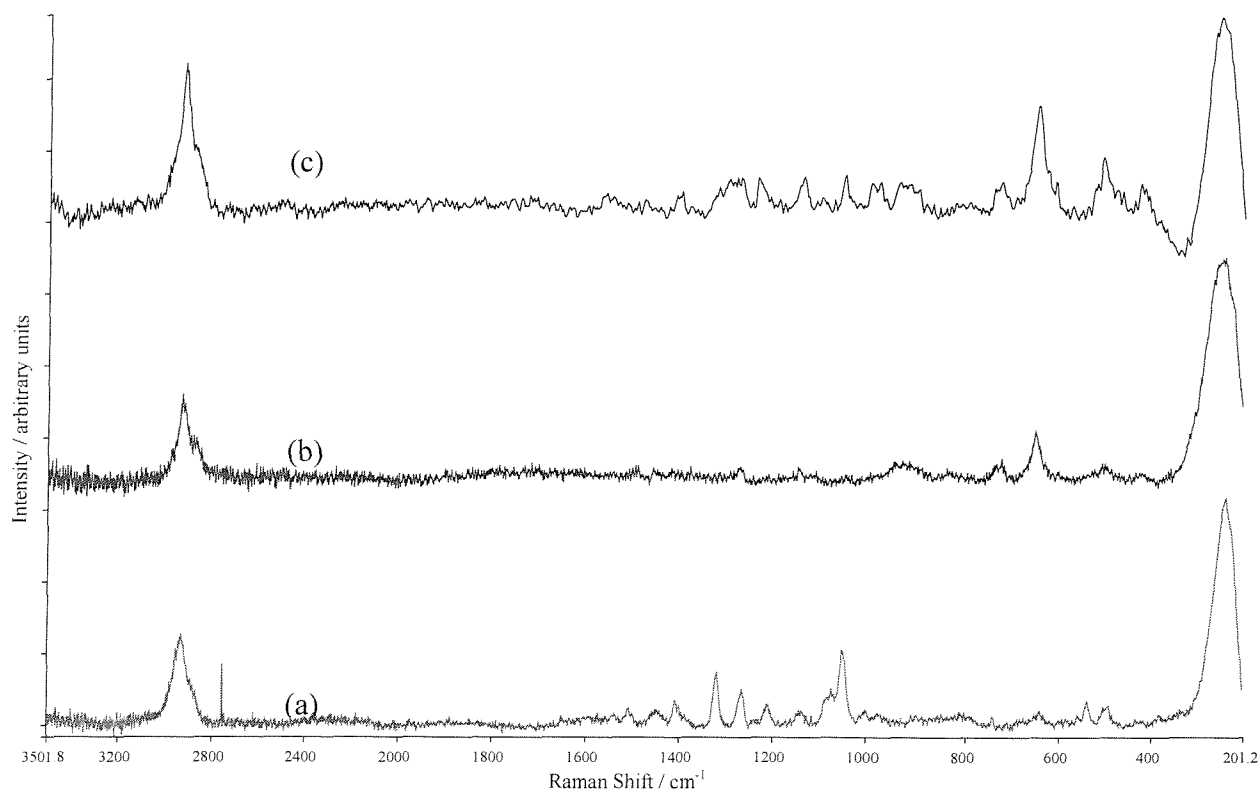


Figure 4-13 SERS spectra of tetramethoxy titanate (a), LP2C (b) and both titanate and LP2C on the same plate (c)

No S – H stretching vibration can be observed in the combined spectra. As discussed previously, in the case of interaction with the silane and in chapter 3, the molecule is very unlikely to stand straight on the top of the adhesion promoter. It is more likely to bend (and then bond) using both chain endings, creating a loop.

As before, a long exposure (8 minutes) to the LP2C experiment has been performed. The resulting spectrum showed a stronger LP2C spectrum but still with some features of the titanate, with decreased intensity. Thus, an even longer experiment (10 minutes) has been carried out, showing the disappearance of all the peaks of the titanate.

This behaviour was predictable. In the previous section, the experiment had been carried out on smaller dithiols. In the case of LP2C, the bonding to the surface occurs via the ending sulphur atoms, such as in the 1,4-butanedithiol. The kinetic factor of this experiment

is due to the length of the molecule: the longer chain needs longer to arrange itself onto the surface.

Once again, the LP2C did not bond to the titanate. The competition process occurred and the affinity of the ending sulphur atoms for the surface was greater than that of the TiO. The titanate was this time again playing the role of slowing down the reaction (hence increasing the cohesion of the material) instead of reinforcing the adhesion to the surface.

1.8.6. ADP1 and the molecules

In figure 4-14, 4-15 and 4-16, the SERS spectra of ADP1 (a), the associated molecule (b) and ADP1 + the molecule (DDS, 1,4-butanedithiol and LP2C respectively) on the same plate (c) can be observed. For each sample, an 8 minutes experiment has also been carried out, but no dependence of the spectra on the exposure time was found.

As the molecular structure of the adhesion promoter ADP1 is commercially sensitive, little information was available to assist in the interpretation of the data. Nevertheless, in the combined spectrum of ADP1 and DDS, one can see the great enhancement of the Raman band situated at 1047 cm^{-1} . This band, first thought to be of the S – C stretching vibration, seems to also appear in the ADP1 + butanedithiol spectrum. This band is probably due to the interaction between the coupling agent and the sulphur of the DDS.

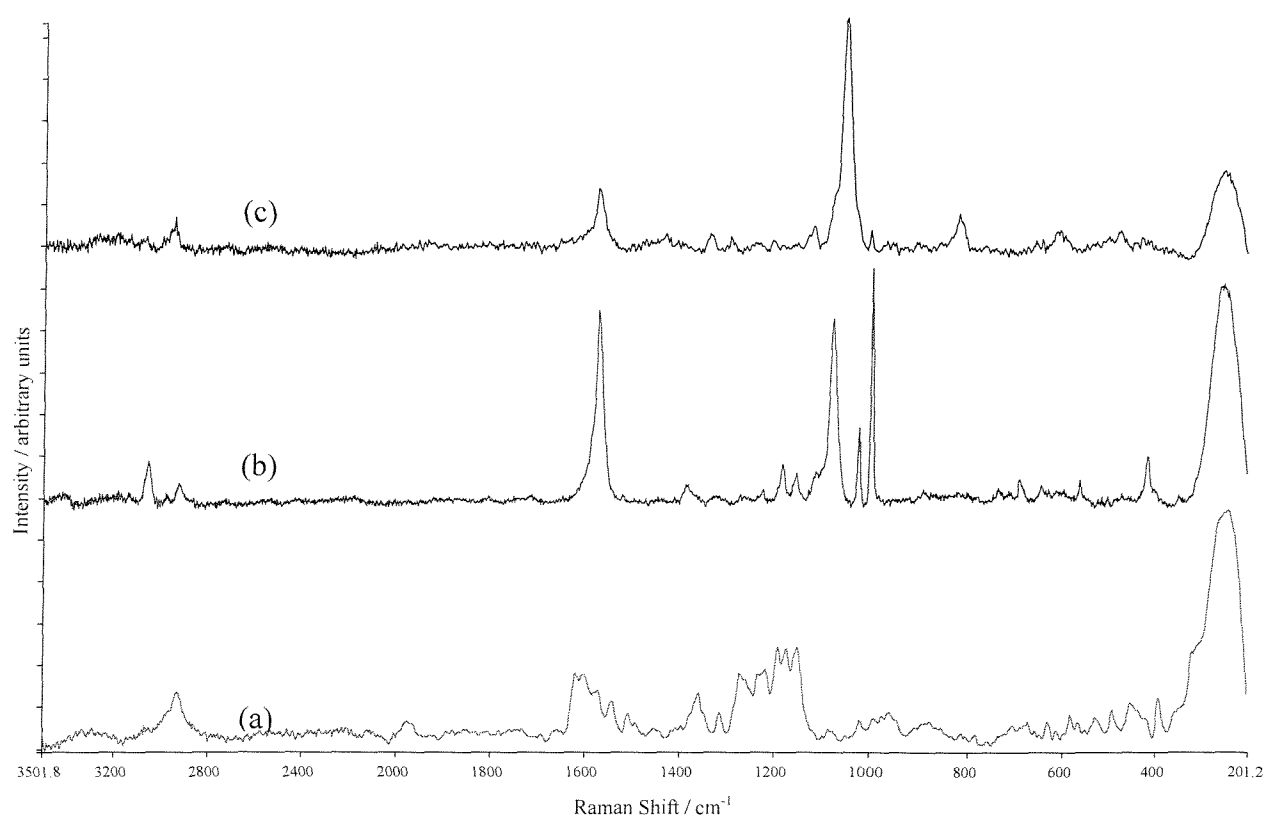


Figure 4-14 SERS spectra of ADP1 (a), DDS (b) and ADP1 and DDS on the same plate (c)

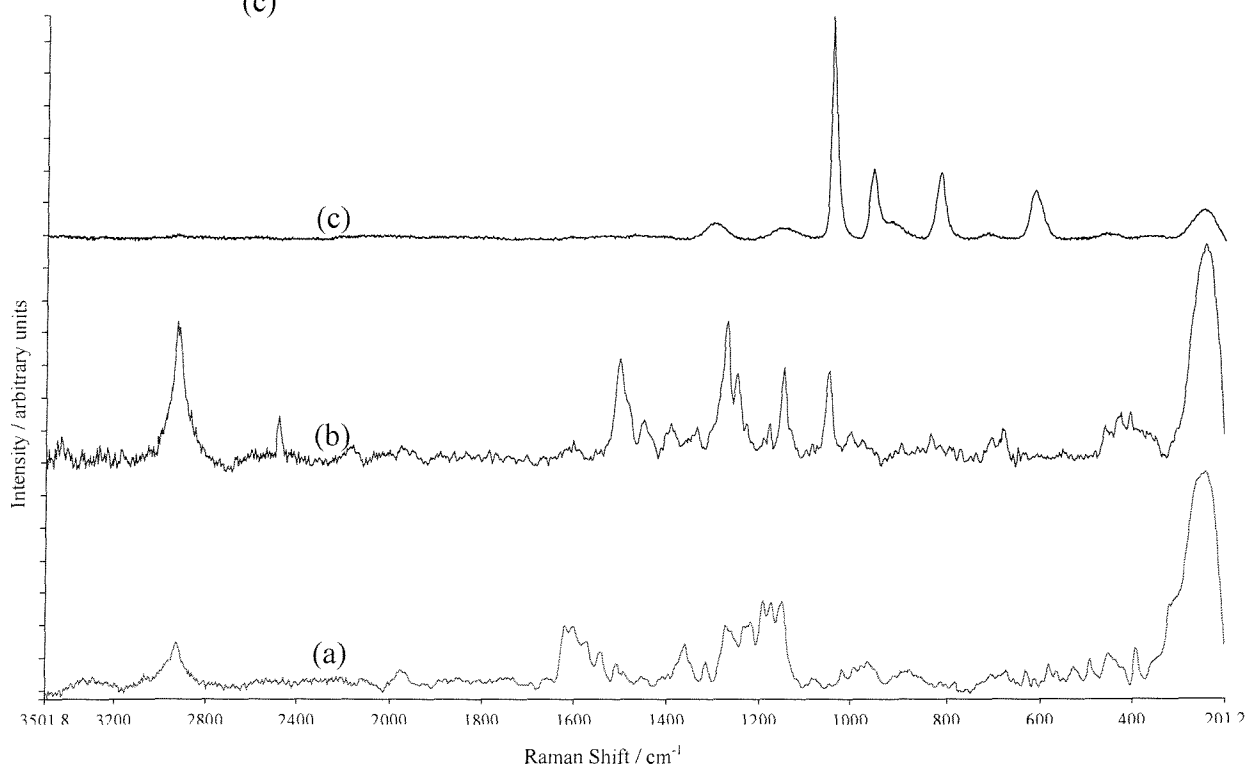


Figure 4-15 SERS spectra of ADP1 (a), 1,4 butanedithiol (b) and both ADP1 and butanedithiol on the same plate (c).

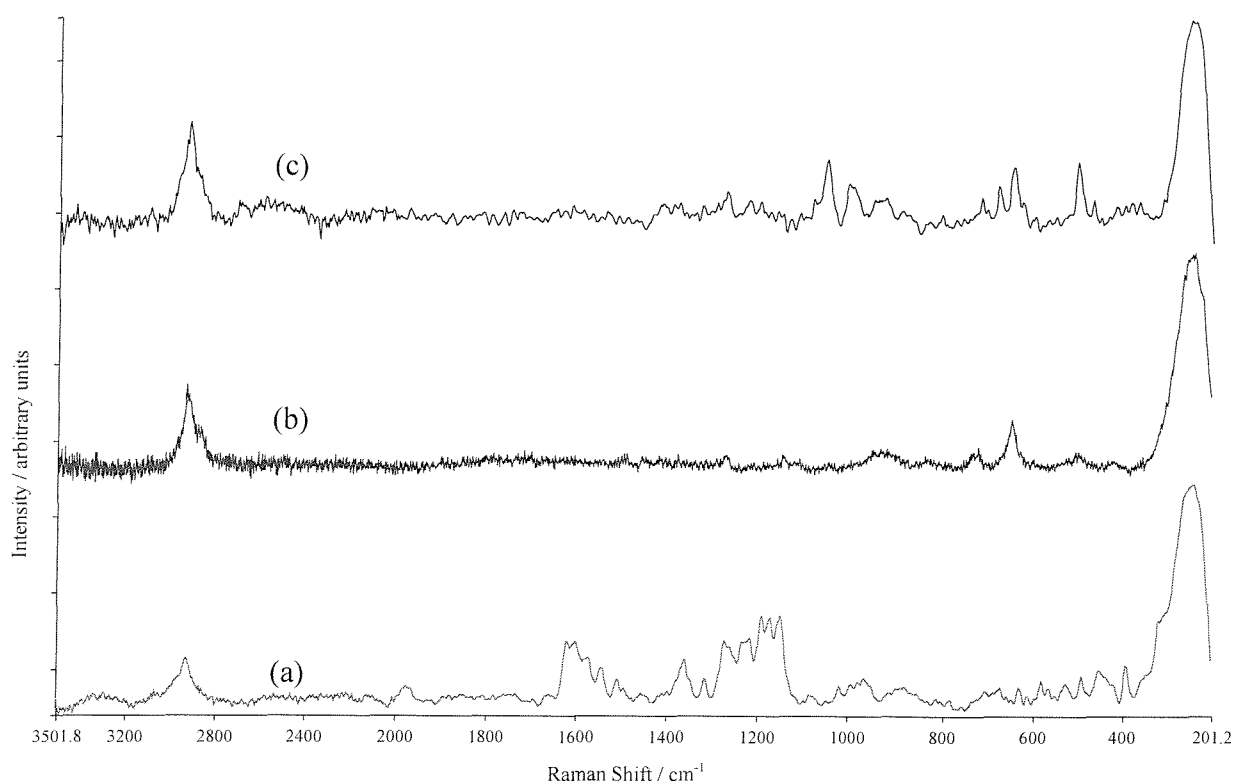


Figure 4-16 SERS spectra of ADP1 (a), LP2C (b) and ADP1 and LP2C on the same plate (c)

The other interesting band is situated at 500 cm^{-1} , which disappears in the combined spectrum. The absence of this band, assigned to the S – S stretching vibration, reveals that the DDS probably bonded to the adhesion promoter dissociatively.

The second spectrum (ADP1+butanedithiol, Figure 4-15) remains a complete mystery. The bands are very broad and intense. Apart from the peak at 1047 cm^{-1} which is the same as in the combined spectrum with DDS, no band seem to correspond to either of the individual exposure spectra. One conclusion could be that the coupling agent ADP1 has been designed to work perfectly with thiols. However, the peak at 640 cm^{-1} is common to the LP2C spectrum and was assigned before to the S – C stretching vibration. Another explanation would be the emergence of a chromophore. This would definitely explain the intensity of the peaks. Due to the nature of the compounds and due to the absence of bands around 1600 cm^{-1} , corresponding to conjugated double bonds, this chromophore would be inorganic and is probably due to the reaction between the different species adsorbed on the

plate. After comparing the spectrum to the Renishaw library of spectra, no clear cut decision could be made about the nature of the species represented. The closest matches were either a phosphate group or a mix of nitrate and oxide. Thanks to the guys at Renishaw for doing the analysis so quick (special thanks to Dr Ian Hayward). More research should definitely be pursued in this direction.

After the spectacular result of the interaction between the dithiol and ADP1, one could expect the same kind of result for the interaction with LP2C, which did not happen. Nevertheless, the usual peaks at 640 cm^{-1} (S – C stretching) and at 505 cm^{-1} (S – S stretching) are present in the spectrum, revealing that the S – S linkage is not broken. Moreover, no S – H vibration is present, the molecule is then probably bonding to the adhesion promoter using the sulphur ending atoms.

When looking at the general aspects of the different interaction spectra, even if in the case of DDS, where the DDS SERS spectrum dominates, some changes occur. In the two other cases, no adsorbate seems to win the competition process, but some re-arrangement process seem to occur in which the studied molecule and the adhesion promoter are partially transformed.

To summarise the results with regards to the commercial adhesion promoter, ADP1, there appears to be a greater change in the presence of thiols rather than with disulfides. When linked to the DDS, the S – S bond breaks, whereas with the liquid polysulfide LP2C, the molecule does not.

Conclusion

The purpose of this chapter was to study the way adhesion promoters, used in the aerospace industry, adsorb onto the surface of the metal plate but also how they combine with the adhesion promoter molecules to reinforce the adhesion process. The technique chosen was

the Surface Enhanced Raman Scattering technique, as it gives information about the surface – molecule interface.

For trading purposes, the formula of the promoters used in the industry remains a secret. Thus, in a first instance, some model molecules have been chosen to simplify the study, knowing that the coupling agents used are mainly composed of titanates and organosilanes. The formulae of the model molecules have also been kept simple, so as not to have a lot of interactions with the adhesive molecule. These molecules reacted very well with the substrate and showed some surprises concerning their conformation on the surface.

The first one, the trimethoxy methyl silane, which is known to form discreet islands on the surface, showed the formation of a Si = O bond that was not predicted by the literature. The tetramethoxy titanate, on the other hand, adsorbs uniformly on the surface without any surprises, compared to what was predicted by the literature. The other discovery is that because these two molecules are hydrolysed when solvated, some methanolate groups also adsorb onto the surface along with the active molecules. Finally, the spectrum of the real adhesion promoter has also been recorded. However, because of all the additives and dyes used in its composition, it was difficult to assign the peaks of the spectrum. Nevertheless, it was revealed to contain some peaks of the titanate and some of the silane as well as the methanolate (because of the hydrolysis process).

Later, in the interaction spectra, for some of the pairs of molecules the spectra were well represented by the sum of the two components. The relative amounts depended on the exposure time as one molecule displaced the other. This is in agreement with the work of Sockalingum *et al.* [23] who found that when two molecules are adsorbed, the spectrum will be dominated by the more strongly adsorbed molecule and will show some features of the other molecule. In practice, a competition process occurs and the molecule with the highest affinity for the surface is adsorbed in greater quantity. It has also been demonstrated that the molecules studied have different behaviours, depending on the pair chosen. Two major behaviours came forward: the combined molecule either links to the adhesion promoter, producing a mixed spectrum, or it slows down the adhesion of the molecule to

the surface and in that case the spectrum is dominated by the thiol molecule. In the latter case, if the sample is exposed longer to the thiol, the spectrum only shows the peaks corresponding to the thiol.

The real adhesion promoter molecule has then been used to observe its reaction when combined with thiols. Unfortunately, no clear behaviour could be highlighted from these experiments. However, larger differences were observed with dithiols rather than the disulfide.

As seen earlier in this chapter, the literature insists on the fact that the titanates are used to slow the curing process, leading to a stronger polymer, as the slow curing is increasing the cross-linking ratio. They also suggest the active group in the adhesion promoters is selected in combination with the kind of adhesive used. In their reviews, Sathyanarayana [7] and Walker [13] give an almost exhaustive list of active groups and adhesive matches. Thus, in the future, some work can concentrate on the more complicated, but more effective, coupling agents and study these in combination with the adhesive molecules.

References

- [1] Urban, M. W. *Vibrational Spectroscopy of Molecules and Macromolecules on Surfaces*; John Wiley & Sons, Inc.: New York, 1993.
- [2] P.C.Hewlett; C.A.Pollard. Adhesion-1; K.W.Allen, Ed.; Applied Science Publishers: London, 1977; pp 35.
- [3] C.G.Munger *Corrosion protection by protective coatings*; National Association of Corrosion Engineers: Houston, TX, 1984.
- [4] Gent, A. N. *Adhesion Age* **1982**, 25, 27.
- [5] Cassidy, P. E.; Johnson, J. M.; Rolls, G. C. *Industrial & Engineering Chemistry Product Research and Development* **1972**, 11, 170.
- [6] Johnson, O. K.; Stark, F. O.; Vogel, G. E.; Fleischmann, R. M. *Journal of Composite Metals* **1967**.
- [7] Sathyanarayana, M. N.; Yaseen, M. *Progress in Organic Coatings* **1995**, 26, 275.
- [8] Pleuddemann, E. F. *Silane Coupling Agents*; Plenum Press: New York, 1982.
- [9] W.E.Driver. *Plastics Chemistry and Technology*; Van Nostrand Reinhold: New York, 117; pp 117.
- [10] *Journal of Coating Technology* **1979**, 51, 38.
- [11] Moskovits, M. *Journal of Chemical Physics* **1978**, 69, 4159.
- [12] Colthrup, N. B.; Daley, L. H.; Wimberley, S. E. *Introduction to Infrared and Raman Spectroscopy*, 2nd ed.; Academic Press: New York, 1975.
- [13] Walker, P. *Surface Coating* **1987**, 1, 189.
- [14] Gettings, M.; Kinloch, J. *Journal of Material Science* **1977**, 12, 251.
- [15] Brown, R. G.; Ross, S. D. *Spectrochimica Acta* **1972**, 28A, 1263.
- [16] Beccaria, A. M.; Poggi, G. *British Corrosion Journal* **1995**, 30, 33.
- [17] White, L. D.; Tripp, C. P. *Journal of colloid and interface science* **2000**, 227, 237.
- [18] Withnall, R.; Andrews, L. *Journal of Physical Chemistry* **1985**, 89, 3261.

- [19] Withnall, R.; Andrews, L. *Journal of Physical Chemistry* **1985**, *107*, 2567.
- [20] *Handbook of Physics and Chemistry*; CRC Press: Cleveland, 1974; Vol. 56.
- [21] Zhang, L.; Dong, J.; Zhou, M. *Journal of Physical Chemistry A* **2000**, *104*, 8882.
- [22] Ault, B. S.; Everhart, J. B. *Journal of Physical Chemistry* **1996**, *100*, 15726.
- [23] Sockalingum, D.; Fleischmann, M.; Musiani, M. M. *Spectrochimica Acta* **1991**, *47A*, 1475.
- [24] Usmani, A. M.; Chartoff, R. P.; Warner, W. M.; Butler, J. M.; Salyer, I. O.; Miller, D. E. *Rubber Chemistry and Technology* **1981**, *54*, 1081.

General Conclusion and Future Work

The aim of this thesis was to investigate the adhesion and the ageing processes involved in the sealing of aircraft fuel tanks.

In **Chapter 2**, the macroscopic part of the study took place. An accelerated screening test had to be designed and tested. During the first stages of the work, a soxhlet extractor had been used, but was unsuccessful because of the problems due to the reduced pressure that had to be used to lower the boiling point of the fuel. It was then replaced by an ultrasonic heated bath. This second device was more appropriate to carry out the experiments. The sealant joint was in constant contact with the fuel mixture. The ultrasonic system provided the agitation of the fuel around the sealant, reproducing the same conditions as in a real aeroplane. Finally the sealant sample could be taken out for testing during the experiment, whereas with the soxhlet extractor, the sample was sealed inside the extractor for the time of the experiment. For each run, the sealant samples were tested for mass uptake, change of hardness and “mini-peel” resistance. These tests were helpful to determine the loss of elasticity of the sealants material. Parallel to this, the fuel mixtures were also analysed using mass spectrometry coupled with gas chromatography and UV/Visible spectroscopy. These tests were used to understand the transfer of matter between the sealants and the solvents. All these procedures gave valuable clues on the degradation process of the sealants. However, to completely understand and evaluate new formula, it is recommended to carry out all of the tests, as well as to test sealants with a known behaviour to compare with. The accelerated ageing test has been accomplished quite successfully.

In the future, it will be important to consider safety measures. The next step in this kind of testing is to test the resistance of the new formulas to high temperature. Thus, perhaps adapting a tap on the top of the bottles containing the hot fuel mixture will help to avoid high vapour pressure. As discussed before, it was difficult to correlate the mini-peel results to the other tests; it could then be interesting to reproduce these tests, probably

repeating the procedure several times on the same sample to get a reproducible value. The stage used to do the mini-peels also presents a temperature control device. As the normal working temperatures of an aeroplane can vary from +80 °C to -50 °C, it would be of interest to try to run the peeling experiments within this temperature range to study the elasticity of the sealants.

In **Chapter 3**, the highlight was given to the microscopic part of the investigation. The Surface Enhanced Raman Scattering (SERS) technique had been chosen because of the information it gives about the molecules at the surface neighbourhood. To understand how the sealants bond to the surface, different small molecules have been chosen to create a model. The liquid polysulfide is a long chain of aliphatic carbon and oxygen atoms, containing a sulphur – sulphur bond in the middle and terminated by two thiol groups. Thus, a disulfide and several thiol and dithiol molecules have been considered. The first molecule, the disulfide, appeared to adsorb dissociatively, i.e. the S – S bond breaks upon its absorption onto the surface of the metal. All the thiols were bonding with the metal surface via the ending sulphur atom, breaking the S – H bond. After comparing this model with the real molecule, two hypotheses were still possible. The first one, that the molecule adsorbed onto the surface at one end and standing straight, the second that the molecule adsorbed at both ends and looped back to the surface. At that point, computer simulations were used to decide which hypothesis was the most probable. As the gain of energy when the molecule bonds twice to the surface was greater than the disruption caused by the steric encumbrance, it was then concluded that the molecule looping on the surface and adsorbing at both ends was the right orientation.

In the future, it would be very interesting to pursue the calculations in order to find more about the geometry of the molecule onto the surface. For example, the program called Liaison helps to estimate the free energy of binding between a receptor and a ligand; this package would then be of great help to determine the difference in energy for binding one or both ends of the molecule to the metal surface. It would also be of interest to synthesize some long disulfide and monosulfide molecules containing a non binding end,

such as a phenyl group (see figure 1), to study their interaction with the support as well as the detection limit with such systems.

There were two major aims in **Chapter 4**, the first one was to have a better understanding of the adhesion promoters. Because of the commercial sensitivity of these compounds, another model has been studied using the SERS technique. As the active molecules used in the adhesion promoters for the Aerospace industry are mainly silanes and titanates, two simple molecules have been chosen. First, the trimethoxymethylsilane was adsorbed as a monolayer. It was then concluded that this molecule was creating a network on the surface by polymerizing. Moreover the molecule is hydrolysed when dissolved, releasing some methanolate groups in the solvent. Some of these methanolate groups were then adsorbed along with the silane molecule.

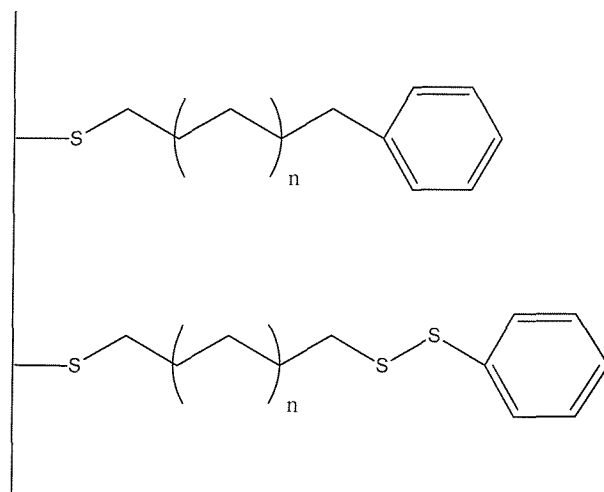


Figure 1 Example of molecules worth studying in the future

The second molecule studied as a model was the tetramethoxy titanate. As in the case of the silane, the titanate polymerises when adsorbed onto the surface, creating a network of molecules. However, at the same time, some methanolate are also adsorbed onto the surface of the metal, exactly like in the silane case. These two model molecules have then been compared to the real adhesion promoter. Unfortunately, because of all the additives and dyes that are included in the formula of the real coupling agent, it was very difficult

to interpret the SERS spectrum. However, it was possible to find some similarities between the adsorbed adhesion promoter and the model molecules.

In a future work, it might be interesting to do more surface experiments on these molecules. Scanning Tunnelling Microscopy (STM) is one of the powerful new techniques that can be used to study the network on the surface. It is probably possible to adsorb the molecules onto the metal surface and observe the creation of the network as a function of time. It will also be interesting to find out more about the formula of the real adhesion promoter to be able to match the active molecule in order to interpret more easily the adsorbed spectra.

The second aim of this chapter was to study the interactions of the coupling agent with the sealant molecules. The two models previously studied in Chapters 3 and 4 have been used again. Some of the results were in accordance with the theory, i.e. when two molecules are adsorbed, the spectrum will be dominated by the more strongly adsorbed molecule and will show some features of the other molecule. However, depending on the pair chosen for the interaction, a second behaviour was observed: time dependence. With some pairs, such as the DDS and the silane, a longer exposure to the DDS led to the removal of the silane monolayers, only a monolayer of DDS remaining on the surface of the metal. This was then interpreted as a slowing down process, i.e. the removal of the layer of coupling agent increases the time it normally takes to the sealant molecule to adsorb onto the metal, allowing the material to cross-link more efficiently on the surface and then increasing the elastic properties of the polymer.

The real adhesion promoter was also studied in combination with the molecules used before: no clear behaviour could be interpreted from these experiments. However, larger differences were observed with dithiols rather than the disulfide.

In these experiments, only a monolayer of molecule was adsorbed onto the surface. However, when the adhesion promoters are used in the industry, a thicker coat is used. The promoter is applied onto the aluminium plate using absorbing paper and the excess wiped off. This creates an infinite coating compared to a monolayer. The prepared plate

is then left to dry for at least ½ an hour (but no longer than 2 hours). This thick layer and the drying period probably allow the adhesion promoter to create a 3 dimensions network which will help the promoting of the adhesion. The polymer is then applied on the top of the adhesion promoter layer.

In the future, it will be interesting to study these interactions with the more appropriate molecules. As these would be designed to properly interact with the thiols, it would be easier to understand their behaviour and then interpret the interaction of the real adhesion promoter with these molecules. Another interesting future work would be to study the interactions *in situ*. After applying the adhesion promoter and the sealant, it is possible to microtome the plate and using microscopic spectroscopy (infrared and Raman) record the spectra of the interface. Finally, in the recent years, a German group from Leipzig [1,2] used Attenuated Total Reflectance Fourier Transform Infrared spectroscopy to study the kinetics of curing of epoxy resins. The same technique could be used to follow the curing of the sealants used in the Aerospace Industry and maybe combine them with the adhesion promoters to follow the cross-linking of the polymer in presence of the coupling agent.

References

- [1] Scherzer, T.; Decker, U. *Vibrational Spectroscopy* **1999**, *19*, 385.
- [2] Scherzer, T.; Decker, U. *Polymer* **2000**, *41*, 7681.